COMPUTATION OF BEARING CAPACITY COEFFICIENTS FOR SHALLOW FOOTINGS ON COHESIONLESS SLOPES USING STRESS - CHARACTERISTICS

BY

MARTIN ANDREWS

A thesis
presented to the University of Manitoba in partial
fulfillment of the requirements for the degree of

MASTER OF SCIENCE

in

CIVIL ENGINEERING

Winnipeg, Manitoba

ISBN 0-315-33910-1

COMPUTATION OF BEARING CAPACITY COEFFICIENTS FOR SHALLOW FOOTINGS ON COHESIONLESS SLOPES USING STRESS CHARACTERISTICS

BY

MARTIN ANDREWS

A thesis submitted to the Faculty of Graduate Studies of the University of Manitoba in partial fulfillment of the requirements of the degree of

MASTER OF SCIENCE

ABSTRACT

Bearing capacity coefficients for shallow footings placed on cohesionless slopes are computed using stress-characteristic solutions. The "basic differential equations" which are obtained by combining the equations of equilibrium with the Coulomb yield criterion, are solved using a numerical procedure. This procedure is based on a finite difference approximation of the equations and was first proposed by Sokolovskii (1960), and improved by Graham (1968). A special computer programme taking into account the effect of the slope on the boundary conditions was developed. The angle of shearing resistance of the soil was taken as being constant throughout the failing domain. The program incorporates some of the general subroutines of Hovan (1985). The solution assumes that the soil is rigid-plastic and thus does not take into account any volume strains prior to failure.

The shape of the elastic wedge beneath the footing is considered to influence the ultimate bearing capacity significantly and it is therefore modelled in the analysis.

The results obtained from the analysis are compared with available large scale field data and other existing theoretical solutions. The bearing capacity coefficients computed using the method developed in this thesis range from 0.64 to 1.35 times the experimental values.

ACKNOWLEDGEMENTS

I wish to express my thanks to Dr. J. Graham for his unwavering guidance and encouragement throughout the development of this thesis, my employers for granting me the opportunity to pursue this course of study, and my wife who has been a constant source of inspiration.

Thanks are also due to Ingrid for her assistance in translating papers written in French, to Roseanne for typing the initial draft, and Sybil for typing the final draft of this thesis.

TABLE OF CONTENTS

CHAPTER PAGE

LIST OF SYMBOLS

a - $\sin(\psi + \mu)/((2\sigma \sin\phi \cos(\psi - \mu)$

b - $-\sin(\psi - \mu)/((2\sigma \sin\phi \cos(\psi + \mu))$

B - Footing breadth

D - depth of footing

e - eccentricity of elastic wedge

H - Set back of footing from crest of slope

l - scale parameter

m - number of radial lines

n - number of spiral lines

$N_{\gamma q}$ - bearing capacity coefficient

q - ultimate bearing pressure

x - coordinate axis

y - coordinate axis

z - coordinate axis

α - slope angle

ξ $\chi + \psi$

ε - inclination of the equivalent slope

ϕ - angle of shearing resistance

LIST OF SYMBOLS (2)

γ - unit weight of soil

η - $\chi - \psi$

μ - $\pi/4-\phi/2$, the angle between the slip lines and the major principal stress direction

σ - normal stress

τ - shear stress

ω - base angle of elastic wedge

χ - $(\ln\sigma)/2 \tan\phi$

ψ - inclination of major principal stress to the vertical axis (counterclockwise positive)

Subscripts

ave - average

f - at failure

H - horizontal

i - initial

ℓ - - left side

max - maximum

min - minimum

n - normal (to the plane of application)

ps - plane strain

r - right side

tx - triaxial

v - vertical

1,2,3 - principal (stresses)

LIST OF TABLES

LIST OF FIGURES

CHAPTER 1

INTRODUCTION

A number of engineering structures, e.g. - structures placed on benches cut into slopes, retaining walls, bridge piers, etc. - require their foundations to be placed on sloping ground. Highway overpass bridges, in particular, frequently require approach fills in the vicinity of 10 m (30 feet) high. It is common in these cases to terminate the fill in a slope face dropping down to the underpass level. Foundations for the end spans of the bridge are often more economical if they are placed in the fill and not excavated or piled to underlying strata. Apart from the obvious economic advantage, there is usually also, an improved level of performance (Shields et al 1980). Supporting the end spans in the approach fill can significantly reduce the severe road maintenance problems that arise when the fills and bridge decks settle by different amounts.

Various theories are available to the design engineer for estimating the bearing capacity of a footing on a slope. As noted by Bauer et al (1981), all these theories give different answers and most theories are applicable only to a footing located right at the crest of a slope.

Because of the uncertainties of the theories, bridge designers adopt a conservative approach, and tend to utilize pile support or other deep foundations for the abutments. In many cases, this approach may not be the most economical solution (Felio and Bauer, 1984). As noted by Bauer and Mowafy (1985), it is economically advantageous to locate the footing as close as possible to the edge of the embankment and to make the slope as steep as possible in order to keep the bridge span to a minimum length.

Several researchers (for example Vesic, 1973; De Beer, 1965), note that the primary framework for design involves both the determination of ultimate loads, as well as the analysis of settlements to ensure that the foundations fulfill their intended function from a structural as well as functional viewpoint.

The particular problem of estimating settlements of foundations located on granular slopes is complicated and not fully understood. At the present time the tendency is to use complicated finite element techniques to study the settlement behaviour of footings located on granular media, e.g. Bauer (1982), Selvadurai et al (1984), Mowafy (1984), Bauer and Mowafy (1985). Since such tools are not readily available to all design engineers, reliable estimates of settlements cannot readily be made. As a result, estimation of the ultimate bearing capacity still constitutes the primary framework for design. It would therefore be helpful to have at the present time, a simple bearing capacity solution which gives reliable results.

This thesis is concerned only with the bearing capacity aspect of the stability problem. Economy in design can be achieved if the ultimate bearing capacity can be accurately determined.

Ultimate bearing capacity of footings is commonly determined by making use of the principle of superposition. That is, the influence of self-weight in the failure zone and surcharge on the free surface are assessed separately and then added together. This thesis uses an alternative approach by Meyerhof (1951) which combines both effects into a single dimensionless factor. $N_{\gamma q}$. The bearing capacity is thus expressed as $q_u = 1/2\ B\ \gamma N_{\gamma q}$. (Notation is summarized at the beginning of the thesis on pages vii to viii).

However in contrast with the theoretical method used by Meyerhof, the thesis uses the method of stress-characteristics (Graham 1968), and develops a soundly based analysis for the capacity of shallow footings near the crest of slopes. It compares the new theoretical results with existing theories and with available field data.

In the analysis, the solution for failure loads starts from a Rankine rectilinear plastic zone exiting the slope below the footing. The geometry and stress conditions in this zone are statically determinate. The back surface of this zone was then used as the starting boundary for a radial transition zone that extends backwards into the slope, and upwards towards the footing. Available information and photographic evidence concerning the shape of the failure zone was studied in order to arrive at realistic assumptions concerning the distorted shape of the domain for the analysis.

It is well known that sand behaviour cannot be adequately described by a straight Coulomb-Mohr strength envelope. That is, the Coulomb-Mohr envelope flattens with increasing stress, resulting in a variable angle of shearing resistance dependent on stress level (Graham and Hovan, (1985). However, the present analysis considers only a constant ϕ solution because at this stage of understanding the mathematical modelling of the problem, further complexity is unwarranted.

In Chapter 2, the most common existing theories are described and reviewed. Chapter 3 summarises the theory of the basic stress characteristic solution and develops the boundary conditions resulting from the presence of a slope close to the footing. Chapter 4 presents an analytical study of the shape of the elastic zone immediately beneath the footing. Chapter 5 considers the special case of a footing at the crest of the slope, and describes the parametric study of the problem that has been conducted using a specially developed computer program, and presents the results for this case. Chapter 6 describes the parametric study and presents the results for the more general case of footing located away from the crest of the slope.

Results, discussions and comparison with other theories and experimental data follows in Chapter 7. Topics for further research and conclusions are presented in Chapter 8.

Appendix 1 contains a listing and typical output of the main computer program.

CHAPTER 2

REVIEW OF EXISTING THEORIES FOR THE BEARING CAPACITY OF FOOTINGS ON SLOPES

2.1 INTRODUCTION

At present there are at least nine theories which can be used to predict the bearing capacity of a footing placed within close proximity of a slope. As noted by Bauer et al (1981) all these theories give different answers and most are applicable only to footings located with one edge right at the crest of the slope. This chapter briefly describes the most commonly available theories and comments on their usefulness and the assumptions made in their development. Comparisons between these existing theories and the new solution developed in this thesis are discussed in Chapter 7.

Prior to describing the distinctive features of each of the bearing capacity theories, it is necessary to place them in perspective by discussing their similarities, and the general framework within which bearing capacity theories are commonly developed.

All of the commonly used theories utilize the concept of "perfect" plasticity, that is failure is assumed to occur with large scale continuous straining after zero initial displacement. That is, the behaviour is assumed to be "rigid-plastic".

Chen and Davidson (1973) suggest that the techniques used to determine the collapse load can be divided into three principal groups utilizing respectively :

i) the stress characteristic or slip line method,

ii) the limit analysis method,

iii) the limit equilibrium method

This grouping is maintained in the ensuing discussions. It will however be evident later that the fundamental approach of the latter two methods are similar. They both start with an assumed failure surface or failure mechanism. Each method then employs a different approach to determine the stresses satisfying static equilibrium at the instant of impending failure. The methods will now be reviewed in turn.

The stress characteristic method combines the Coulomb-Mohr yield criterion with the equations of static equilibrium to give a set of hyperbolic differential equations of plastic equilibrium. When taken together with the stress boundary conditions for a given problem, the equations can be used to investigate the stresses in the soil beneath the footing at the instant of impending plastic flow (Sokolovskii 1960). In problem solving, it is often convenient to transform this set of equations to curvilinear co-ordinates whose directions at every point in the yielding region coincide with the directions of failure or the slip plane. These slip directions are known as slip lines in physical modelling or stress characteristics in mathematical modelling.

Kotter (1903) was the first to derive these stress characteristic equations for the case of plane deformations. Prandtl (1920) subsequently obtained a closed form solution to these equations for a footing on a weightless soil possessing both cohesion and friction. The important inclusion of soil weight into the analysis considerably complicates the mathematical solution. Sokolovskii (1960) adopted a numerical procedure based on a finite difference approximation of the stress characteristic equation. Graham (1967, 1974) made a significant improvement to the Sokolovskii solution by including a better approximation of the effects of stress variation along the slip lines.

Graham and Stuart (1971) suggested that this method is superior to the other methods since it offers the opportunity of investigating a wider range of boundary and field assumptions. In particular it permits more realistic modelling of the sand properties (see for example, Graham and Hovan, 1985). This form of analysis will be used in the theoretical solution derived in Chapter 3.

The second type of analysis, namely limit analysis, is based on the upper and lower bound limit theorems of Drucker et al (1952). These theorems were developed for an elastic perfectly plastic material with an associated flow rule.

The lower bound theorem of limit analysis states that if a distribution of stress over the domain in question can be found which satisfies the equations of equilibrium, the stress boundary conditions and the yield criterion, the load associated with this stress condition is less than or at best equal to the true ultimate load.

The upper bound theorem states "if the power of the external load is greater than or equal to the rate of internal energy dissipation associated with a kinematically admissible velocity field, then the load must be greater than or at best equal to the true ultimate or limit load" (Chan, 1975). The upper bound theorem may also be stated as follows: if a kinematically admissible velocity field can be found, uncontained plastic flow must impend, or have taken place previously.

By suitable choice of stress and velocity fields, the above upper and lower bound theorems enable the required collapse load to be bracketed.

The limit equilibrium method has been the most commonly used method for obtaining approximate solutions for bearing capacity. It can be best described as depending on a quasi-static analysis or approximations to the slip line fields. It generally entails using an assumed failure surface comprising various simple shapes, for example plane, circular or logarithmic spiral. To allow an equation of equilibrium to be written for bearing capacity determination (or indeed for other classes of problems such as slope stability) it is necessary to make sufficient assumptions about the stress distribution within the soil domain bounded by the failure surface so that the analysis becomes determinate in terms of resultant forces or moments. This method (and indeed all three of these methods) gives no consideration to soil kinematics, or to the displacements preceeding failure.

All available theories for determining the bearing capacity of footings on slopes fall within the general framework of one of the three methods outlined above. The methods by Meyerhof (1957); Mizuno (1960); Kovalev (1964); Brinch Hansen (1970); Giroud and Tran Vo Nhiem (1971); Chen (1975); Bowles (1975); Bowles (1977); Kusakabe (1981); will now be discussed in turn. They are presented in the chronological order based on the publication date.

2.2 Meyerhof's (1957)

Meyerhof's method is a limit equilibrium method. His original theory which was developed for level ground (Meyerhof, 1951) was a modification of the earlier Terzaghi (1943) solution. The failure mechanism based on logarithmic spirals used by Terzaghi is shown on Fig. 2.1. He assumed that the soil of depth D above the level of the foundation base manifests itself only by its weight, and offers no support to the foundation loads through its shearing resistance. In his development of this analysis. Meyerhof assumed that the failure surface extends right of the surface (Fig.2.2). He includes in his analysis an "equivalent free surface" subjected to "equivalent free surface stresses". (Fig. 2.2).

The solution for footings on a slope uses a development of the same procedure (Fig. 2.3). In this case, the weight of the soil wedge AEF in Fig. 2.2 is replaced by the equivalent stresses p_o and s_o normal and tangential, respectively to the equivalent free surface AE.

It is not clear from the literature whether Meyerhof included the influence of the soil on the upslope side of the foundation when calculating the ultimate bearing capacity.

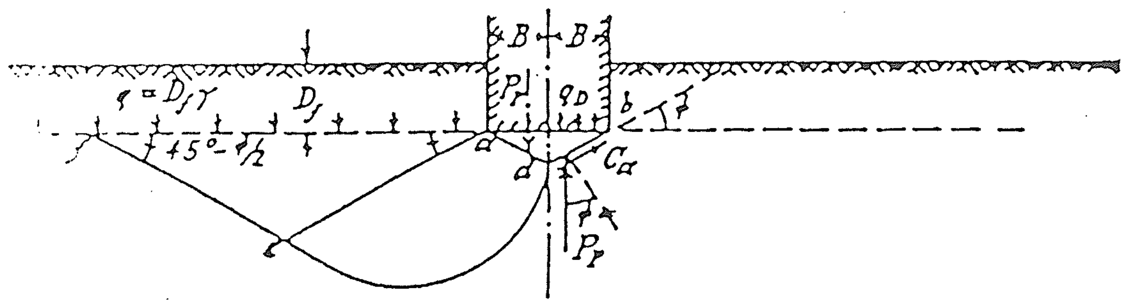

FIGURE 2.1 TERZAGHI FAILURE MECHANISM FOR A FOOTING ON LEVEL GROUND

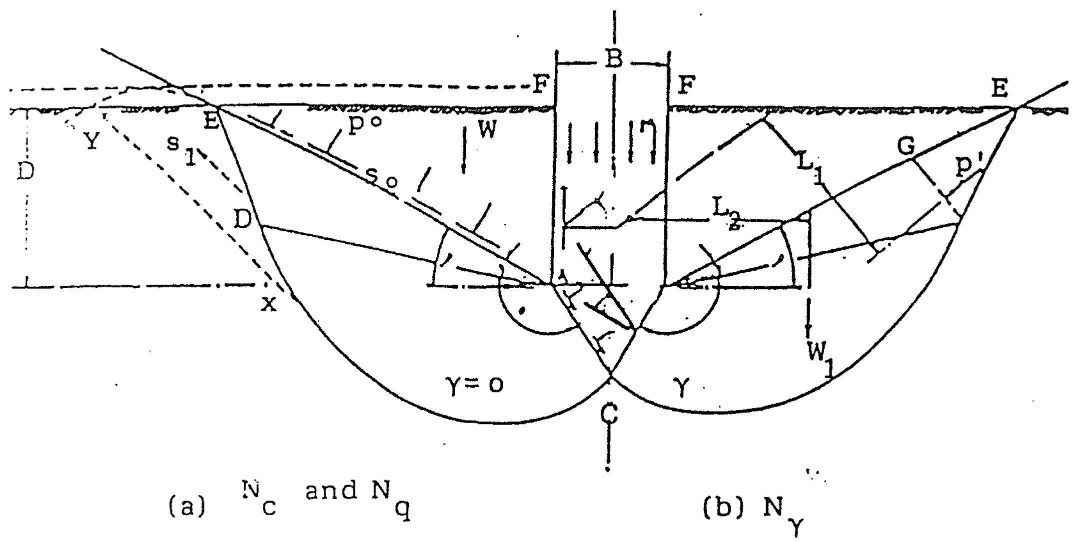

FIGURE 2.2 MEYERHOF FAILURE MECHANISM FOR A FOOTING ON LEVEL GROUND

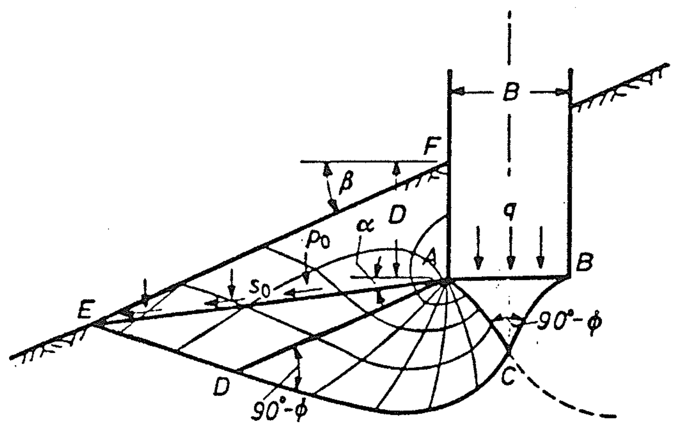

FIGURE 2.3: MEYERHOF FAILURE MECHANISM FOR A FOOTING ON A SLOPE (after Meyerhof 1957).

2.3 Mizuno (1960)

Mizuno et al (1960) calculated the bearing capacity of a slope of cohesionless soil under a uniform load acting upon its horizontal top. The method employed is a limit equilibrium method. The analysis is similar in principle to the case of a footing on a horizontal surface presented earlier by Mizuno (1948, 1953), which is about the same time that Meyerhof published his theory concerning the ultimate bearing capacity of foundations on level ground (Meyerhof, 1951). It is therefore reasonable to assume that the work of Meyerhof and Mizuno was carried out independent of each other. This is in fact evidenced by the completely different approaches adopted by the authors to the analysis of the bearing capacity problem.

Mizuno et al, assume that at the instant of failure, a wedge of active earth pressure is formed directly below the load, while a region of passive earth pressure is formed adjacent to the slope (Fig. 2.4). The boundary of the passive pressure region is determined from the Mohr's circle (Fig. 2.5) as a fraction of the slope angle and the angle of internal friction ϕ of the soil.

By considering the static equilibrium of the elastic wedge, the stress acting on the wedge at the instant of failure is calculated, as a function

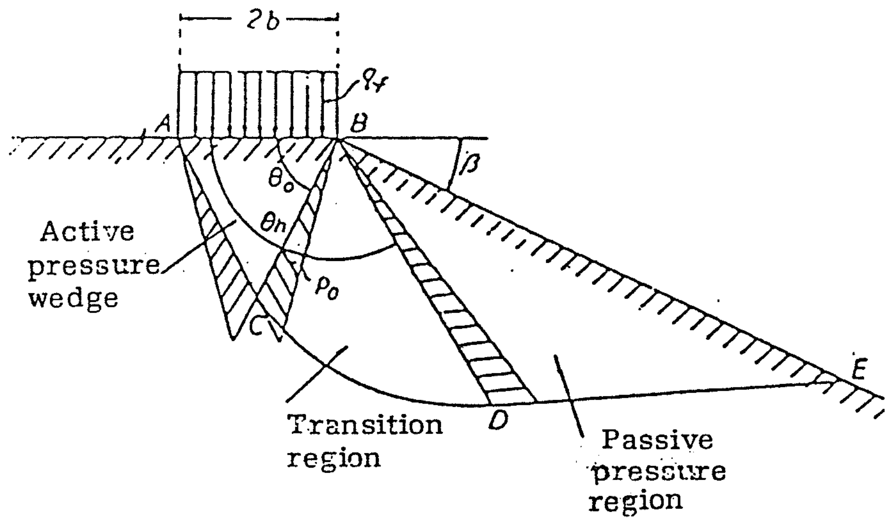

FIGURE 2.4: MIZUNO ET AL FAILURE MECHANISM FOR A FOOTING ON A SLOPE (after Mizuno et al 1960)

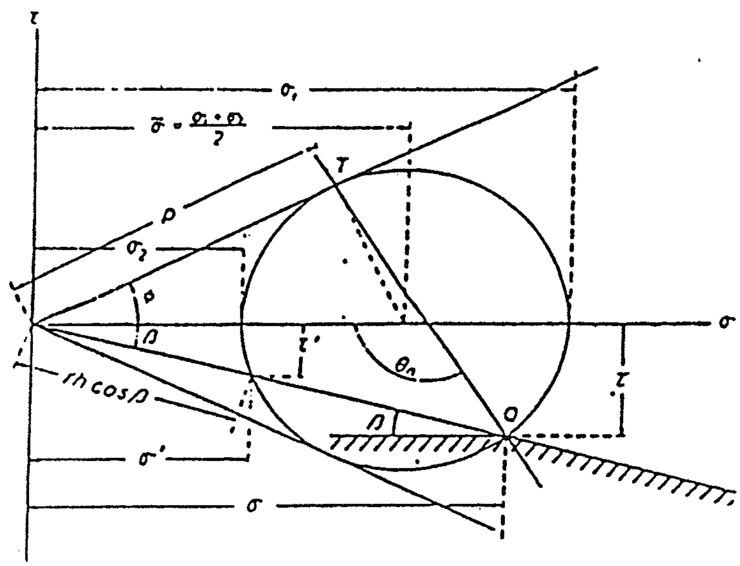

FIGURE 2.5: MOHR CIRCLE USED BY MIZUNO TO DETERMINE BOUNDARY CONDITIONS (after Mizuno et al 1960)

of the ultimate load, the wedge geometry and the unit weight of the soil. Similarly, by considering the static equilibrium of the region of passive pressure adjacent to the slope, the stresses on the boundary BD (Fig. 2.4) are calculated.

The transition region, which is defined as the region between the active and passive pressure regions, as described above, is then divided into a series of small wedges having equal vertex angles. If the stresses on one side of any of the wedges and the length of that side are known, then the stresses on the other as well as its length can be determined from the equilibrium conditions of the wedge. The shape of the sliding surface is thus also generated from the equilibrium conditions.

The bearing capacity is determined by first assuming a value for the stress distribution on the boundary of the elastic wedge beneath the footing, which is a multiple of the unit weight of the soil and half the footing breadth. Then, starting from this assumed value the stresses on the dividing lines between the wedges and the sliding surface are calculated as outlined above. The initally assumed value is then adjusted until the stresses on the last wedge coincides with the passive earth pressure. Since the apex angle of the transition zone as a function of the slope angle is known, then the slope angle corresponding to the calculated value is determined.

The authors present their results in the form of curves of the dimensionless bearing capacity coefficient N_{γ}, plotted against the slope angle, for various values of ϕ ranging from 15 degrees to 40 degrees.

The analysis does not account for the embedment depth of the footing or the distance between the shoulder of the slope to the edge of the footing. The results are therefore applicable only to footings sitting at the top of a slope with one edge at the crest of the slope.

2.4 Kovalev (1964)

Kovalev's method for the determination of the bearing capacity of a footing on a slope can best be described as a limit equilibrium method. He developed a simplified shape of the slip lines generated using Sokolovskii stress characteristic method and used this simplified shape to obtain an approximate estimate of the ultimate bearing capacity of the soil. It is worthy of note that Kovalev's expressed rationale for using a simplified failure surface is to avoid the great amount of calculations required for solving the basic differential equations, and determination of the slip line field for the variety of combinations of slope angle and soil shear strength parameters. Although such an argument may have been valid at the time when the paper was first published, the availability of the digital computer has substantially changed matters. It is now possible to carry out a series of such calculations with little human effort and at relatively low cost and in a very short time.

Kovalev, using the approach of Sokovskii (1960), treats the bearing capacity problem as being identical to a slope stability problem with a surcharge at the crest of the slope. It is obvious that this approach does not take into account the important effect of the interaction between the soil and the base of the footing. In fact, the footing load is simply treated as an artifical surcharge. A typical slip line field generated using this approach is shown on Figure 2.6. This diagram shows that the slip line field continues right up to the base of the footing on the horizontal ground surface.

The simplified failure surface considered by Kovalev for a surface footing is shown on Figure 2.7. He states that it was based on actual stress characteristic fields for 'c, ϕ', soils with ϕ varying between 30 and 40 degrees. The proposed failure surface consists of two parts: a straight line section 'ab' inclined at an angle $\pi/4 - \phi/2$ to the sloping ground surface, and, a circular segment 'bd' with centre O' (Figure 2.7).

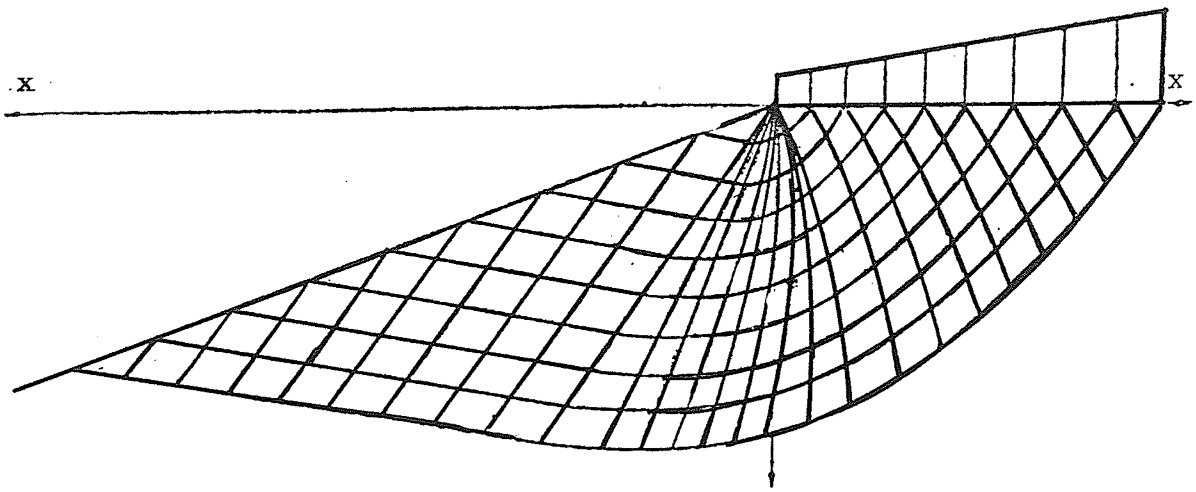

FIGURE 2.6: TYPICAL SLIP LINE FIELD BASED ON SOKOLOVSKII SOLUTION

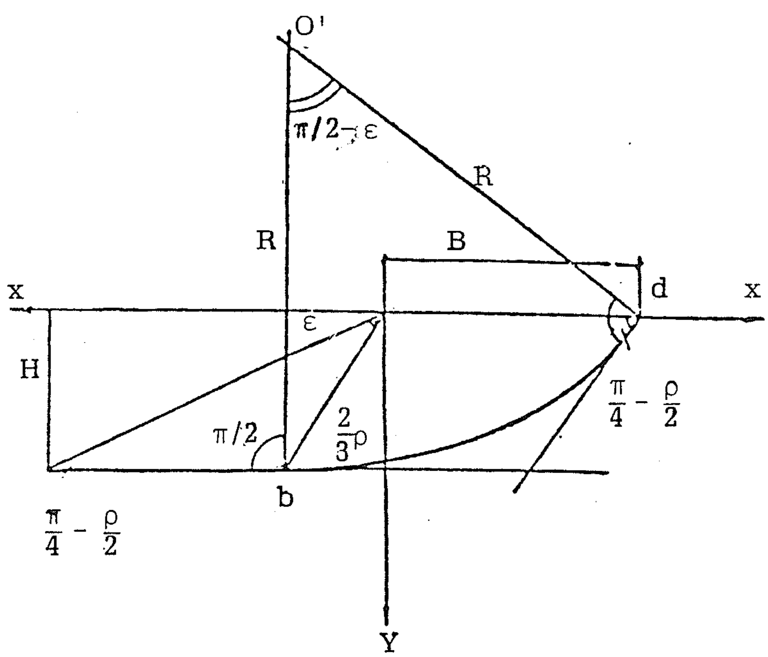

FIGURE 2.7: KOVALEV'S FAILURE MECHANISM FOR A FOOTING ON A SLOPE

The centre of the circular segment is found by ensuring that the rupture line meets the ground surface at the "statically correct angle" of $\pi/4 + \phi/2$. The statically correct angle is the angle at which a rupture line intersects a boundary so that statical equilibrium conditions at the point of intersection are fully satisfied.

Although it is not explicitly acknowledged by Kovalev, he makes use of Kotter's equation to determine the state of stress along the assumed rupture line and subsequently the ultimate bearing capacity of the footing.

Kotters equation relates the limiting state of stress on a rupture line, to two variables, namely, the resultant stress σ, and the angle θ between the rupture line and the horizontal (Kotter, 1903).

The equation may be expressed as

$$\frac{d\sigma}{ds} - 2\sigma \tan\phi \frac{d\theta}{ds} = -\gamma \frac{\cos\theta}{\cos\phi} \qquad \text{.........2.1}$$

By combining Kotter's equation with the known boundary conditions, e.g. the known statically correct angle where the rupture line meets the surface, Kovalev determined the vertical stress at the base of the footing.

This is expressed as

$$p' = A_1 \gamma B + C_1 c$$

where γ, B, and c have the same usage as elsewhere in the thesis (see pages vi to vii for a definition of the notation used), and A_1 and C_1 are coefficients depending on the soil properties ϕ and the problem geometry i.e. α.

Comparing Equation 2.2 to the commonly used expression for bearing capacity of a surface footing (D = 0).

$$q_u = 1/2\ B\ \gamma\ N\gamma + cN_c \quad \ldots\ldots\ldots\ldots 2.3$$

we note that

$$A_1 = N_{\gamma/2}, \text{ and}$$

$$C_1 = N_c$$

Kovalev indicates that the maximum difference between the results obtained by his proposed method, and those obtained by solving the basic differential equations numerically is 12%.

Thus far, we have only discussed the case of a surface footing. The case of a shallow footing, that is, one placed at small depth in the soil was also studied by Kovalev. The soil layer above the base of the footing is treated as a uniform surcharge which is in turn resolved into two components perpendicular and parallel respectively to the surface of the slope (Figure 2.8).

The analysis assumes that the failing domain can be divided into two zones as shown on Figure 2.9.

The approximate sliding surface for this case, like the case of surface footing, is considered to consist of a straight line portion and a circular arc. (Figure 2.10). The straight line portion cuts the slopes surface at an angle of $\varepsilon + \alpha - \phi$. The angle α is defined in Figure 2.9 and from Mohr circle considerations, its value is given by

$$\alpha = 1/2 \{ \pi /2 - \text{arc sin} (\sin \varepsilon / \sin \phi) - \varepsilon + \phi \}$$

Again by applying Kotter's equation, Kovalev obtained a solution for the bearing capacity coefficients N_γ and N_q. For this case N_c was not determined since only cohesionless soil was considered.

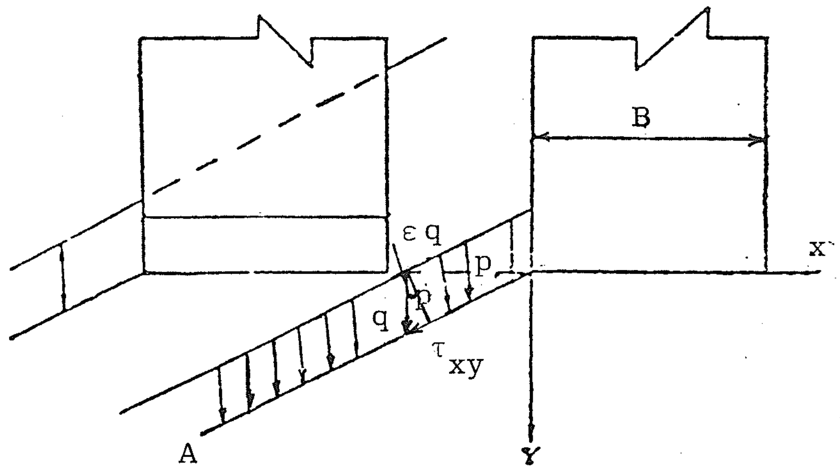

FIGURE 2.8: UNIFORM SURCHARGE ON A SLOPE

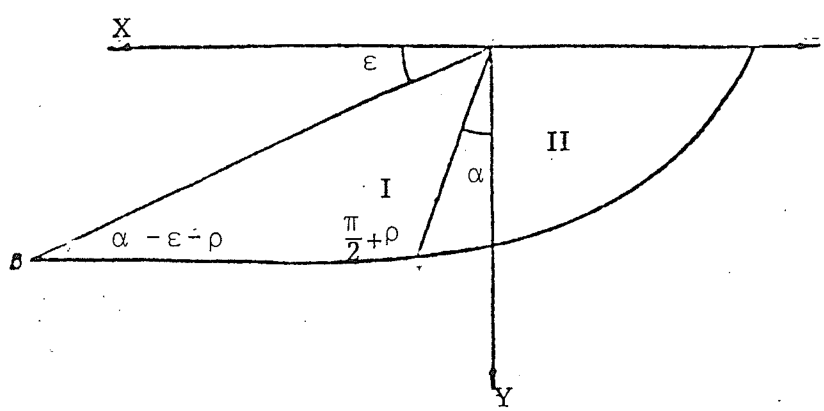

FIGURE 2.9: DIVISION OF THE FAILING DOMAIN INTO TWO ZONES (after Kovalev 1964)

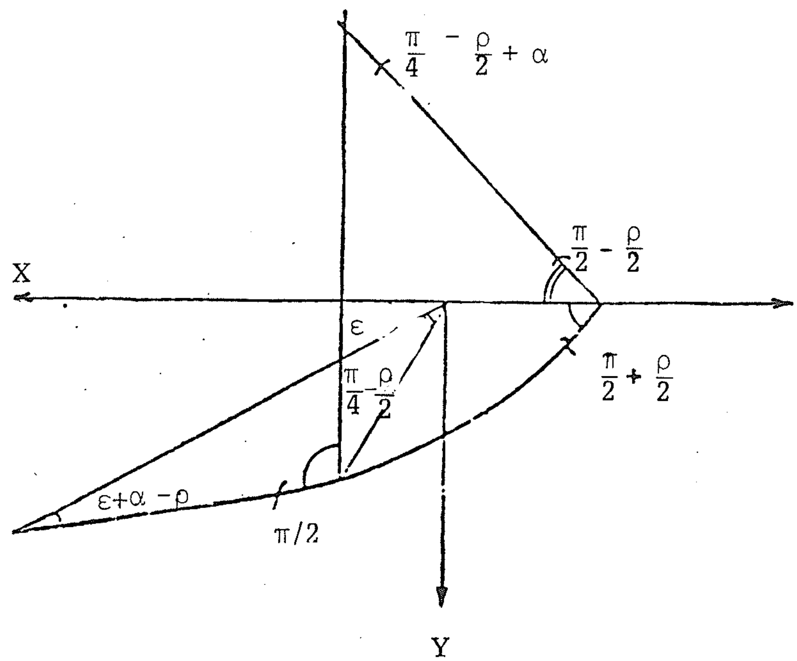

FIGURE: 2.10: FAILURE MECHANISM FOR A SHALLOW FOOTING ON A SLOPE (after Kovalev 1964)

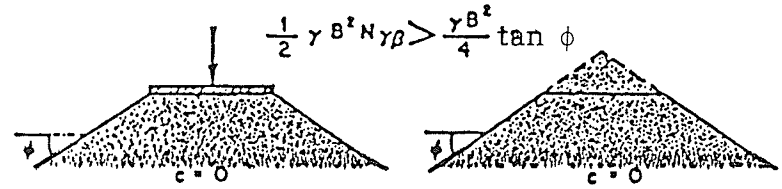

FIGURE 2.11: COMPARISON OF THE BEARING CAPACITY PROBLEM WITH THE SLOPE STABILITY PROBLEM (after Giroud 1971).

The important case of a footing with its leading edge located away from the crest of the slope was not addressed. As noted earlier, the analysis is based on the assumption that the bearing capacity of a footing on a slope is identical to the problem of stability of a slope with a surcharge placed at the crest. This approach is here considered to be too simplistic since it does not take into account the important effect of the soil-footing interaction. This view agrees with the view point of Giroud et al (1971) who have indicated diagramatically (Figure 2.11) that the load that can be supported by a footing at the top of a symmetrical embankment is greater than the weight of soil required to transform the embankment into a triangle.

2.5 Brinch Hansen (1970)

In 1961, Brinch Hansen published "A General Formula for Bearing Capacity (Hansen, 1961)". This publication does not give a 'new' method for bearing capacity determination, but generalizes the Terzaghi (1943) bearing capacity formula to take into account the dimensions, shape and depth of the footing, as well as the inclination and eccentricity of the foundation load. This was done by multiplying each term of the Terzaghi formula with a shape, depth and inclination factor . The general equation was then written as

$$q_u = 1/2\, B_\gamma N_\gamma s_\gamma d_\gamma i_\gamma + \gamma D \quad N_q s_q d_q i_q + c \quad N_c s_c d_c i_c \,,$$

The method employed by Brinch Hansen in determining the new factors is semi empirical. For example, with respect to N_γ, Brinch Hansen states that Meyerhof's values are too high while those of Lundren and Mortenson are too low. Reasoning that the correct value of N_γ, must be between these two values he gives a 'better' approximation of the N_γ value as $N_\gamma = 1.8 \ (N_q - 1) \tan \phi$.

Approximate formulae are also presented for the factors s,d and i.

In 1970 Brinch Hansen published "A Revised and Extended Formula for Bearing Capacity (Hansen (1970). In this paper, two other factors were added to account for base inclination and ground inclination. The ground inclination factor was intended to apply to the case of a footing located close to a slope. The failure mechanism assumed for calculation of the new factors b and g is shown on Figure 2.12. The factors g_q and g_γ are given as

$$g_\gamma = g_q = (1 - 0.5 \tan \alpha)^5$$

For a horizontal footing $b_\gamma = 1$. Hence setting the terms which are not applicable to unit, Brinch Hansen's formula can be written as

$$q_u = 1/2 \, B_\gamma N_\gamma g_\gamma + \gamma D \ N_q g_q d_q \quad \ldots\ldots\ldots\ldots 2.4$$

For a shallow footing, that is $0 \leq D_f \leq B$), and with ϕ ranging from 30 to 45 degrees d_q varies within the relatively narrow range of 1.1 to 1.3.

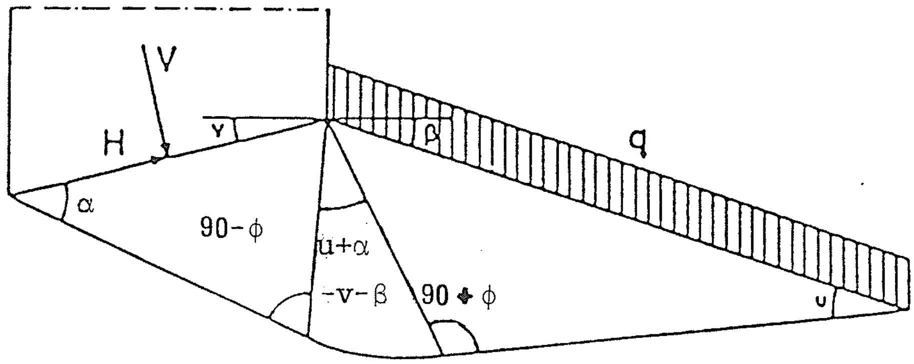

FIGURE 2.12: FAILURE MECHANISM FOR A FOOTING ON A SLOPE (after Brinch Hansen 1970).

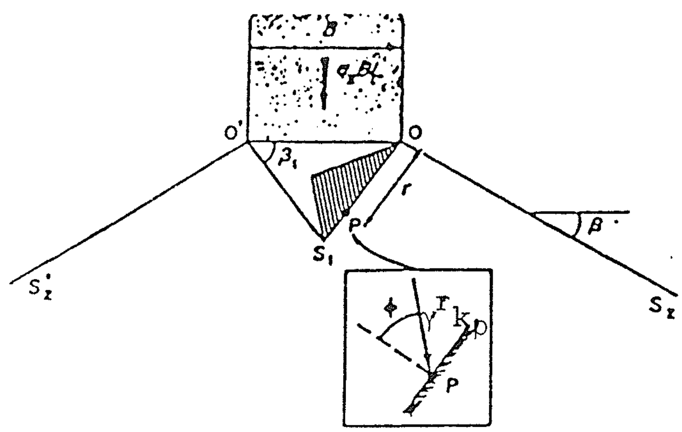

FIGURE 2.13 N_γ DETERMINATION (after Giroud 1971)

Taking an average value of 1.2, Equation 2 can be rewritten as

$$q_u = 1/2\, B\gamma\, N_\gamma\, g_\gamma + 1.2\, \gamma D\, N_q\, g_q$$

The equivalent Meyerhof bearing capacity factor $N_{\gamma q}$ based on this method can therefore be expressed as

$$N_{\gamma q} = N_\gamma\, g_\gamma + 2.4\, \frac{D}{B}\, N_q\, g_q$$

As noted previously, the Brinch Hansen method is not a 'new' method for determination of bearing capacity. It is essentially a semi-empirical method based on Terzaghi's analysis which allows for greater flexibility with respect to practical applications.

2.6 Giroud and Tran-Vo-Nhiem (1971)

These authors developed a bearing capacity theory for a footing placed at the top of an embankment which slopes equally on either side of the foundation (Figure 2.11). The slope starts right at the edge of the footing. The method employed in determining the bearing capacity coefficients, is essentially a limit equilibrium method. It is assumed that a rigid wedge which is symmetrical about the centre line of the foundation, is formed beneath the footing. The bearing capacity coefficient, is obtained as a function of the wedge angle, the angle of internal friction of the soil ϕ, and a thrust coefficient on the surface OS, (Figure 2.13). This is done by considering the equilibrium of the wedge OS_1O' and equating the vertical thrust force on OS, due to the soil in the dihedral S_1OS_2 to the sum of load on the footing and weight of soil in the wedge OS_1O_1.

The thrust coefficient defines the stress distribution of OS_1 which is assumed to be triangular with a value of zero at O, that is, the slope of the triangular stress distribution is the thrust coefficient. The authors refer to the coefficient as the coefficient of passive earth pressure. This term is considered to be misleading since the coefficient is not in fact the "coefficient of passive earth pressure" as it is commonly used in traditional Soil Mechanics. The term thrust coefficient is preferred, and is used in the ensuing discussion.

The authors state that the value of the thrust coefficient is deduced after determining the network of characteristics in the dihedral OS_1S_2 by a finite-difference method. No further details of the method are given. For any given values of ϕ and α, the value of ω_r which yields a minimum $N\gamma$ is determined. This value is taken to be the value for use in design.

The authors also present an approximate method of determining the bearing capacity coefficient in the instance when the leading edge of the footing is located some distance away from the crest of the slope.

It consists of first determining the "equivalent slope", which is defined as the slope starting from the foundation which gives the same bearing capacity as that of the real soil mass, (Figure 2.14). The method is based on the assumption that the failure mechanism in the actual soil medium, and in the fictitious medium is the same.

The bearing capacity factors are listed in tables for a range of α from 0 to 50 degrees, and ϕ from 0 to 50 degrees.

2.7 Chen (1975)

Chen (1975) obtained the bearing capacity of a footing on a slope of cohesionless soil using the so-called "limit analysis" method. Chen states that this method enables a definite statement to be made about the collapse load without carrying out a step-by-step elastic plastic analysis. The analysis employs the upper bound limit theorem to generate an approximate solution to the bearing capacity problem. The soil is modelled as an elastic-perfectly plastic material which obeys the associated flow rule. They physical validity of this flow rule is however questionable (Graham, 1968).
however questionable (Graham 1968).

The analysis is a modification of the solution for a shallow footing on level ground (Chen, 1975). For horizontal ground the failure mech-

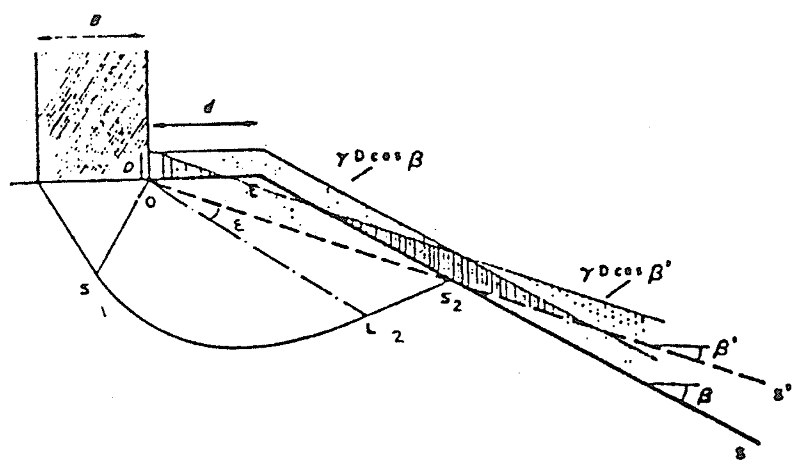

FIGURE 2.14: DETERMINATION OF THE "EQUIVALENT SLOPE" FOR A FOOTING LOCATED AWAY FROM THE CREST OF THE SLOPE (after Giroud 1971).

anisms utilized in the analysis are the Prandtl and Hill mechanism (Figures 2.15 and 2.16 respectively). For sloping ground, the area bef (Figure 2.15) is set equal to zero and the angle which 'eb' makes with the horizontal is taken as being negative in the analysis. These conditions therefore represent the case of a footing on a slope.

In accordance with the upper bound theorem of limit analysis, the power of the external loads is equated with the rate of internal energy dissipation for the assumed failure mechanism. For a soil possessing both cohesion and friction, Chen divides the radial shear zone into a series of small triangles (Figure 2.15) in order to compute the rate of energy dissipation in this region. The triangles are assumed to translate as rigid bodies in directions that make an angle ϕ with the slope of the local segment of cd. The rate of energy dissipation is obtained as a function of the soil cohesion and the relative velocity between the two adjacent soil masses, that is, the soil in the failure zone and the soil outside the zone.

For cohesionless soil, Chen assumes that the rate of internal energy dissipation is zero. On this basis, it is therefore only necessary to calculate the rate of external work done. External power or work done is contributed by gravity forces and the footing load. The bearing capacity factor of the soil is this determined from the expression resulting from equating the rate of external work to zero.

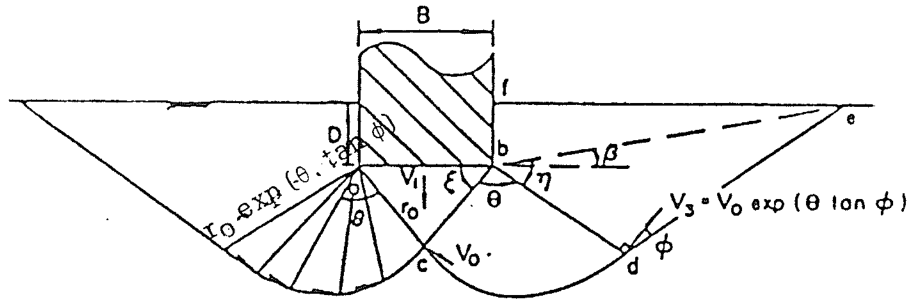

FIGURE 2.15: THE PRANDTL FAILURE MECHANISM

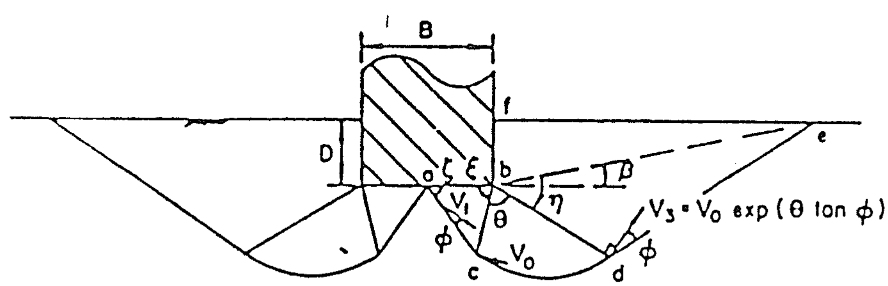

FIGURE 2.16: THE HILL FAILURE MECHANISM

The analysis is carried out for both the Prandtl and Hill mechanisms, and the absolute minimum value of $N\gamma$ is obtained. The results presented by Chen (1975) apply only for the case of a footing at the top of a berm which slopes equally on either side.

2.8 Bowles (1975)

Bowles (1975) proposed a graphical method for the determination of the bearing capacity of a footing on a slope, which he states is a modification of Brinch Hansen's (1966) equilibrium method. Reference to the original Brinch Hansen publications (1957 and 1966) (see Section 2.5). indicates that he approximates the limiting rupture line to a circular arc (Figure 2.17). Static equilibrium conditions are then applied to determine the components N and T of the internal stresses in the circle, and the moment M_R, as a function of the problem geometry and the stresses on the assumed rupture line. Use is then made of Kotter's equation, and the known boundary stresses to determine the stresses along the rupture surface, and hence the unknowns N, T and M_R. Simple static equilibrium considerations can then be applied to determine the ultimate bearing capacity.

The graphical procedure developed by Bowles is presented in principle in Figure 2.18.

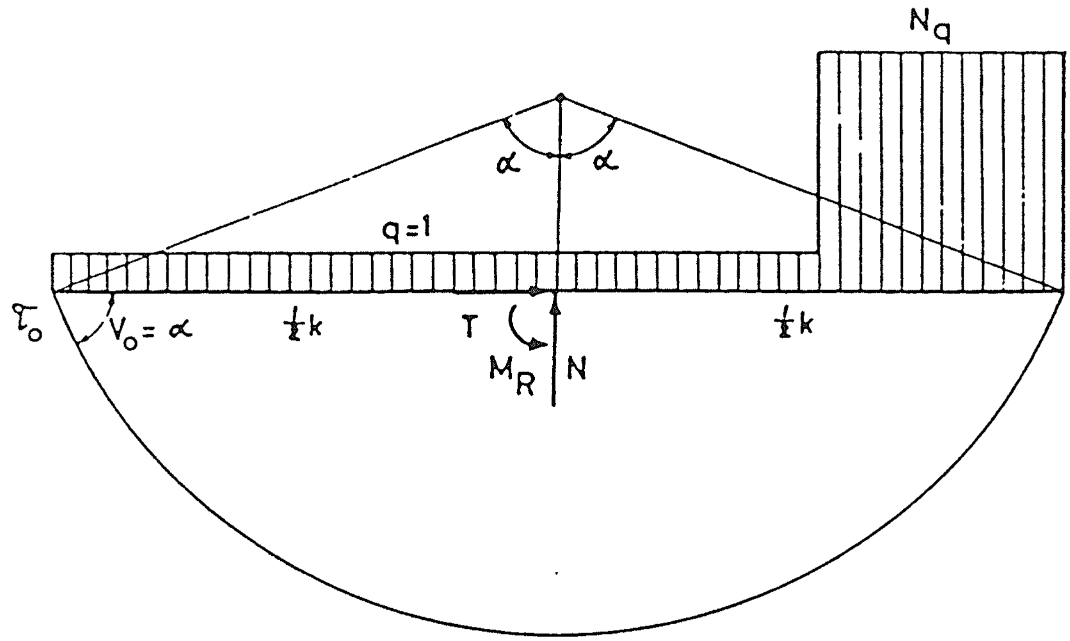

FIGURE 2.17: BRINCH HANSEN'S CIRCULAR RUPTURE SURFACE (after Brinch Hansen 1966)

It consists essentially of drawing the system to scale, and using a graphical procedure to construct the presumed failure surface which is comprised of a circular arc and a straight line. The weight of the soil in the different segments of the failing mass are then computed. The frictional resistance to sliding is computed from the weights, and static equilibrium conditions are supplied to determine the bearing capacity.

The only aspect of this method which is similar to the "so-called" equilibrium method of Brinch Hansen (1966) is that a segment of the failure surface assumed to be circular.

The method used for determination of the ultimate load is not the direct application of Kotter's equation, but considers only simple static equilibrium of the system. Furthermore, the validity of a circular failure surface is questionable since it does not conform to the surface observed in experimental work.

Lee (1978) has computed the bearing capacity factor $N_{\gamma q}$ (as defined by Meyerhof, 1951) using Bowles's (1975) method for a cohesionless sand with $\phi = 35°$ and $\phi = 40°$ with footings located up to 5B from the crest of the slope, with depths ranging from 0 - 3B. A slope with a gradient of 1 vertical to 2 horizontal was considered.

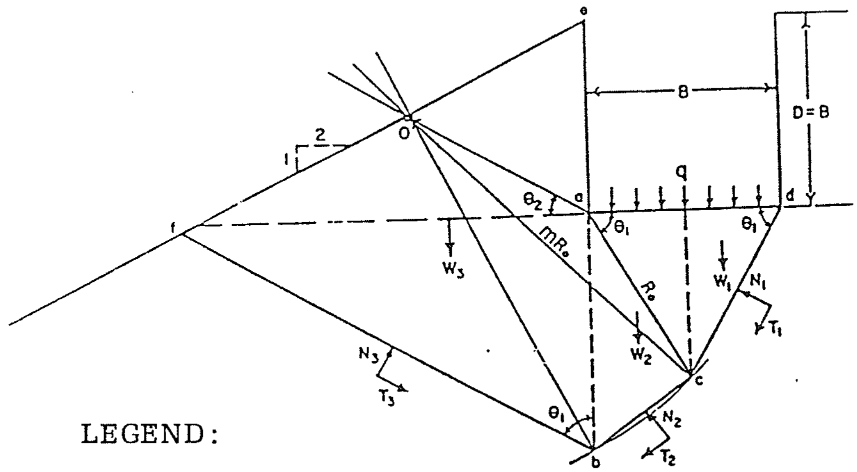

LEGEND:

θ_1 = 45° + ϕ/2

θ_2 = 45° - ϕ/2

ϕ = INTERNAL FRICTION ANGLE

B = FOOTING WIDTH

D = FOOTING FOUNDING LEVEL

FIGURE 2.18: GRAPHICAL PROCEDURE FOR BEARING CAPACITY DETERMINATION (after Bowles 1975).

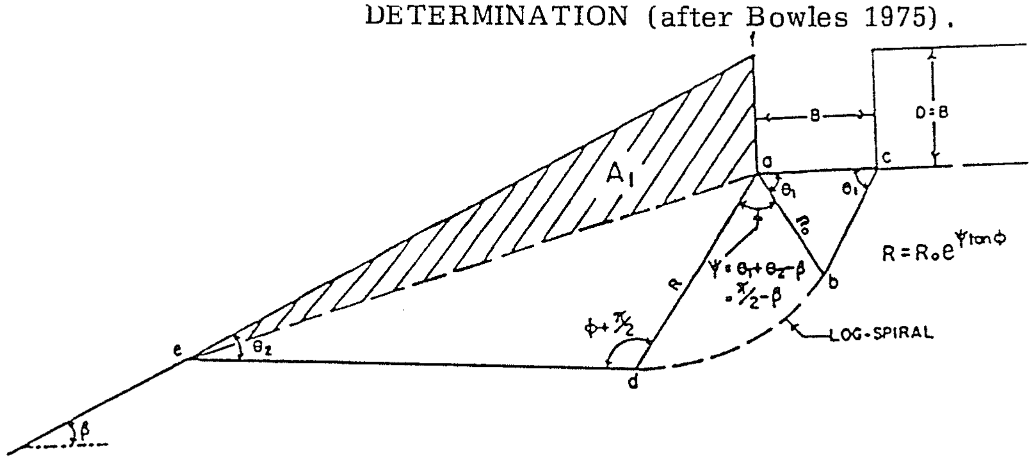

FIGURE 2.19: BOWLES (1977) FAILURE MECHANISM (after Lee 1978).

2.9 Bowles (1977)

The method proposed by Bowles like the one described in Section 2.8 is also graphical procedure. It is based on an assumed failure surface consisting of a log-spiral and a straight line which is consistent with that used by Terzaghi (1943). In contrast to Terzaghi;s solution however, the base angle is assumed to be equal to $\pi/4 + \phi/2$, value same as that assumed by Meyerhof, (1957). As such, the proposed method does not involve any novel approaches to solving the problem, or any attempt to provide a more soundly based analysis The assumed failure mechanism is shown on Figure 2.19.

For a general soil, that is, one possessing both cohesion and friction, revised bearing capacity factors N'_c and N'_q were determined by comparing the geometries of the case under consideration with that of a footing on level ground.

For example, N'_c is given by

$$N'_c = N_c \frac{L_1}{L_o}$$

L_o is the length of the surface 'cbde' in Figure 2.20 and L_1 is the length of the surface 'cbde' in Figure 2.19.

Similarly, N'_q is given by

$$N'_q = N_q \frac{A_1}{A_o} \quad \text{where } A_o \text{ and } A_1$$

are the shaded areas in Figure 2.20 and 2.19 respectively.

Bowles states that the bearing capacity factor $N\gamma$ requires no modification for slope effects because it depends on the wedge 'cba' (Figure 2.19). It assumes therefore that the shape of the wedge is also not modified by slope effects. In contrast, the analysis considered later in this thesis is based on the hypothesis that the shape of the elastic wedge is fundamentally influenced by the effect of the slope.

When the area A_1 is greater than A_o, Bowles (1977) proposed that N'_q be taken as being equal to N_q. This is based on the understanding that the bearing capacity of a footing influenced by a slope will be less than that of footing on level ground.

In order to compare Bowles (1977) bearing capacity factors with Meyerhof (1957) values, Lee (1978) combined the former bearing capacity factors as follows:-

$$N_{\gamma q} = N_\gamma + \frac{2D}{B} N'_q \, d_q$$

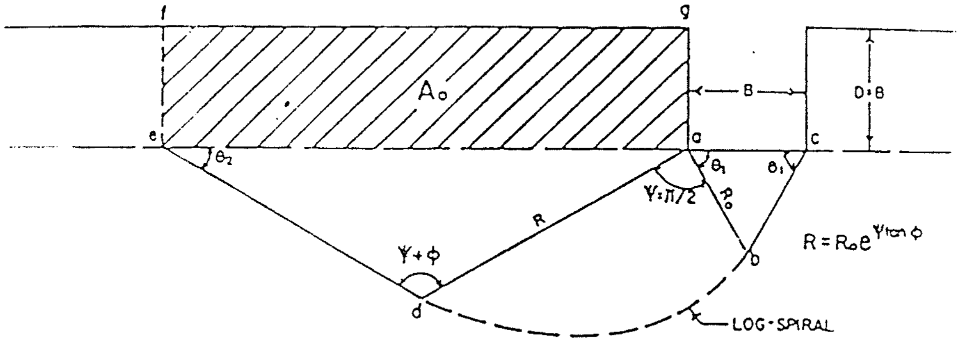

LEGEND

ϕ = INTERNAL FRICTION ANGLE

Θ_1 = $45° + \phi/2$

θ_2 = $45° - \phi/2$

FIGURE 2.20: FOOTING ON HORIZONTAL GROUND

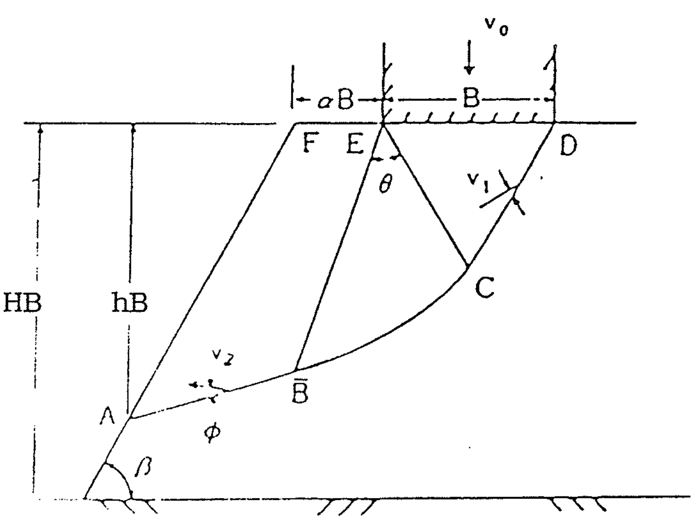

FIGURE 2.21: FAILURE MECHANISM FOR FOOTING ON A SLOPE
(after Kusakabe et al 1981)

Lee (1978 and 1981) calculated the $N_{\gamma q}$ values based on Bowles's method for $\phi = 35°$ and $\phi = 40°$ and a slope with a gradient of 1 vertical to 2 horizontal for footings located at distances up to 5B for the crest of the slope, and depths up to 3B deep.

2.10 Kusakabe et al (1981)

The method employed by these authors to determine the bearing capacity of a footing on a slope is a limit analysis technique using the upper bound theorem. The solution considers the failure mechanism shown on Figure 2.21. It consists of a triangular region immediately beneath the footing which is an active wedge, and a rupture line which consists of a logarithmic spiral and a straight line exiting at the toe of the slope.

The authors state only that a straight line connects with the logarithmic spiral smoothly and passes through the inclined surface of the slope. No further details of the failure mechanism are presented. From the geometry of the problem, and the upper bound theorem a relationship is derived for bearing capacity by equating the rate of internal energy dissipation to the rate of external work.

The authors present a number of charts giving bearing capacity for various combinations of the problem variables, namely the slope angle, the footing distance from the edge of the slope, the slope height (as a multiple of the foundation width), the strength parameters c, and ϕ of the soil. The authors have not considered the particular case of cohesionless soil which is addressed in this thesis. However, their results are quite comprehensive and therefore potentially of practical significance.

The general features of the analysis is similar to that used by Chen (1975). That is, a failure mechanism is assumed, and the rate of internal energy dissipation is equated to the external work done for the assumed mechanism. The resulting equation yields a relationship for $N\gamma$ which is function of ϕ , the apex angle of the radial transition zone BEC (Figure 2.21) and the area of quadrilateral ABEF. The angle ϕ is defined for a given problem. The angle BEC and the area of the quadrilateral ABEF are determined from the geometry of the assumed failure mechanism. The accuracy of the solution is therefore dependent upon how well the assumed failure surface models the actual soil behaviour.

2.11 Summary

In Sections 2.2 to 2.10 nine methods which are presently available for determination of the bearing capacity of a footing on a slope have been outlined. The methods employed in developing the theories are limit equilibrium and limit analysis methods. Comparison of the results of the theories is presented in Chapter 7. However, it is evident from the foregoing discussion that despite the relatively large number of theories which have been advanced over the last three decades, there is as yet no theory which analyses all the special features of the problem in an attempt to provide a realistic estimate of the ultimate bearing capacity.

In contrast to the solution developed in this thesis, all of the existing theories require assumptions to be made with respect to the shape of the failure surface. Additionally, it is not clear whether the downslope failure surface direction is carefully treated in some of the solutions (e.g. Kusakabe, 1981).

At least three of the theories, (Giroud, Chen and Mizuno et al) consider only the case of a footing located at the crest of an embankment which slopes equally on either side. The limited practical application of this solution is immediately obvious. Another method (Kovalev) considers the bearing capacity problem to be identical to a slope stability problem, and hence does not include the important effect of soil-footing interaction. The basis for the failure mechanisms proposed by Bowles is not clear. Additionally, none of the methods consider how the soil on the upslope side of the footing influence the ultimate bearing capacity. These aspects are considered in this study in order to develop a soundly based analysis for the problem.

CHAPTER 3

THE STRESS CHARACTERISTIC METHOD

3.1 INTRODUCTION

The stress characteristic method involves the integration by a numerical procedure of known boundary conditions to unknown boundary stresses in a field or domain in which the strength properties are defined everywhere. At failure, the soil beneath a footing is stressed to its limiting or yield condition. The Coulomb-Mohr yield criterion is assumed to apply in the failing region.

Sokolovskii (1965) developed the stress characteristic method to compute the stresses beneath the footing at failure. The numerical accuracy of the basic method was improved by Graham (1968). For convenience, the development of the numerical procedure is briefly outlined here, following the approach given by Graham. The computer program is based on the work of Hovan (1985) but has involved a significant amount of reprogramming for the particular question being examined.

3.2 THEORY

Points in a two dimensional plastic field are defined in terms of physical plane co-ordinates x and z where the positive z axis is oriented vertically downwards (in the direction of gravity) to simplify the resulting differential equations (Figure 3.1).

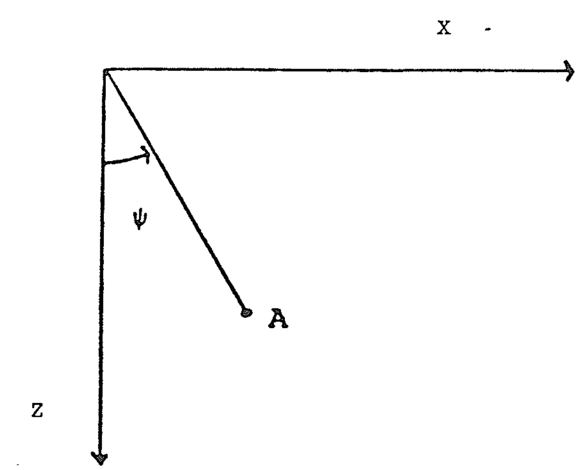

FIGURE 3.1: GENERAL SYSTEM OF COORDINATES

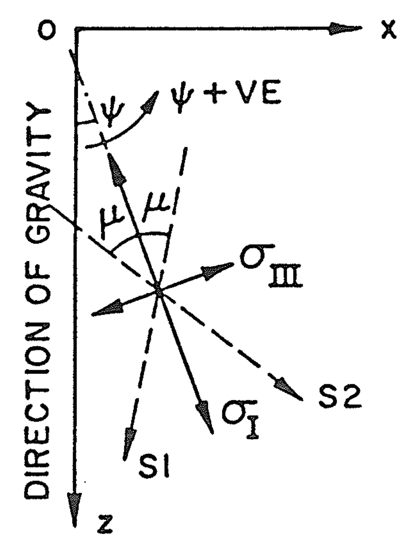

FIGURE 3.2 SIGN CONVENTION

A soil element in this two dimensional field which is about to fail, must also be in a state of plastic equilibrium. The stresses in a soil element in a state of plastic or limiting equilibrium are considered to be controlled by the Coulomb-Mohr failure criterion.

The criterion is stated as follows:

$$\tau_f = c + \sigma_n \tan \phi \quad \ldots\ldots\ldots\ 3.1$$

For cohesionless soil, c = o so the equation can be written as

$$\tau_f = \sigma_n \tan \phi \quad \ldots\ldots\ldots\ldots\ 3.2$$

Effective stresses have not been indicated by the normal ' superscript but are assumed throughout.

Figure 3.2 shows the direction of the major principal stress, σ_1 in a typical soil element, inclined as an angle ψ to the z - axis. The slip lines S_1 and S_2 along which failure will occur are inclined at an angle $\mu = (\pi/4 - \phi/2)$ to the direction of σ_1. The Mohr's circle representation of this state of stress is shown in Figure 3.3. From the Mohr circle,

$$\left.\begin{matrix}\sigma_z \\ \sigma_x\end{matrix}\right\} = \sigma (1 \pm \sin \phi \cos 2\psi)$$

and,

$$\tau_{xz} = \sigma \sin \phi \sin 2\psi \quad \ldots\ldots\ldots\ldots 3.3.$$

A two dimensional soil element which is just about to fail, must

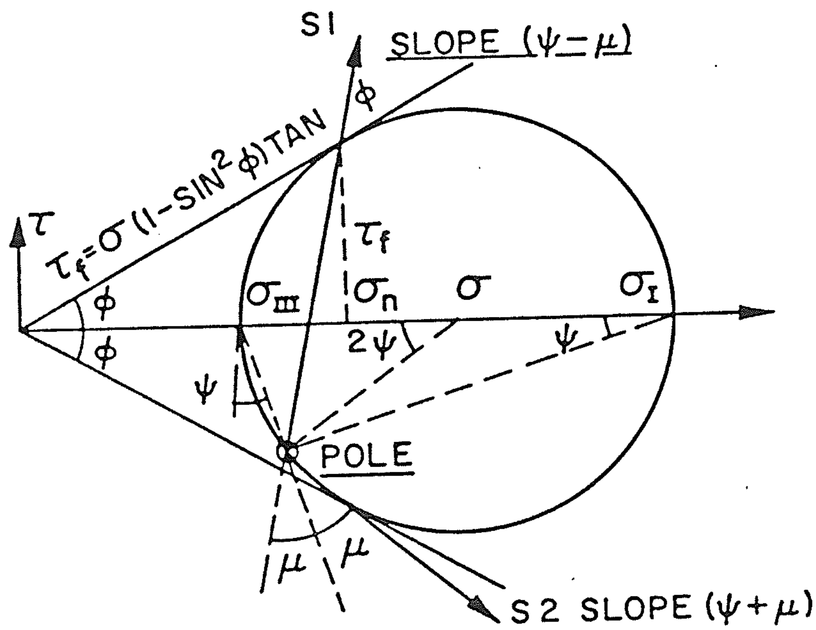

FIGURE 3.3. MOHR CIRCLE FOR FAILURE CONDITION

satisfy the equations of static equilibrium.

$$\frac{\partial \sigma_x}{\partial x} + \frac{\partial \tau_{xz}}{\partial z} = 0$$

$$\frac{\partial \sigma_z}{\partial z} + \frac{\partial \tau_{xz}}{\partial x} = \gamma \qquad \ldots\ldots\ldots\ldots\ 3.4$$

The unit weight of the soil is considered to be the only body force.

It is convenient to express these equations in dimensionless terms by substituting $x = x_r/\ell$, $z = z_r/\ell$, $\sigma = \sigma_r/\gamma\ell$ and $\tau = \tau_r/\gamma\ell$. The parameter ℓ is called the scale parameter or characteristic length. γ is the unit weight of the soils and x_r, z_r, σ_r, and τ_r are dimensional real parameters. Dimensionless parameters have been used throughout the rest of the analysis. Euqations 3.3 and 3.4 may be rewritten in dimensionless form as

$$\left.\begin{matrix}\sigma_x\\ \sigma_z\end{matrix}\right\} = \sigma\,(1 \mp \sin\phi \cos 2\psi)$$

$$\tau_{xz} = \sigma \sin\phi \sin 2\psi \qquad \ldots\ldots\ldots\ldots 3.3a$$

and

$$\frac{\partial \sigma_z}{\partial z} + \frac{\partial \tau_{xz}}{\partial x} = 1$$

$$\frac{\partial \sigma_x}{\partial x} + \frac{\partial \tau_{xz}}{\partial z} = 0 \qquad \ldots\ldots\ldots\ldots 3.4a$$

Substitution of Equations 3.4a into 3.3a gives

$$\frac{\partial \sigma}{\partial z} (1 + \cos 2\psi \sin \phi) + \frac{\partial \sigma}{\partial x} (\sin 2\psi \sin \phi)$$

$$- 2 \sigma \sin \phi (\sin 2\psi \frac{\partial \psi}{\partial z} - \cos 2\psi \frac{\partial \psi}{\partial x}) = 1$$

and,

$$\frac{\partial \sigma}{\partial x} (1 - \cos 2\psi \sin \phi) + \frac{\partial \sigma}{\partial z} (\sin 2\psi \sin \phi)$$

$$- 2 \sigma \sin \phi (\sin 2\psi \frac{\partial \psi}{\partial x} + \cos 2\psi \frac{\partial \psi}{\partial x}) = o \qquad \ldots\ldots\ldots\ldots 3.5$$

Equations 3.5 are statically determinate but cannot in general be integrated in closed form because they are non-linear. Closed form solutions can be obtained for special cases with the simplifying assumption for example $\phi = 0$, or $\gamma = 0$ (Wu, 1966; Graham 1968).

Sokolovskii suggested using the following logarithmic transformations to simplify the equation

$$\chi = \frac{\ell n \sigma}{2 \tan \phi}$$

$$\xi = \chi + \psi$$

$$\eta = \chi - \psi$$

Substitution of these new variables into Equations 3.5 gives after mathematical manipulation the following equations

$$\frac{d\eta}{dz} = a - \tan(\psi - \mu) \frac{\partial \eta}{\partial x} + \frac{\partial \eta}{\partial x} \cdot \frac{dx}{dz}$$

$$\frac{d\xi}{dz} = b - \tan(\psi + \mu) \frac{\partial \xi}{\partial x} + \frac{\partial \xi}{\partial x} \cdot \frac{dx}{dz} \qquad \text{............3.6}$$

where,

$$a = \frac{\sin(\psi + \mu)}{2\sigma \sin \phi \cos(\psi - \mu)}$$

and,

$$b = \frac{-\sin(\psi - \mu)}{2\sigma \sin \phi \cos(\psi + \mu)}$$

For any line in the physcial plane with slope $\frac{dx}{dz} = \tan(\psi \mp \mu)$, the last two terms of Equations 3.6 are equal and opposite, and therefore cancel. The stress field can now be described by two families of slip lines

$$\frac{d\eta}{dz} = a \text{ for slip lines } S_1 \text{ with slope } \frac{dx}{dz} = \tan(\psi - \mu)$$

and,

$$\frac{d\xi}{dz} = b \text{ for slip lines } S_2 \text{ with slope } \frac{dx}{dz} = \tan(\psi + \mu) \qquad \text{......3.7}$$

From the Mohr circle (Figure 3.3) it can be seen that the two lines through the pole having inclinations of $(\psi \mp \mu)$ are in the directions of the slip lines S_1 and S_2 in the physical field. That is, the solved system in logarithmic stress space provides a set of slip lines or a slip line field whose positions are known in the physical (x, z) plane.

The values of the four parameters x, z, σ, ψ, describing a point P in a plastic field are found by solving Equations 3.7 along each of the characteristics through the point. To provide a definite integral, two previously known points, one lying on each of the characteristics must be available. In Figure 3.4 the new point C lies on the intersection of the S_1 line from point B $(x, z, \sigma, \psi,)_B$ with the S_2 line from point A $(x, z, \sigma, \psi)_A$.

Rewriting Equations 3.7 in finite differences form yields

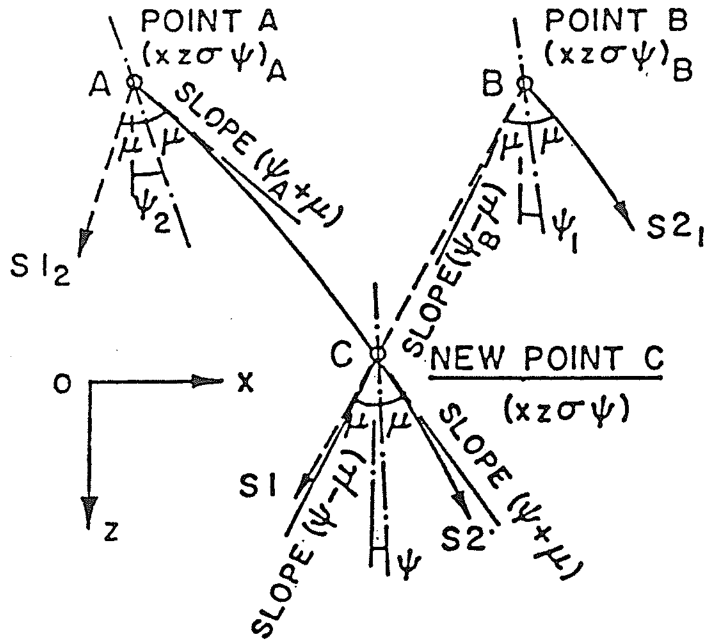

FIGURE 3.4: COMPUTATION OF A NEW POINT C FROM KNOWN POINTS A AND B.

$$\frac{\Delta \xi}{\Delta z} = b = - \frac{\sin (\psi - \mu)}{2 \sigma \sin \phi \cos (\psi + \mu)}$$

$$\frac{\Delta \eta}{\Delta z} = a = \frac{\sin (\psi + \mu)}{2 \sigma \sin \phi \cos (\psi - \mu)} \qquad \ldots\ldots\ldots\ldots\ldots\ 3.8$$

As a first approximation, the assumptions are made that the slip line AC and BC in Figure 3.4 are straight, and that they have directions of $(\psi_A + \mu)$ and $(\psi_B - \mu)$ at C respectively.

The slip line through A has the gradient

$$\frac{dx}{dz} = \tan (\psi_A + \mu)$$

therefore,

$$x_C - x_A = (z_C - z_A) \tan (\psi_A + \mu)$$

Similarly, for the slip line through B, we have

$$x_C - x_B = (z_C - z_B) \tan (\psi_B - \mu)$$

Solving for x_C and z_C gives

$$x_C = x_B + (z_C - z_B) \tan (\psi_B - \mu)$$

$$z_C = \frac{z_B \tan (\psi_B - \mu) - x_B - z_A \tan (\psi_A + \mu) + x_A}{\tan (\psi_B - \mu) - \tan (\psi_A + \mu)}$$

From Equations 3.8

$$\xi_C = \xi_A - \frac{(z_C - z_A)\sin(\psi - \mu)}{2\sigma_A \sin\phi \cos(\psi + \mu)}$$

$$\eta_C = \eta_B + \frac{(z_C - z_B)\sin(\psi + \mu)}{2\sigma_B \sin\phi \cos(\psi - \mu)} \qquad \ldots\ldots\ldots\ldots\ldots\ldots 3.9$$

From ξ_C and η_C, the values of σ_C and ψ_C can be computed from the following expressions by reversing the log-transform.

$$\sigma_C = \exp\ \{\tan\phi\ (\ \xi + \eta\ )\ \}$$

and,

$$\psi_C = 1/2\ (\ \xi - \eta\ )$$

The simple form of the finite difference relations given is very approximate since no account is taken of the curvature of the slip lines between the known point A and B, and the new point C. The accuracy of the solution was improved by Sokolvskii (1960) by substituting $1/2\ (\psi_A + \psi_C)$ and $1/2\ (\psi_B + \psi_C)$ for ψ_A and ψ_C respectively once the initial value of ψ_C has been determined. This process is continued until the value of ψ_C from two successive iterations converge to an acceptable tolerance. This is the so-called " ψ iteration" method (Graham, 1968). The solution is much improved by the additional substitution $\sigma_{A,B} = 1/2\ (\sigma_C + \sigma_{A,B})$ for σ_A and σ_B and carrying out the iterative process until the σ values converge to a specified tolerance. This method is the so-called " σ, ψ iteration" method, which was proposed by Graham (1968).

3.3 DETERMINATIONS OF THE SLIP LINE FIELD

The computation begins at a boundary where the parameters x, z, σ and ψ are known.

In this work, the known boundary is the edge of the passive zone beneath the sloping surface (Figure 3.5) which Graham (1966) has shown to have straight slip lines when the magnitude of the surface loading is zero (Figure 3.5).

If point O (Figure 3.6) is taken as the origin of the adopted system of physical co-ordinates the slip line field in the transition zone consists of two families of characteristics.

1. a set of curved radial lines originating from point O.
2. a set of spiral lines intersecting the radial lines in turn at an angle of $2\mu = \pi/2 - \phi$

Point O is a unique point in the field, at which there is a sudden jump in the values of σ and ψ when moving from right to left say, through

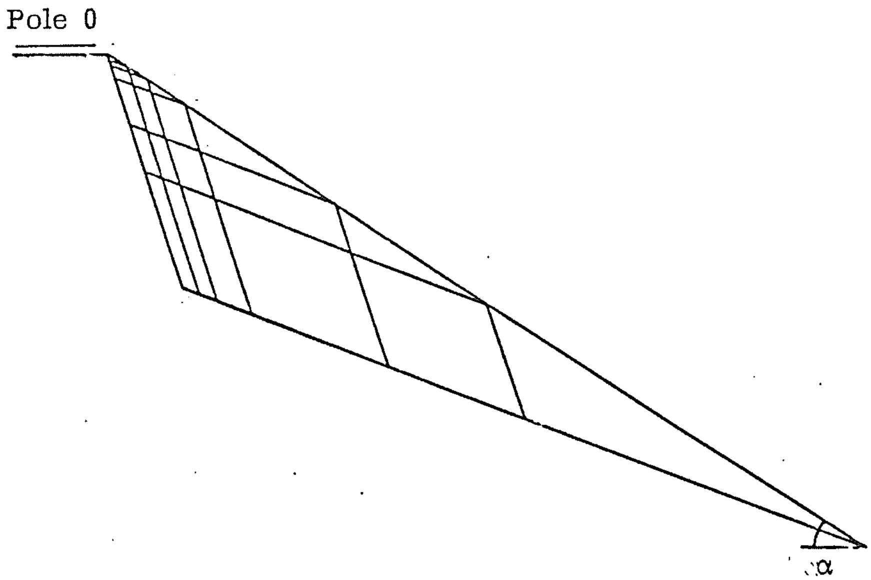

FIGURE 3.5: TYPICAL SLIP LINE FIELD IN THE PASSIVE ZONE BENEATH A STRESS FREE SLOPE.

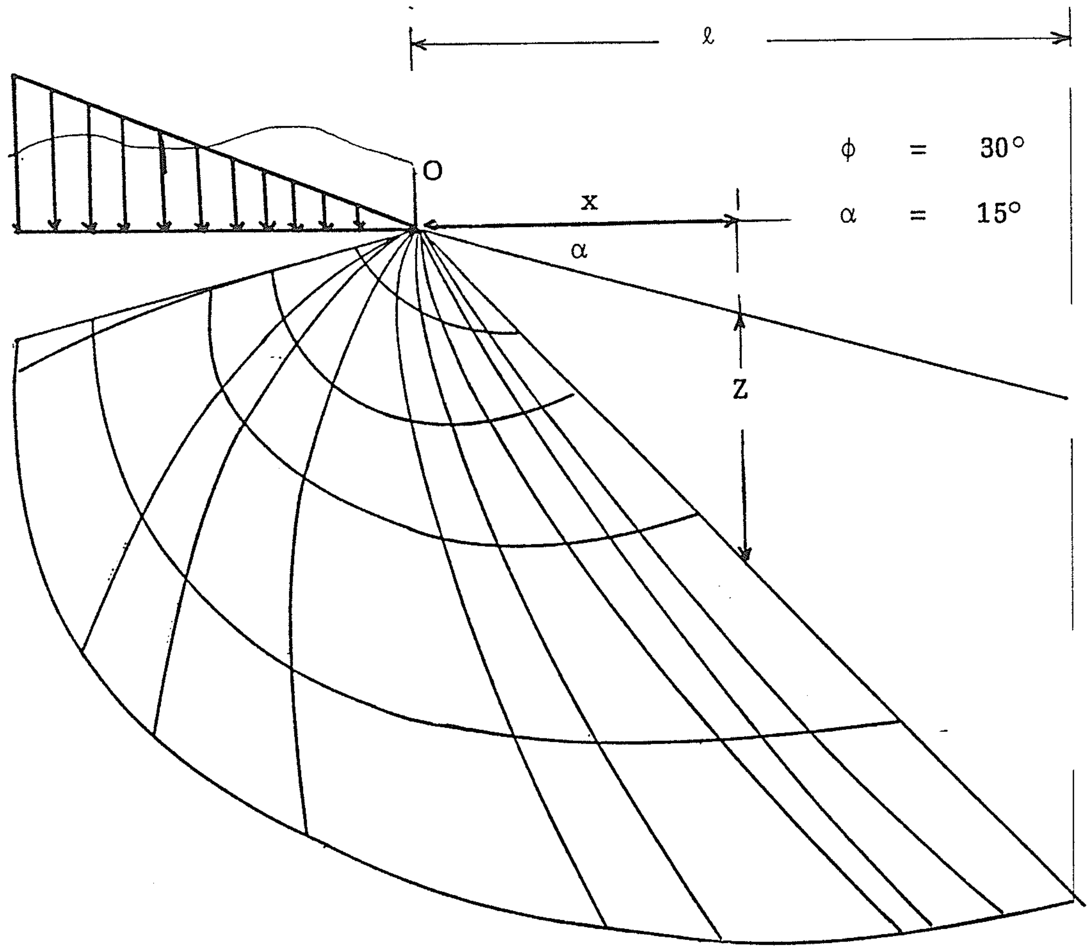

FIGURE 3.6: TYPICAL SLIP LINE FIELD IN TRANSITION ZONE

O. The value of ψ describing the direction of the major principal stress is fixed at the beginning and end of the transition zone by the physical formulation of the problems as outlined in Sections 3.4 and 3.5. This means that ψ undergoes a total change of say $\Delta\psi$ at O. The slip lines themselves have no physical reality, but only describe the directions of slipping at any point in the field. The radial lines can therefore be specified in number by dividing $\Delta\psi$ into a suitable number of intervals, each corresponding to a separate member of the radial family. The parameters X and Z are constant and fixed at O by the formulation of the problem, and each radial line has a different, arbitrarily selected value of ψ and hence σ along the inner limiting member of the spiral family, surrounding O at an infinitesimally small distance. The assumption is made that close to O, self weight forces do not affect the stress distribution. Hence, the values of σ predicted for a weightless material are considered to be applicable around the inner limiting spiral curve (Graham 1966). Thus, if the boundary of the uniquely defined zone forming the initial radial line has values of σ_i and ψ_i at O, the value of σ_j on the j.th radial line having $\psi = \psi_j$ at O, will be given by

$$\sigma_j = \sigma_i \,.\, \exp \{ 2 \tan \phi \, (\psi_j - \psi_i) \}$$

Points determined in this way provide the second set of known boundary conditions required to begin the computation. The computation of the entire field is then routine using the numerical procedure outlined in Section 3.2 above. The computation of the slip line field is carried out until the end boundary where the failure stresses are to be evaluated is reached.

Since point O (Figures 3.5 and 3.6) is a singular point of the slip-line field, it represents a point of discontinuity in the mathematical solution of the basic equations. At stress levels equal to zero, the logarithmic transformations that are involved in the solution tend to infinity. In order to handle this problem, Graham (1968) introduced a surcharge term, in the computation of the slip line field, that allows the logarithmic stress range to remain finite. The effect of the surcharge term is then reduced by 'shrinking' the field by a factor of 10 n, where n is the number of scale reductions necessary to eliminate the effect of the surcharge to an acceptable tolerance. It is important to note that this scale reduction process does not itself introduce any scale effects since all computations are carried out in dimensionless terms. The present study has retained this procedure for handling the singularity at point O.

3.4 THE INITIAL BOUNDARY CONDITION

It is necessary to determine values of the parameters x, z, σ and ψ on the starting boundary, that is the edge of the rectilinear passive zone in order to begin computation of the stress characteristic field.

The parameter x is the horizontal distance from the point O (Figure 3.6).

The coordinate z is the depth of soil from the sloping ground surface to the boundary of the passive zone (Figure 3.6). The inclination of the passive zone boundary is a function of the angle ψ_i, the value of ψ in the passive zone.

z is also a function of ψ_i and is given by

$$z = x \cdot \left\{ \frac{1}{\tan(\psi_i - \mu)} - \tan\alpha \right\}$$

The value of ψ_i is determined from the Mohr circle of Figure 3.7, and is given by

$$2\psi_i = \pi - \alpha - \sin^{-1}(\sin\alpha / \sin\phi)$$

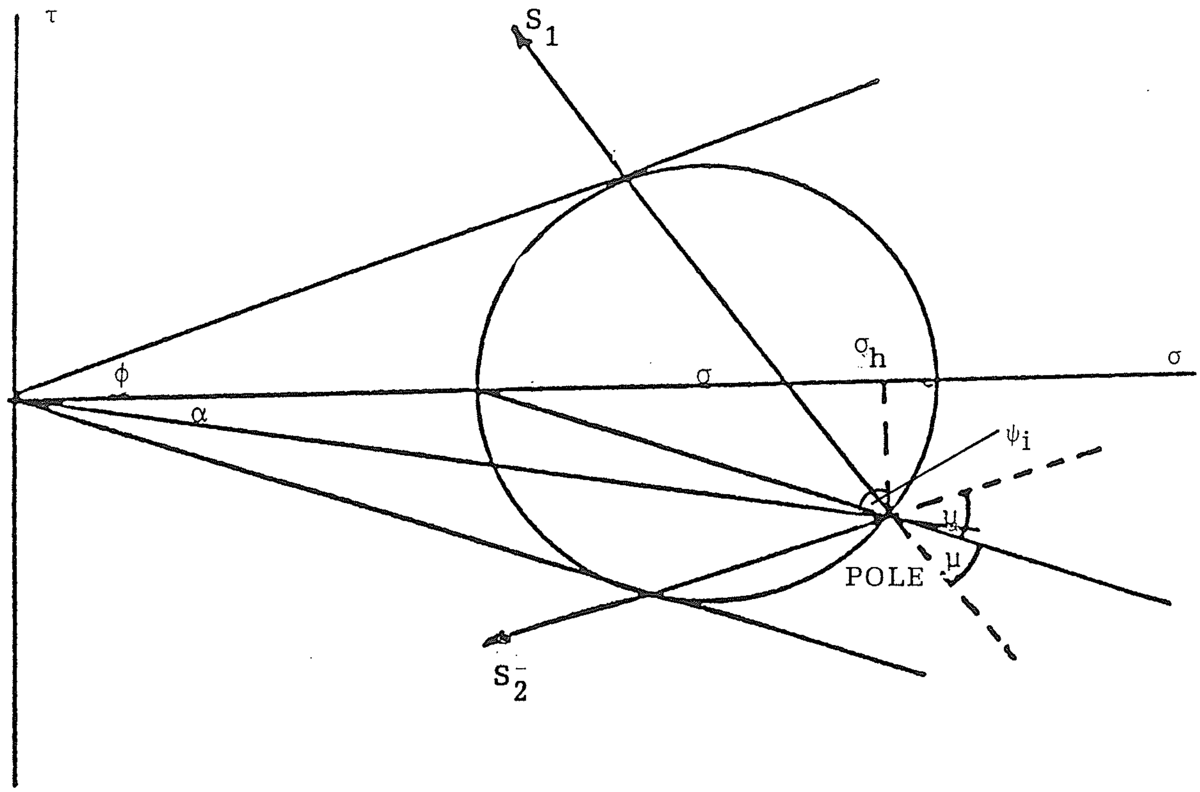

FIGURE 3.7: MOHR CIRCLE SHOWING STRESS CONDITION IN THE UNIQUELY DEFINED ZONE AT THE SURFACE OF THE SLOPE.

The value of σ is also determined from the Mohr's circle as,

$$\sigma = \frac{1.0 + Z}{1 + \sin\phi \cos 2\psi_i}$$

where 1.0 is a surcharge term assumed for the present to be constant along the free surface of the slope.

3.5 THE END BOUNDARY CONDITION

For a footing on level ground, it is generally assumed that an elastic wedge of soil is trapped beneath the footing and that failure consists of two symmetrical zones flowing outwards from the centre line.

The end boundary in the stress field computation is normally taken as the lower edge of the elastic wedge for example by Graham and Stuart (1971), Suppiah (1981) and Hovan (1985). This boundary is also a slip line and is inclined at an angle of ϕ with the footing base.

For the case of a footing on sloping ground the elastic wedge is not symmetrical about the centre line of the base of the footing. The analytical solution to its precise geometry however has never been addressed nor defined in any of the existing theories. This thesis addresses that problem. A study of the shape of the elastic wedge and the determination of a likely shape for use in the computations is presented in Chapter 4. It is important to note that the inclination and conditions along this boundary have significant effect on the computed bearing capacity.

Vertical stresses on the two lower boundaries of the wedge are calculated from the stress characteristic solution, and then expressed as the dimensionless parameter $N_{\gamma q}$.

3.6 OTHER INPUT PARAMETERS

In order to facilitate the computations, other parameters must be carefully chosen. These are discussed below.

3.6.1 Scale Parameter ℓ

All the variables throughout the computation of the stress characteristics were expressed in dimensionless terms, that is they were written $\sigma = \sigma_r / \gamma\ell$, $x = x_r/\ell$, $z = z_r/\ell$, where ℓ is a scale parameter used to convert the real physical plane dimensional parameters σ, x, z, into dimensionless ones for computational purposes, and vice-versa. The scale parameter ℓ was chosen as the horizontal component of the edge of the passive zone (Figure 3.6).

3.6.2 Number of Spiral and Radial Lines

It has become also customary in stress characteristic solutions to use ten spiral and twenty radial lines (e.g. Graham 1968 and Hovan 1985). As noted by Hovan (1985), a higher number of spiral and radial lines would improve the accuracy only slightly. It would also lengthen the computation time. This thesis uses ten spiral and twenty radial lines for all the computations.

3.7 VALIDITY OF THE COMPUTER PROGRAM

The numerical accuracy of the results produced by the basic computer program was established by computing N_γ for a footing on level ground for a series of ϕ values from 30 to 42 degrees.

The computation values were compared with the results obtained previously by Graham and Stuart (1971), and Hovan (1985). These results are summarized in Table 3.1.

The computed N_γ values agree very closely with those of Graham and Stuart, and compare within -1.9% and + 0.2%. These differences in N_γ may arise from slightly different procedures for integrating the pressure distributions for determining the failures loads. Graham used essentially semi-graphical procedures, whereas more recent approaches by Suppiah (1984), Hovan (1985) and the author use numerical procedures. The results also compare reasonably well with those obtained by Hovan (1985) except at high ϕ values where the N_γ values differ by about 11%. The reason for this discrepancy is not known. It should be noted that this favourable comparison with N_γ values for surface footings on horizontal grounds does not however confirm the validity of the new EDGPA subroutines written by the Author.

ϕ angle	N_γ Graham & Stuart	N_γ Hovan	N_γ Author
30	22.4	23.17	21.97
32	31.4	31.25	31.29
34	45.0	45.60	44.93
35	54.5	-	54.03
36	65.0	69.20	65.14
38	96.0	98.90	95.14
40	143.0	147.90	142.09
42	216.0	242.97	214.65

TABLE 3.1 CHECK ON NUMERICAL ACCURACY OF THE COMPUTER PROGRAM - COMPARISON OF N_γ VALUES FOR A FOOTING ON LEVEL GROUND.

CHAPTER 4

THE SHAPE OF THE TRAPPED ELASTIC WEDGE

4.1 INTRODUCTION

Vesic (1973) in his extensive review of the ultimate bearing capacity of shallow foundations on level ground concluded that the stress and deformation pattern under compressed areas is such that it always leads to the formation of single wedges immediately beneath the footing. The roughness of the footing base was deduced to have little effect on the bearing capacity as long as the applied external loads remained vertical. In their recent paper on model tests of bearing capacity problems in a centrifuge, Kimura et al (1985) state that their current experimental observations concur with the analytical theories suggesting a single wedge failure mechanism regardless of the roughness of the failure footing base. This means that the "Prandtl type" failure mechanism and not the "Hill type" mechanism is the likely failure type (Figures 2.15 and 2.16).

For footings on level ground this wedge of soil is commonly assumed to be symmetrical about the centre line of the footing and have a base angle of ϕ to $45 + \phi/2$ degrees. Graham and Stuart (1971) and Hovan (1985) used a base angle of ϕ degrees in their "ϕ - wedge" analyses.

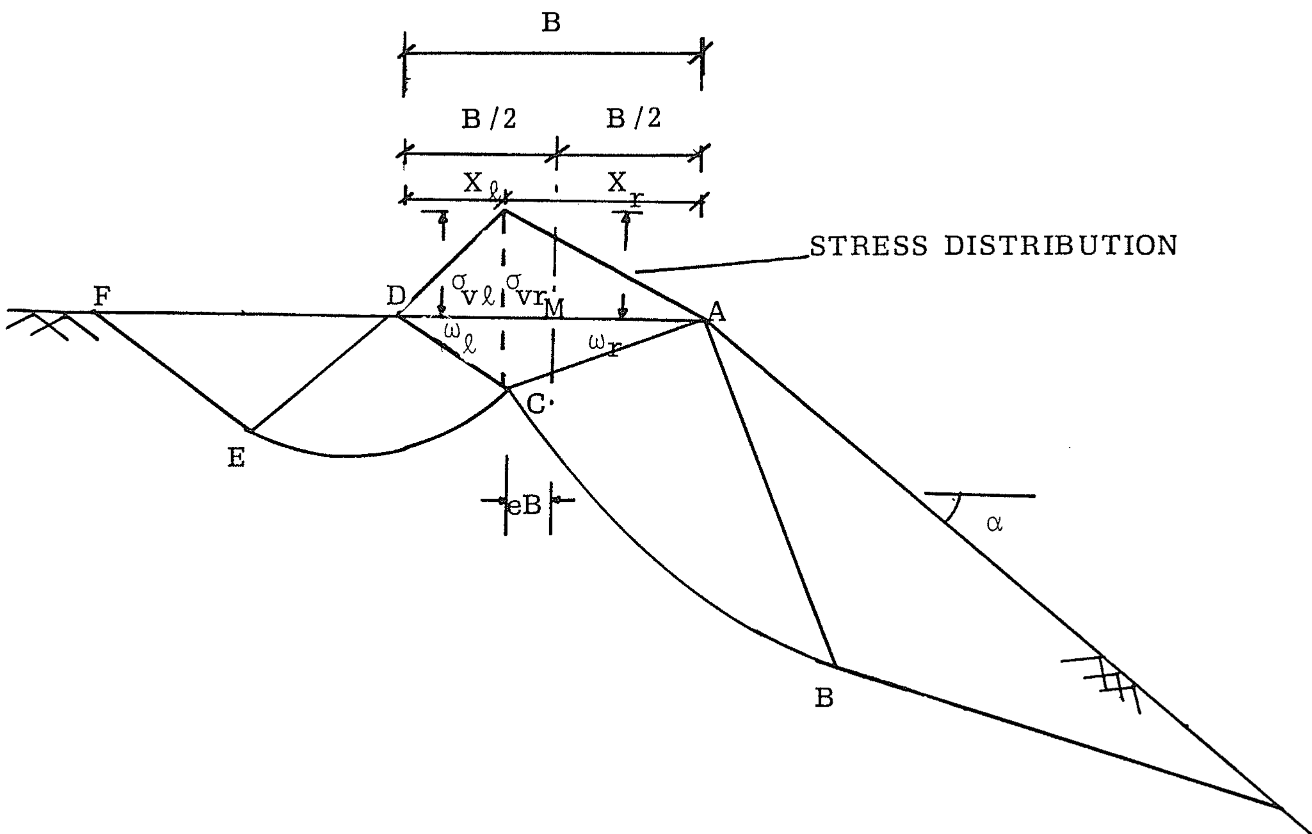

FIGURE 4.1: STRESS DISTRIBUTION AND TRAPPED WEDGE FOR A FOOTING CLOSE TO A SLOPE

The case of a footing close to the crest of a slope with one side (A) adjacent to level ground (Figure 4.1) is however more complex. Because of its physical geometry, the problem is clearly asymmetrical. The stability of such a footing will be influenced by the reduced support available on the side with the slope. It can be expected that the ultimate bearing capacity will be reduced from the level-ground case. Failure will commence in the weakest region of the foundation soil, that is, in soil adjacent to the slope, and will propagate inwards towards the footing. The overall behaviour of the soil in the failing domain to either side of the centre line of the footing is not yet fully understood. However, it can be reasonably expected that if the foundation is constrained to move downwards vertically, then displacement of the soil mass will occur on both sides of the footing.

The earliest known experimental investigation of the behaviour of footings on slopes was reported by Peynircioglu (1948). This work indicated among other things that the trapped elastic wedge beneath the footing is probably not symmetrical about the centre line of the footing base. As mentioned in Section 3.5, the lower edges of this wedge form the end boundary for the stress characteristic solution. It is therefore necessary that their location should be carefully modelled if the stresses acting on them are to be determined accurately. Various analytical models for determining the shape of the wedge are studied in this Chapter.

4.2 Photographic Evidence For the Shape of the Wedge

Experiments that indicate the shape of the trapped wedge for footings located close to slopes have been reported by Peynircioglu (1948), Mizuno et al. (1960), and Giroud and Tran-Vo-Nhiem (1971). The recently reported work of Kimura et al. (1985) based on model tests in a centrifuge also provides limited information on the shape of the slip lines at failure.

Peynircioglu carried out small scale tests on two types of sand in a glass box with dimensions 55 x 33 x 26 cm. The physical properties of the sands are summarized on Figure 4.2. The movement of the sand particles during the loading process was recorded by means of time exposure photography. Although the friction between the sand and the sides of the glass box obscures the development of the failure zone, some important conclusions can be drawn from the observations, these are as follows:-

(1) It is very clear that the trapped wedge beneath the footing is asymmetrical, and that the base angle ω_r on the side nearest the slope is less than $\pi/4 + \phi/2$.

SOIL PROPERTY	S_1	S_2
Specific Gravity	2.613	2.591
Unit Weight in the loosest state	1.405 t/m^3	1.385 t/m^3
Unit Weight in the densest state	1.584 t/m^3	1.610 t/m^3
Porosity in the loosest state	46.2%	46.5%
Porosity in the densest state	39.3%	37.9%
Angle of internal friction	38°	36°

FIGURE 4.2 PROPERTIES OF THE SANDS USED BY PEYNIRCIOGLU (1948)

(2) The greater the slope inclination, the greater is the asymmetry of the wedge.

A summary of the relevant results of this work is shown in Table 4.1, which also shows a summary of the experimental works of Giroud (1971) and Kimura (1985) and comparisons of these results with the models developed later in this Chapter.

Mizuno (1960) studied the problem with the aid of small, two-dimensional model where the soil is represented by small cylindrical bamboo sticks, 5 mm in diameter. They reported good agreement between the observed slip lines and a failure zone calculated by assuming a symmetrical soil wedge with a base angle of $\pi/4 + \phi/2$. This is in direct contradiction to the observations by Pernircioglu (1948) described previously. The reasons for this apparent discrepancy are not known.

Giroud and Tran-Vo-Nhiem (1971) carried out their experiments with a two dimensional model similar to that used by Mizuno et al (1960) but used duralumin rods to represent the soil medium. The soil movement and failure mechanism were observed by means of both a camera attached to the moving footing and by a fixed camera. The results clearly indicate than an asymmetrical wedge is formed beneath the footing and that this asymmetry increases with the inclination of the slope. The base angle of the wedge immediately adjacent to the slope ω_r (Fig. 4.1) is observed to be less than $\pi/4 + \phi/2$. The results in general agree with those of Peynircioglu (1948) and the pertinent details are summarized on Table 4.9.

AUTHOR	α degrees	ϕ degrees	ω_ℓ					ω_r					x_ℓ/x_r				
			OBS (4)	M1	M2	M3	M4	OBS (4)	M1	M2	M3	M4	OBS (4)	M1	M2	M3	M4
Peynircioglu 1948	6.8	36	34.1	36.0	36.0	36.0	36.0	26.0	(3)	(3)	(3)	(3)	0.72	(3)	(3)	(3)	(3)
	12.9	38	43.8	38.0	38.0	38.0	38.0	32.0	31.0	23.7	26.8	23.2	0.65	0.77	0.61	0.70	0.51
	17.7	36	39.5	36.0	36.0	36.0	36.0	25.0	23.5	17.0	20.5	15.5	0.54	0.61	0.43	0.56	0.36
Giroud et al 1971	15	26	35.0	26.0	26.0	26.0	26.0	27.0	22.7	15.5	19.0	-	0.63	0.70	0.53	0.64	0.44
Kimura et al 1985	30	49	65	49.0	49.0	49.0	49.0	70	(3)	(3)	(3)	(3)	>1.0	0.26	0.17	0.22	0.13

NOTES:

(1) The deductions from the photographs and sketches are not considered to be very accurate.

(2) Observed values by the Author were determined on the basis of visual interpretation. No further efforts were made to improve the comparisons between the theory and the observed values.

(3) The analyses were carried out for $10 < \alpha < 45$. For smaller values of α, $x_\ell/x_r = 1.0$ (approx.). and $\omega_\ell = \omega_r$ (approx.)

(4) These values are based on observations.

(5) M1 refers to Model 1, M2 refers to Model 2, etc.

TABLE 4.1 COMPARISON OF MODELS 1 to 4 WITH AVAILABLE PHOTOGRAPHIC EVIDENCE

4.3 Analytical Study Of The Shape Of The Trapped Elastic Wedge

4.3.1 Introduction

In this section four different models for the shape of the wedge are developed and analysed. For a footing with its edge at the crest of the slope, the geometry of the wedge is a function of the slope angle α, and the angle of internal friction ϕ of the soil. The variables which define the shape of the wedge are the x_ℓ / x_r ratio, ω_ℓ and ω_r (Figure 4.1). These variables are mutually dependent and can be expected to vary with the basic parameters α and ϕ. The models which are developed all start from the premise that the left base angle of the trapped wedge is equal to ϕ (Figure 4.3). That is, when failure occurs it will do so simultaneously to both sides of the footing, with failure zones of different sizes extending to both the slope surface on the right in Fig. 4.3 and to the horizontal ground surface on the left. As mentioned previously in Section 4.1 the base angle of the trapped wedge is normally taken as being equal to ϕ in the stress characteristic solution for footings on level ground. The development of the models is now described in turn.

4.3.2 Development of Model 1

The stress on the boundary AB (Figure 4.3) of the rectilinear passive zone adjacent to the slope is determinate (Graham 1968). Its value

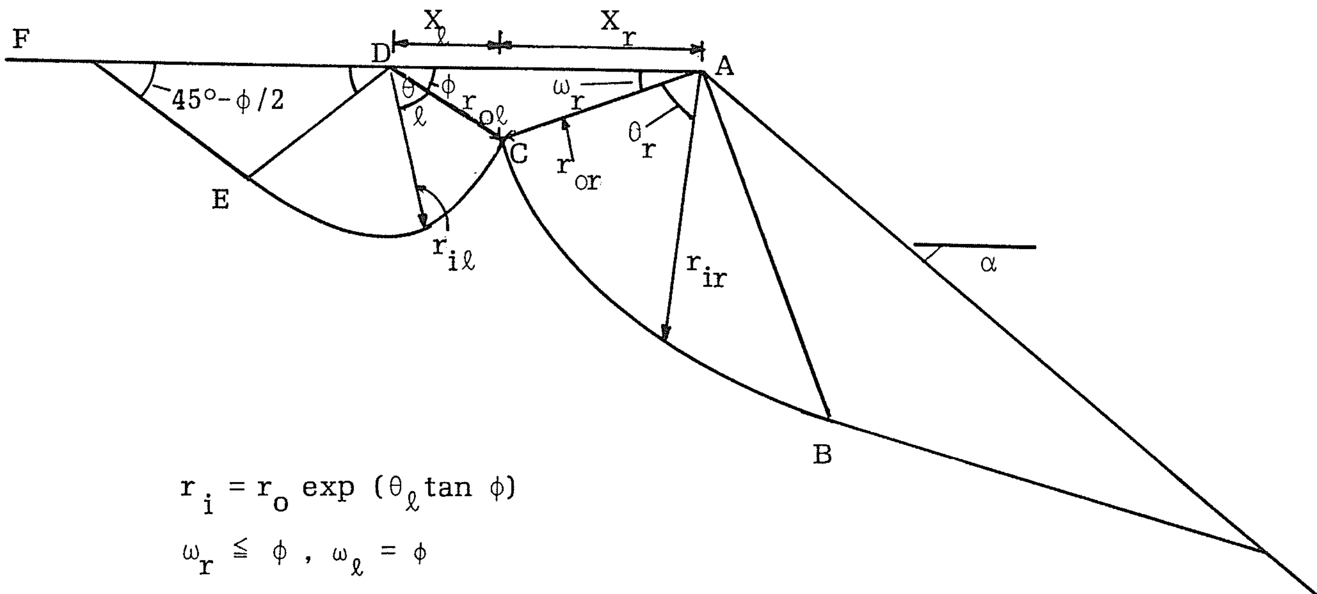

$r_i = r_o \exp(\theta_\ell \tan\phi)$

$\omega_r \leqq \phi$, $\omega_\ell = \phi$

$\alpha \geqq 0$

FIGURE 4.3 BASIC ASSUMPTIONS FOR THE DEVELOPMENT OF MODEL 1.

was determined in Section 3.3 and is given by

$$\sigma_i = x_i \{[1/\tan(\psi_{ir} - \mu)] - \tan\alpha\} \cdot \frac{1}{1 + \sin\phi \cos 2\psi_{ir}} \qquad \ldots\ldots\ldots 4.1$$

At the start of the extreme spiral at B bounding the failing soil mass,

$$\sigma_i = \ell\{[1/\tan(\psi_{ir} - \mu)] - \tan\alpha\} \cdot \frac{1}{1 + \sin\phi \cos 2\psi_{ir}} \qquad \ldots\ldots\ldots 4.2$$

In the region close to O (Figure 4.4) where the effect of self weight can be neglected, the stress on the j^{th} radial line is given by

$$\sigma_j = \sigma_i \exp(2\,\Delta\psi \tan\phi) \qquad \ldots\ldots\ldots 4.3$$

If this can be applied to the entire failing mass (and this is strictly correct only if the entire domain is weightless) then

$$\sigma_{jr} = \ell\{[1/\tan(\psi_{ir} - \mu)] - \tan\alpha\}.\exp(2\,\Delta\psi \tan\phi) \cdot \frac{1}{(1 + \sin\phi \cos 2\psi_{ir})} \qquad \ldots\ldots\ldots 4.4$$

The verical stress σ_{vr} at point C is therefore

$$\sigma_{vr} = \ell\{[1/\tan(\psi_{ir} - \mu)] - \tan\alpha\} \frac{\{1 + \sin\phi \cos 2\psi_{fr}\}}{\{1 + \sin\phi \cos 2\psi_{ir}\}} \cdot \exp\{2\tan\phi(\psi_{fr} - \psi_{ir})\} \qquad \ldots\ldots\ldots 4.5$$

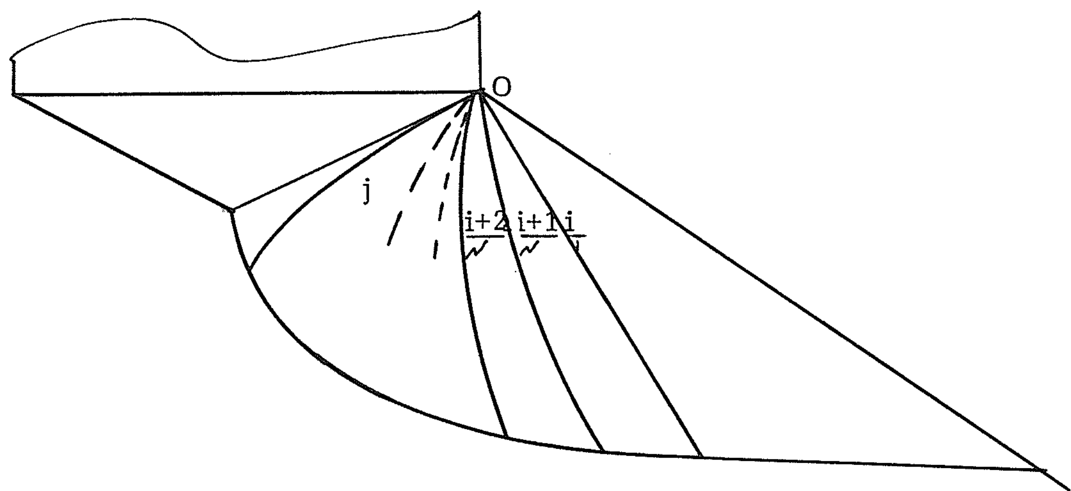

FIGURE 4.4. NUMBERING SEQUENCE FOR THE RADIALS EMANATING FROM O.

The value of ψ_{ir} was determined in Section 3.4. and is a function of α. It is expressed as

$$\psi_{ir} = 1/2 \{\pi - \alpha - \sin^{-1}(\sin \alpha/\sin \phi)\} \quad ....4.6$$

The parameter ψ_{fr} is a function of ω_r and can be expressed as

$$\psi_{fr} = \omega_r - \pi/4 - \phi/2 \quad ....4.7$$

The value of σ_{vr} as expressed in Equation 4.5 is thus a function of ω_r, α and ϕ.

It is clear that good mathematical modelling should not introduce a stress discontinuity at any intermediate point on the footing base. Hence there can only be one value for the stress at point M (Figure 4.1). The Model 1 analysis assumes that the vertical stress σ_{vr} at point M decreases linearly to zero at D, the left edge of the footing. The rate of stress decrease to D obtained from a surface footing calculation will define the location of the left edge of the footing. This establishes the value of x_ℓ/x_r, that is, the skewness of the elastic wedge.

Since we have assumed that the failure surfaces are logarithmic spirals then the length x_r in Fig. 4.3. is

$$x_r = \ell \cos \omega_r / \{\sin (\psi_{ir} - \mu)\} . \exp\{\theta_r \tan \phi\} \quad ....4.8$$

From the physical geometry of the wedge

$$x_\ell = x_r \frac{\tan \omega_r}{\tan \phi} \qquad \ldots\ldots\ldots 4.9$$

By combining Equation 4.8 and 4.9, the following expression for x_ℓ is obtained.

$$x_\ell = \frac{\ell \cos \omega_r}{\sin (\psi_{ir} - \mu) \tan \phi} \cdot \exp \{\theta_r \tan \phi\} \qquad \ldots\ldots\ldots\ldots 4.10$$

If we further assume that the rate of stress decrease to 'D' is in accordance with the Terzaghi N_γ value (here called $N_{\gamma T}$) for a fully rough ϕ wedge, then

$$\sigma_{v\ell} = 2\, x_\ell\, N_{\gamma T} \qquad \ldots\ldots\ldots\ldots 4.11$$

This is also based on the assumption that the failure surface is a logarithmic spiral.

Substitution of Equation 4.10 into Equation 4.11 yields

$$\sigma_{v\ell} = \ell \frac{2 \cos \omega_r}{\sin (\psi_{ir} - \mu) \tan \phi} \cdot \exp \{\theta_r \tan \phi\}\, N_{\gamma T} \qquad \ldots\ldots 4.12$$

Equations 4.5 and 4.12 therefore provide values for the stress at point M as functions of ω_r. As noted earlier, to avoid a discontinuity:

$$\sigma_{vr} = \sigma_{v\ell} \qquad \ldots\ldots\ldots\ldots 4.16$$

The resulting expression can be solved for ω_r provided that α and ϕ are defined. It was solved by computer by assuming an initial value for ω_r and determining the resulting σ_{vr} and $\sigma_{v\ell}$, values. These values were compared to determine whether the absolute difference met a specified tolerance that is $(\sigma_{vr} - \sigma_{v\ell}) / \sigma_{rv} < 0.01$. If this tolerance was exceeded, then ω_r was adjusted until the convergence criterion was met. Using this procedure, ω_r was computed for values of ϕ ranging for 30 to 45 degrees and values of α ranging from 10 degrees to $(\phi - 5)$ degrees. for each ϕ considered.

4.3.3 Results From Model 1

The results showing the computed values of ω_r and x_ℓ / x_r are summarized in Table 4.2. Also shown in this table, is the eccentricity of the apex of the asymmetrical wedge which is defined on Figure 4.1. It is a relative measure of the skewness of the wedge and gives a more convenient quantitative measure of the asymmetry than the parameter x_ℓ / x_r. Table 4.2 shows that the value of 'e' varies within the range of .02 B to .35 B as α varies from 10 to 40 degrees.

ϕ (degrees)	α (degrees)	ω_r (degrees)	ω_ℓ (degrees)	x_ℓ / x_r	'e' (x1/B)
30	5.0	30.0	30.0	1.0	0.0
	10.0	27.4	30.0	0.90	0.02
	15.0	22.0	30.0	0.70	0.08
	20.0	16.9	30.0	0.53	0.15
	25.0	12.4	30.0	0.38	0.22
35	10.0	33.2	35.0	0.93	0.02
	15.0	26.8	35.0	0.72	0.08
	20.0	20.7	35.0	0.54	0.15
	25.0	15.4	35.0	0.39	0.22
	30.0	11.0	35.0	0.28	0.28
40	10.0	36.7	40.0	0.89	0.03
	15.0	29.6	40.0	0.68	0.09
	20.0	22.9	40.0	0.50	0.17
	25.0	16.9	40.0	0.36	0.23
	30.0	12.1	40.0	0.26	0.29
	35.0	8.4	40.0	0.17	0.35
45	10.0	41.5	45.0	0.88	0.03
	15.0	33.0	45.0	0.70	0.08
	20.0	26.3	45.0	0.49	0.17
	25.0	19.6	45.0	0.36	0.23
	30.0	14.0	45.0	0.25	0.30
	35.0	9.8	45.0	0.17	0.35
	40.0	6.6	45.0		

TABLE 4.2 SUMMARY OF CALCULATED x_ℓ / x_r AND ω_r VALUES FOR MODEL 1.

From Table 4. 2, it is immediately obvious that the skewness of the trapped wedge, as represented by both x_ℓ/x_r and e, is largely independent of the value of ϕ. Average values of e and x_ℓ/x_r for a given α are summarized on Table 4. 2 . The variation of e with α, and x_ℓ/x_r with α are shown on Figures 4. 5 and 4. 6 respectively. These graphs also show results from further Models 2 to 4 which were also examined. Both the curves for Model 1 (Figures 4.5 and 4.6) indicate that the asymmetry or skewness of the wedge becomes more pronounced as the slope inclination increases. Figure 4.6 is basically a repetition of Figure 4.5, but is reproduced because of its usefulness in the later numerical work.

The general trends resulting from this solution agree quantitatively with those obtained from the experimental observations by Peynircioglu (1948), and Giroud and Tran-Vo-Nhiem (1971).

The variation of ω_r with α for various ϕ angles is shown on Figure 4.7. These curves are useful for determining ω_r values which define the final boundary in the N_γ calculations, which will be described in Chapter 5.

From the above analysis, the approximate shape of the trapped elastic wedge can be determined for any combination of ϕ and α. However, when

SLOPE ANGLE α (degrees)	ECCENTRICITY OF WEDGE 'e' $(x \frac{1}{B})$	x_ℓ / x_r
10	0.026	.90
15	0.08	.70
20	0.16	.52
25	0.225	.37
30	0.29	.26
35	0.35	.17
40	0.50	

TABLE 4.3 AVERAGE VARIATION OF 'e' AND 'x_ℓ / x_r' WITH 'α' BASED ON MODEL 1.

Note: The values of 'e' and x_ℓ / x_r quoted above are the arithmetic means of the values shown on Table 4.2 for any specified value of α .

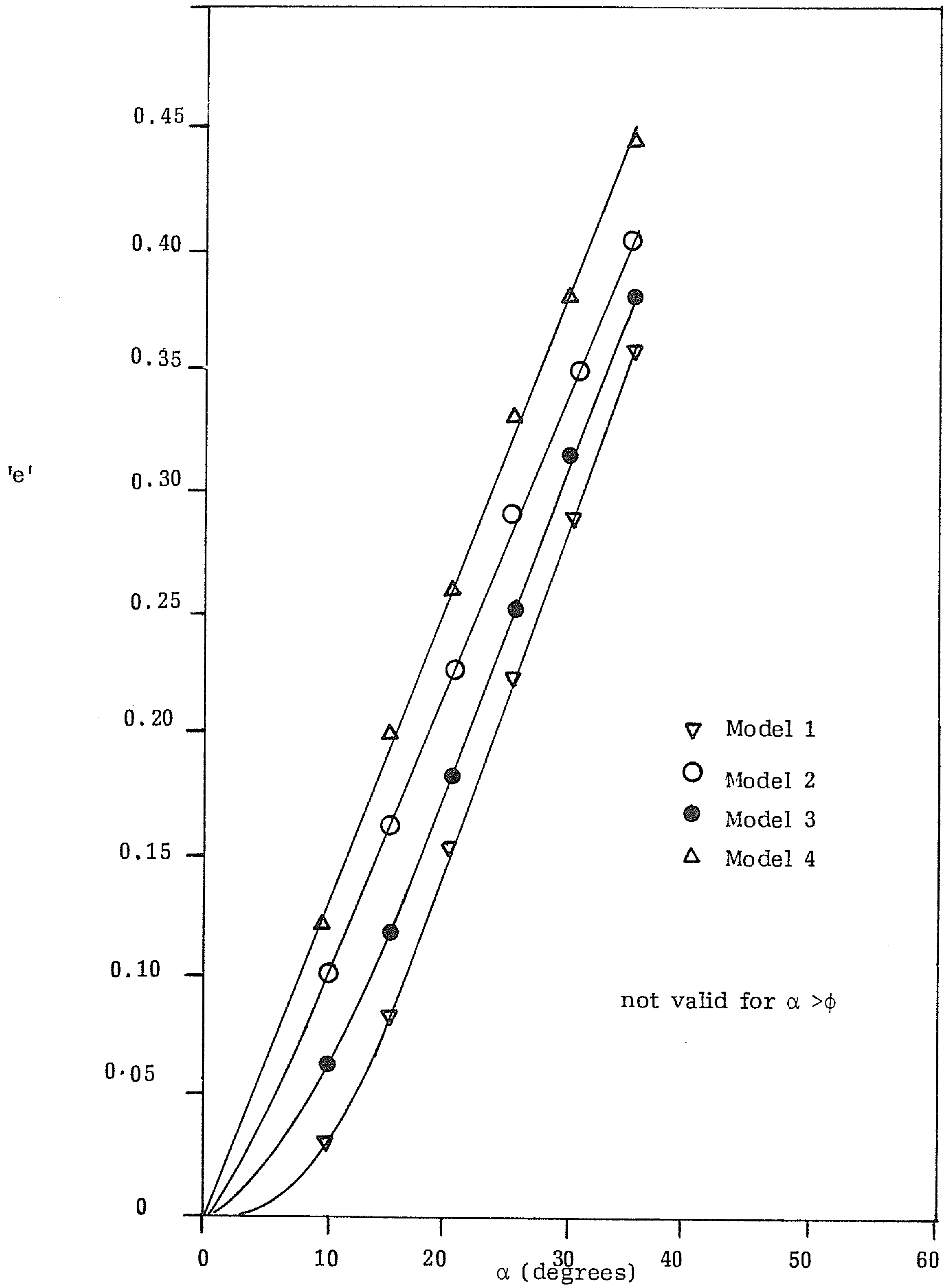

FI

FIGURE 4.5. VARIATION OF 'e' WITH α FOR MODELS 1 TO 4.

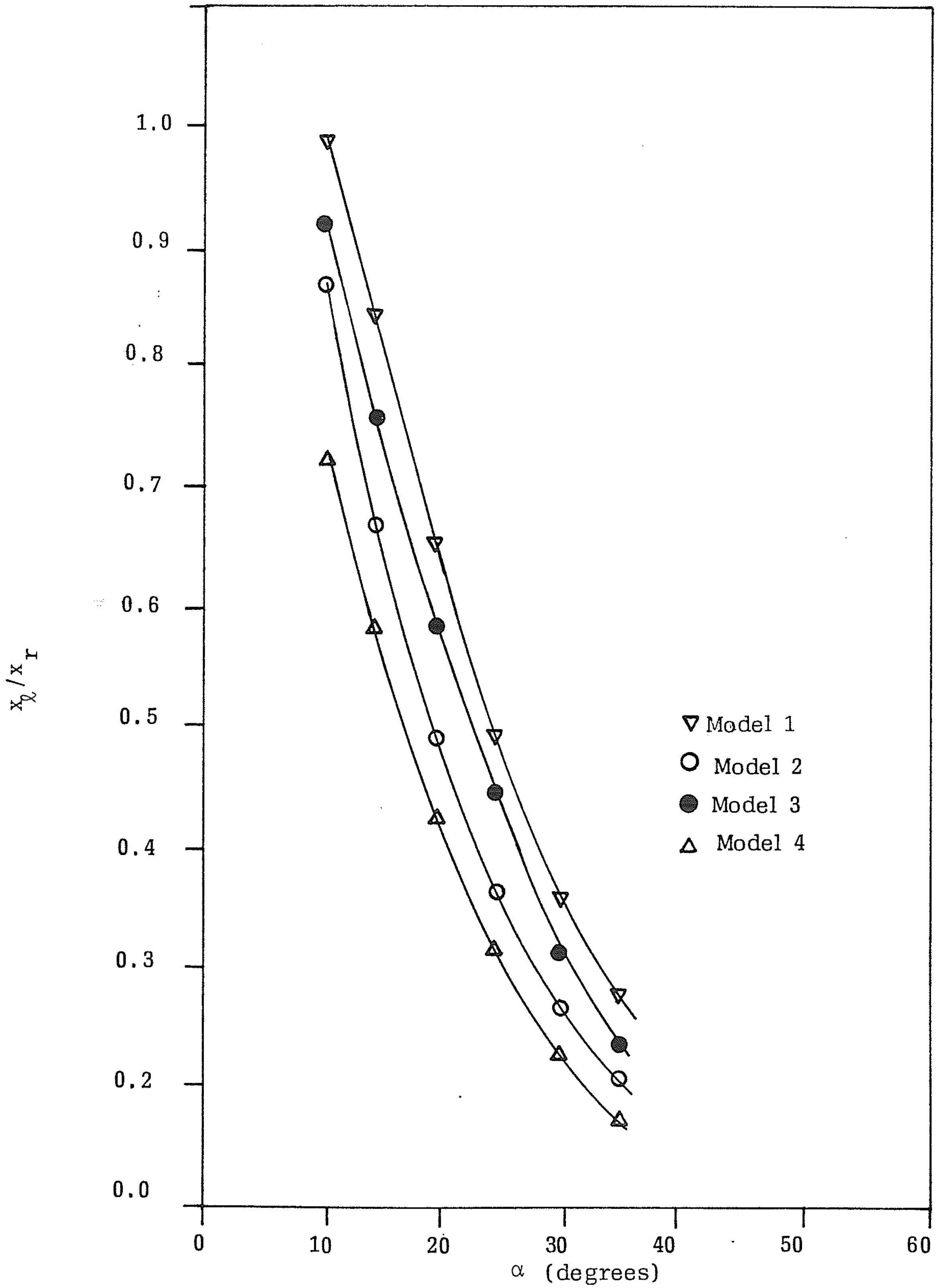

FIGURE 4.6 VARIATION OF x_ℓ/x_r WITH α FOR MODELS 1 TO 4.

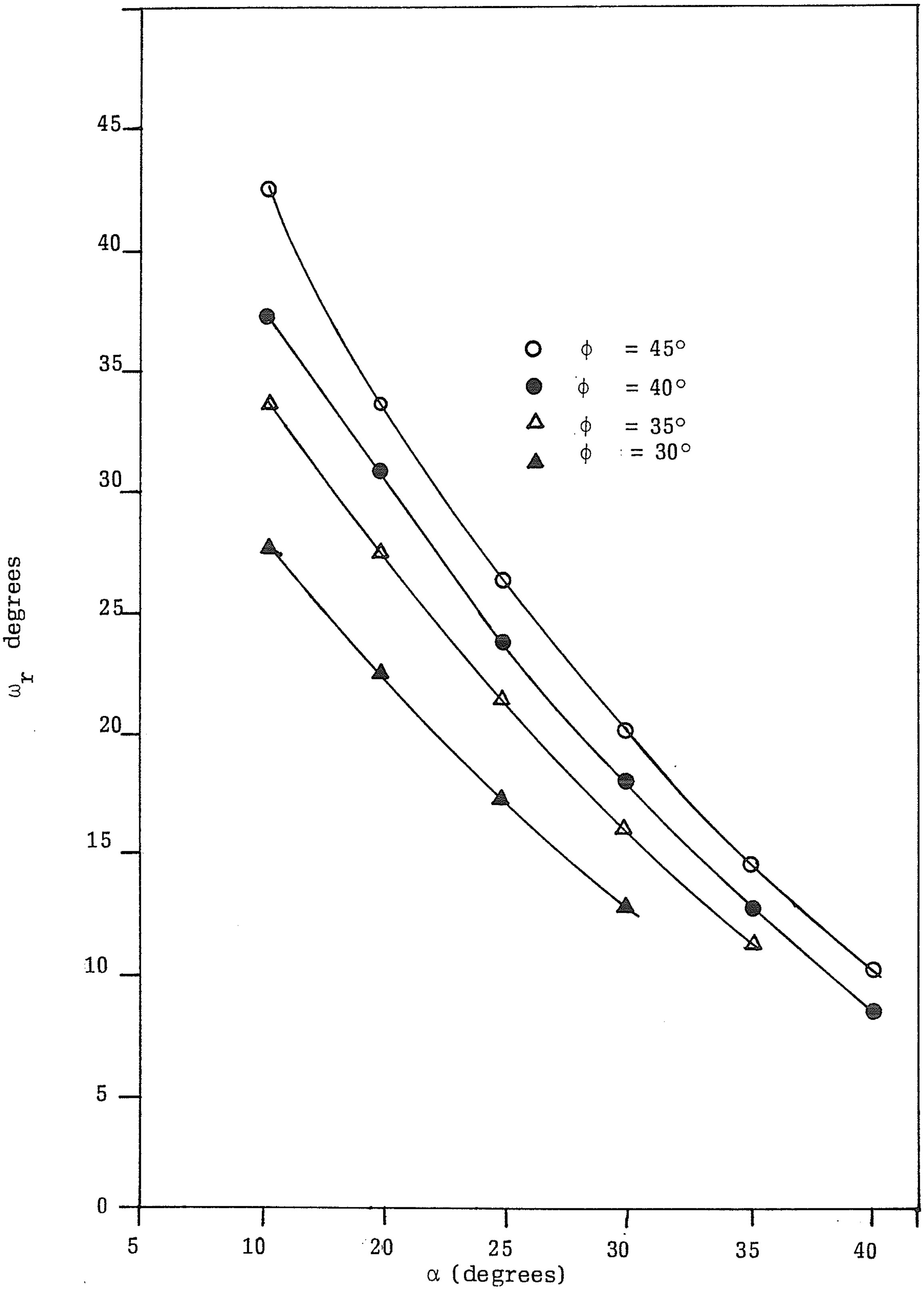

FIGURE 4.7 VARIATION OF ω_r WITH α MODEL 1.

comparisons were made between experimental and theoretical values of N_γ, the agreement was not acceptable. Further models (2 to 4) were then developed to improve the level of agreement. These are described in the following sections.

4.3.4 Development Of Model 2

This model is similar in several respects to Model 1. It starts from the same premise that the left base angle of the wedge is equal to ϕ. It also computes the vertical stress 'σ_{vr}' at point M on the base of the footing by starting with the known stress on the edge of the rectilinear passive zone adjacent to the slope and computing the stress on the end boundary, i.e. the lower right edge AC of the elastic wedge by assuming that the stresses in the transition zone are related by the expression.

$$\sigma_j = \sigma_i \exp \left(2 \Delta\psi \tan \phi \right)$$

The difference between Models 1 and 2 is that σ_{vr} is computed independently by assuming a logarithmic spiral stress distribution in the failing domain on the left rather than the Terzaghi distribution and then computing the vertical stress on the end boundary (Figure 4.3) which was defined by a base angle ϕ, as a function of ω_r.

The resulting expression for $\sigma_{v\ell}$ is

$$\sigma_{v\ell} = \frac{x_\ell \sin \mu \exp \{ 3 \Delta\psi \tan \phi \}}{\cos \phi \ (1-\sin \phi) \ (1 + \sin \phi \cos 2\mu)} \quad \ldots\ldots\ldots\ldots 4.17$$

where

$$x_\ell = \frac{\sin \omega_r}{\tan \phi \ \{ \sin (\psi_{ir} - \mu) \}} \cdot \exp \{ - \theta_r \tan \phi \} \ldots\ldots\ldots 4.18$$

By equating $\sigma_{v\ell}$ (Equation 4.17) to σ_{vr} (Equation 4.5) an expression which contains the single unknown ω_r is obtained. This was solved using the iterative procedure outlined in Section 4.3.2.

4.3.5 Results From Model 2

The values of the computed parameters defining the geometry of the wedge are summarized on Tables 4.4 and 4.5. The variation of ω_r with α for ϕ angles varying from 30 to 45 degrees is shown on Figure 4.8. The general trends which resulted from Model 1 are also observed for Model 2. That is, the degree of asymmetry of the trapped wedge increases

ϕ (degrees)	α (degrees)	ω_r (degrees)	ω_ℓ (degrees)	x_ℓ / x_r	'e' $(x \frac{1}{B})$
30	5	26.2	30.0	0.85	0.04
	10	21.8	30.0	0.69	0.09
	15	17.2	30.0	0.54	0.15
	20	13.0	30.0	0.40	0.21
	25	9.4	30.0	0.29	0.27
35	10	25.1	35.0	0.67	0.10
	15	19.7	35.0	0.51	0.16
	20	14.7	35.0	0.37	0.22
	25	10.7	35.0	0.27	0.28
	30	7.5	35.0	0.19	0.34
40	10	28.8	40.0	0.66	0.10
	15	22.4	40.0	0.49	0.17
	20	16.6	40.0	0.36	0.23
	25	11.9	40.0	0.25	0.30
	30	8.3	40.0	0.17	0.35
	35	5.6	40.0	0.11	0.40
45	10	32.7	45.0	0.64	0.11
	15	27.5	45.0	0.52	0.15
	20	18.9	45.0	0.34	0.25
	25	13.3	45.0	0.24	0.31
	30	9.2	45.0	0.16	0.36
	35	6.2	45.0	0.10	0.41
	40	4.1	45.0	0.07	0.43

TABLE 4.4 SUMMARY OF CALCULATED x_ℓ / x_r AND ω_r VALUES BASED ON MODEL 2.

SLOPE ANGLE α (degrees)	ECCENTRICITY OF WEDGE 'e' (x 1/B)	x_{ℓ}/x_r
10	0.096	0.80
15	0.15	0.53
20	0.22	0.38
25	0.29	0.26
30	0.35	0.17
35	0.40	0.10
40	0.43	0.17

TABLE 4.5 AVERAGE VARIATION OF 'e' AND 'x_{ℓ}/x_r' WITH 'α' BASED ON MODEL 2.

Note: The values of 'e' and 'x_{ℓ}/x_r' quoted above are the arithmetic means of the values shown on Table 4.3 for any specified value of α.

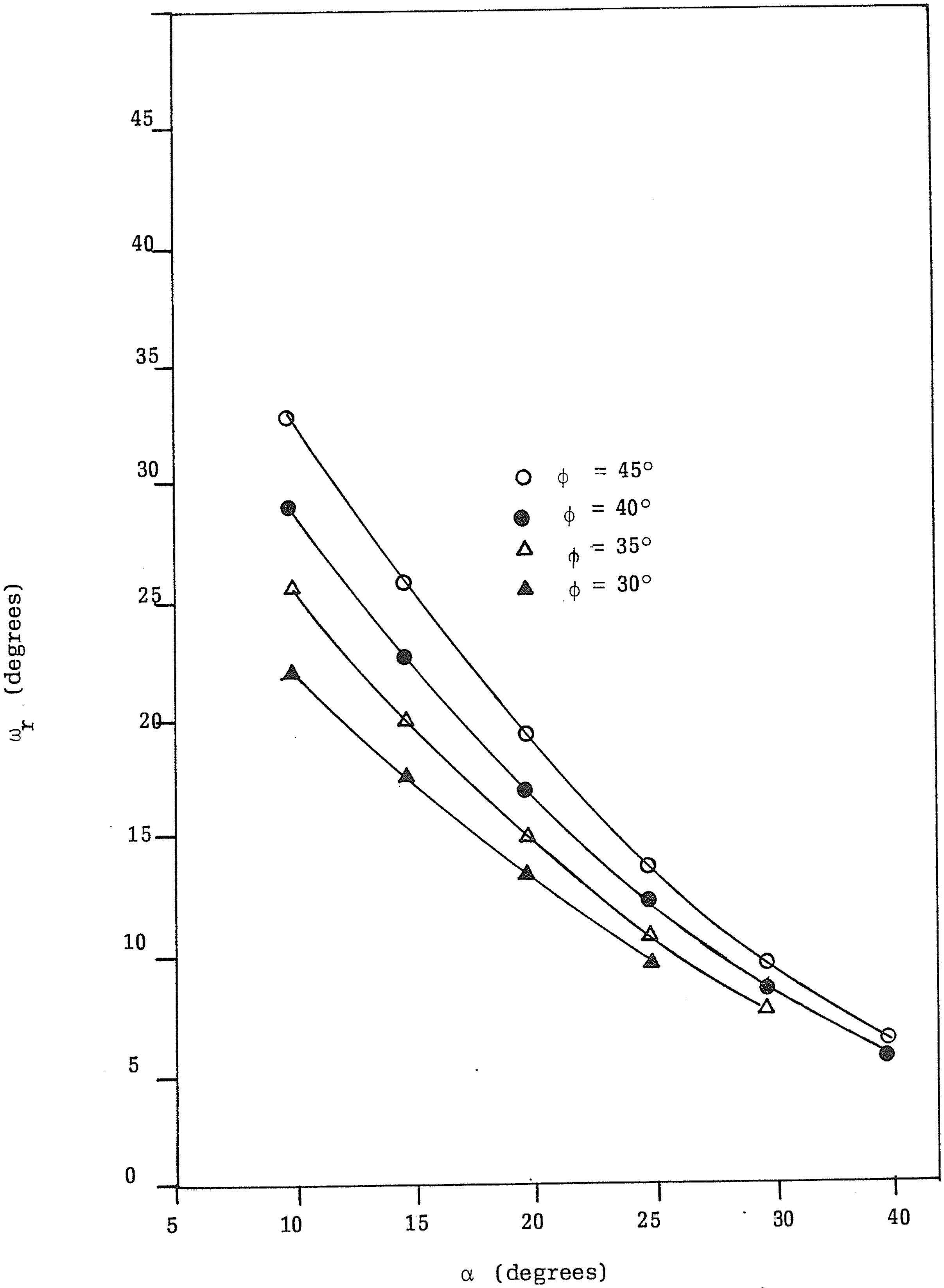

FIGURE 4.8: VARIATION OF ω_r WITH α MODEL 2

as α increases. However, the estimated amount of skewness as measured by e and x_ℓ/x_r of the wedge varies by a significant amount between the two models.

4.3.6 Development of Model 3

The feature of this model which is different from the two presented previously is that the stress $\sigma_{v\ell}$ at M (Figure 4.1) calculated by working from the left is calculated using the N_γ values of Graham and Stuart (1971) That is $\sigma_{v\ell} = 2\ x_\ell\ N_{\gamma G}$

The simplifying assumption of a log-spiral shaped failing domain applied for Models 1 and 2 is no longer used. This means that the effect of soil weight is now partly accounted for in the analysis.

Equation 4.12 can therefore be written as

$$\sigma_{v\ell} = \ell \frac{2 \cos \omega_r}{\sin (\psi_{ir} - \mu) \tan \phi} N_{\gamma G} \ . \ . \exp \{\theta_r \tan \phi \} \qquad \ldots\ldots\ldots 4.19$$

σ_{vr} is given by Equation 4.5.

The expression resulting from equating σ_{vr} (Equation 4.5) to σ_{vl} (Equation 4.19) is again solved for ω_r using the iterative procedure outlined above (Section 4.3.2).

4.3.7 Results From Model 3

The calculated values of ω_r and x_ℓ/x_r are summarised on Tables 4.6 and 4.7. The results are presented graphically on Figures 4.5, 4.6 and 4.9. In general, it is observed that the estimated eccentricity of the wedge is intermediate between the values computed using Model 1 and 2 respectively (Figures 4.5 and 4.6).

4.3.8 Development of Model 4

The approach to the formulation of Model 4 is considered to be much more rigorous than those discussed previously and will form the principal basis for subsequent calculations. In this case the approach starts from the 'free' ground surface (DF in Fig. 4.1) and works towards the right.

It combines the stress characteristic fields obtained for a footing on level ground with those obtained for a footing at the top of an embankment sloping equally on either side. This provides a solution for the condition where the footing is seated at the crest of a slope with level ground on the left side (Figure 4.1). The model is arranged so that it ensures there is no stress discontinuity along the footing base.

ϕ (degrees)	α (degrees)	ω_r (degrees)	ω_ℓ (degrees)	x_ℓ/x_r	'e' $(x\frac{1}{B})$
30	5	30.0	30.0	1.0	0.00
	10	25.5	30.0	0.82	0.05
	15	20.4	30.0	0.64	0.11
	20	15.6	30.0	0.48	0.17
	25	11.4	30.0	0.35	0.24
35	10	29.3	35.0	0.80	0.05
	15	23.3	35.0	0.62	0.12
	20	17.7	35.0	0.46	0.18
	25	13.0	35.0	0.33	0.25
	30	9.1	35.0	0.23	0.31
40	10	31.6	40.0	0.73	0.08
	15	25.0	40.0	0.56	0.14
	20		40.0	0.50	0.17
	25	13.6	40.0	0.29	0.27
	30	9.6	40.0	0.20	0.33
	35	6.5	40.0	0.14	0.38
45	10	36.1	45.0	0.73	0.08
	15	32.2	45.0	0.63	0.12
	20	21.6	45.0	0.40	0.21
	25	15.5	45.0	0.28	0.28
	30	10.8	45.0	0.19	0.34
	35	7.4	45.0	0.13	0.38
	40	4.9	45.0	0.08	0.42

TABLE 4.6 SUMMARY OF CALCULATED x_ℓ / x_r AND ω_r VALUES BASED ON MODEL 3.

SLOPE ANGLE α (degrees)	ECCENTRICITY OF WEDGE 'e' (x 1/B)	x_{ℓ}/x_r
10	0.07	0.75
15	0.11	0.64
20	0.17	0.49
25	0.25	0.33
30	0.33	0.20
35	0.38	0.14
40	0.42	0.097

TABLE 4.7 VARIATION OF 'e' AND x_{ℓ}/x_r WITH 'α' - BASED ON MODEL 3.

Note: The values of 'e' and x_{ℓ}/x_r quoted above are the arithmetic means of the values shown on Table 4.5 for any specified value of α.

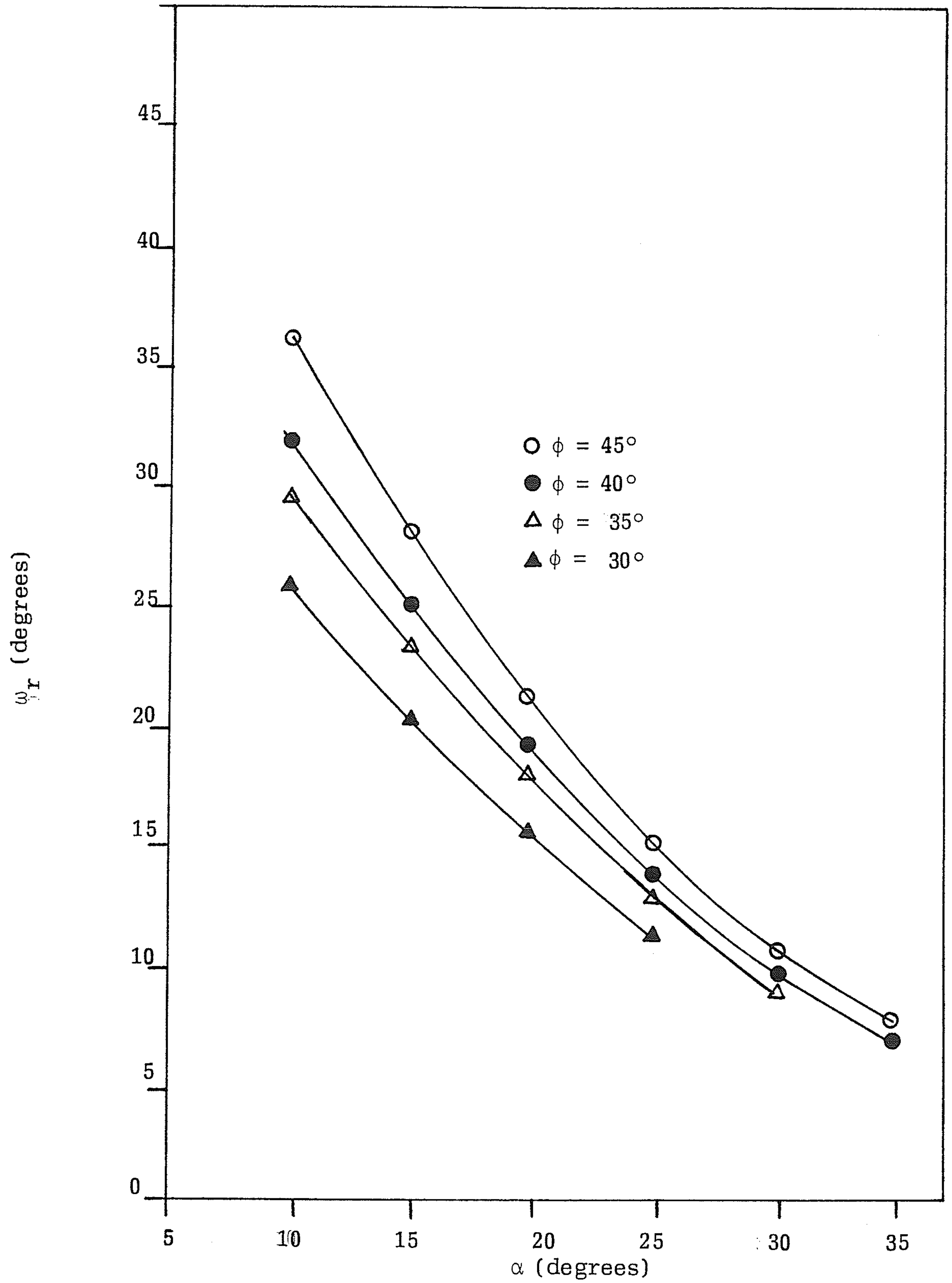

FIGURE 4.9: VARIATION OF ω_r WITH α (MODEL 3)

The model employs the stress characteristic solution to obtain the shape of the trapped wedge and does not presuppose a failure surface. In this respect it is superior to the models considered previously.

In Model 4, the stress characteristic solution for the $\alpha = 0$ condition (that is for a footing on level ground) is employed to determine the stress $\sigma_{v\ell}$ as well as the length x_ℓ (Figure 4.10) This ensures that the effect of soil weight in the failing domain is accounted for in the analysis. The length z_ℓ is also determined, since

$$z_\ell = x_\ell \tan \phi$$

The next stage of the modelling consisted of working from the sloping ground surface, that is, the right hand side of Figure 4.10, and using the stress characteristic solution developed in Chapter 3, to determine the base angle ω_r for which the stress $\sigma_{vr} = \sigma_{v\ell}$ and $z_\ell = z_r$ simultaneously. These conditions ensured that there is no stress discontinuity beneath the footing or physical discontinuity on the trapped wedge.

The procedure for doing this consists of computing the slip line field and hence $N_{\gamma\alpha}$ (which is proportional to σ_{vr}) for specified values of ϕ, α and ω_r. The values of

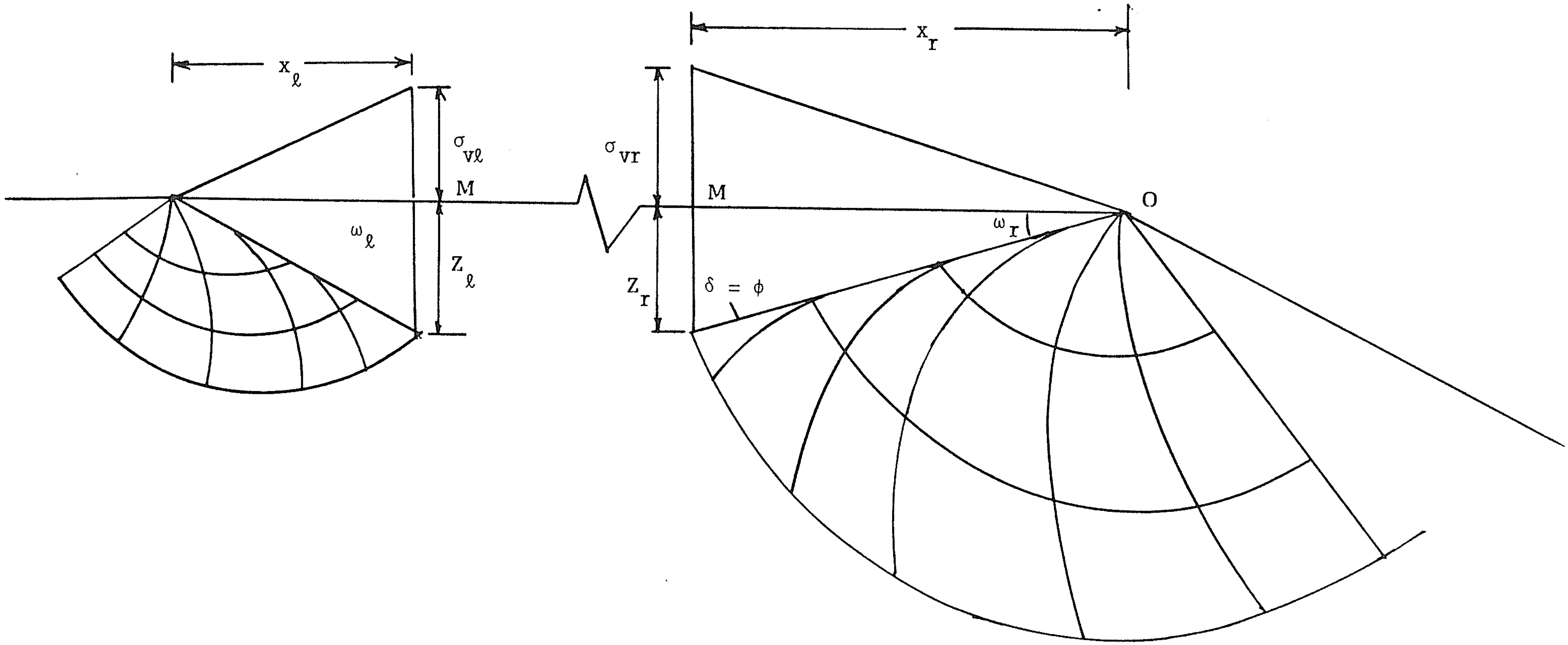

FIGURE 4.10 DEVELOPMENT OF MODEL 4.

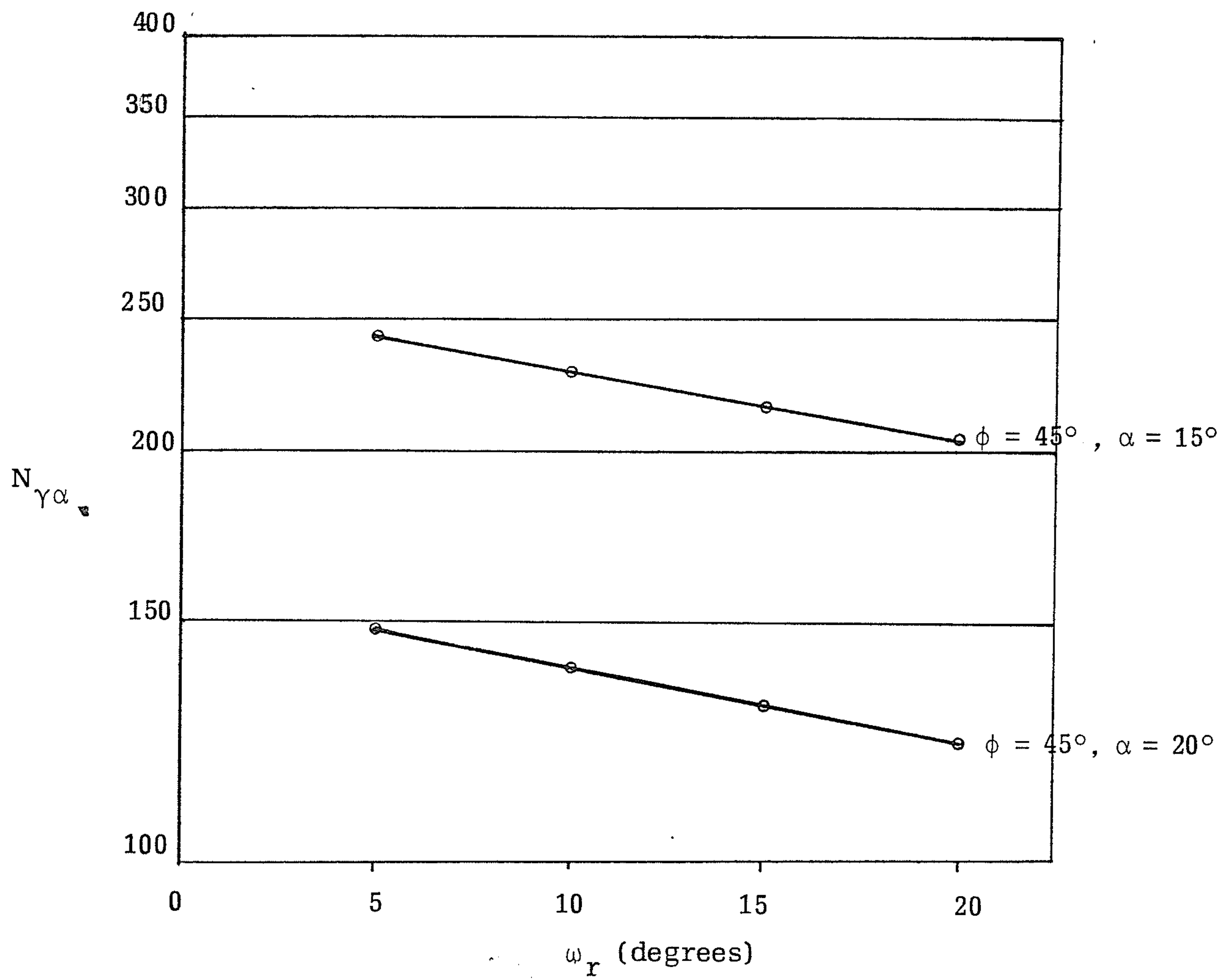

FIGURE 4.11: TYPICAL VARIATION OF $N_{\gamma\alpha}$ WITH ω_r.

ϕ considered, ranged 'rom 30 to 45 degrees in intervals of 5 degrees and α from 10 degrees to ϕ-5 degrees. For each combination of ϕ and α, ω_r was varied through a range of values and $N_{\gamma\alpha}$ computed for each value of ω_r considered. A typical variation of $N_{\gamma\alpha}$ with ω_r is shown on Figure 4.11. This Figure shows that as ω_r decreases, $N_{\gamma\alpha}$, and therefore σ_{vr} increases. A schematic illustration of this phenomenon is shown on Figure 4.12. It is therefore evident that there must exist a unique value of ω_r for which $\sigma_{vr} = \sigma_{v\ell}$ and $z_r = z_\ell$ simultaneously. In order to obtain this ω_r value, the computed σ_{vr} and z_r values were combined with the initially defined z_ℓ and $\sigma_{v\ell}$ values to give to ratio of σ_{vr} to $\sigma_{v\ell}$ and z_r to z_ℓ. By interpolation between the calculated values of the ratio, the exact values of ω_r for which the ratios are equal to 1.0 was determined. The geometry of the elastic wedge was therefore obtained.

4.3.9 Results of Model 4

The geometry of the wedge computed using Model 4 is summarized on Tables 4.8 to 4.9. The results show similar trends to those obtained from Models 1 to 3. A plot of the variation of 'e' with 'α' is shown on Figure 4.5 while the variation of ω_r with a α, is shown on Figure 4.13 Model 4 predicts a higher degree of skewness of the elastic wedge than Models 1 to 3 inclusive.

ϕ (degrees)	α (degrees)	ω_r (degrees)	ω_ℓ (degrees)	x_ℓ / x_r	'e' ($x \frac{1}{B}$)
30	10	20.0	30.0	0.63	0.63
	15	14.7	30.0	0.41	0.41
	20	10.5	30.0	0.31	0.31
	25	6.7	30.0	0.17	0.17
35	10	23.5	35.0	0.60	0.60
	15	17.7	35.0	0.43	0.43
	20	12.7	35.0	0.31	0.31
	25	8.5	35.0	0.19	0.19
	30	5.3	35.0	0.13	0.13
40	10	29.0	40.0	0.66	0.10
	15	21.0	40.0	0.46	0.18
	20	15.0	40.0	0.32	0.26
	25	10.5	40.0	0.21	0.33
	30	6.8	40.0	0.13	0.38
	35	4.0	40.0	0.05	0.45
45	10	31.5	45.0	0.60	0.13
	15	26.0	45.0	0.43	0.20
	20	18.0	45.0	0.32	0.26
	25	12.5	45.0	0.21	0.33
	30	8.0	45.0	0.13	0.38
	35	5.0	45.0	0.09	0.42
	40	4.2	45.0	0.07	0.43

TABLE 4.8 SUMMARY OF CALCULATED x_ℓ / x_r AND ω_r VALUES BASED ON MODEL 4.

SLOPE ANGLE α (degrees)	ECCENTRICITY OF WEDGE 'e' (x 1/B)	x_ℓ / x_r
10	0.12	0.62
15	0.20	0.43
20	0.26	0.31
25	0.33	0.20
30	0.38	0.13
35	0.44	0.07
40	0.44	0.07

TABLE 4.9 VARIATION OF 'e' AND x_ℓ / x_r WITH ' α ' BASED ON MODEL 4.

Note: The values of 'e' and x_ℓ / x_r quoted above are the arthimetic means of the values shown on Table 4.7 for any specified value of α .

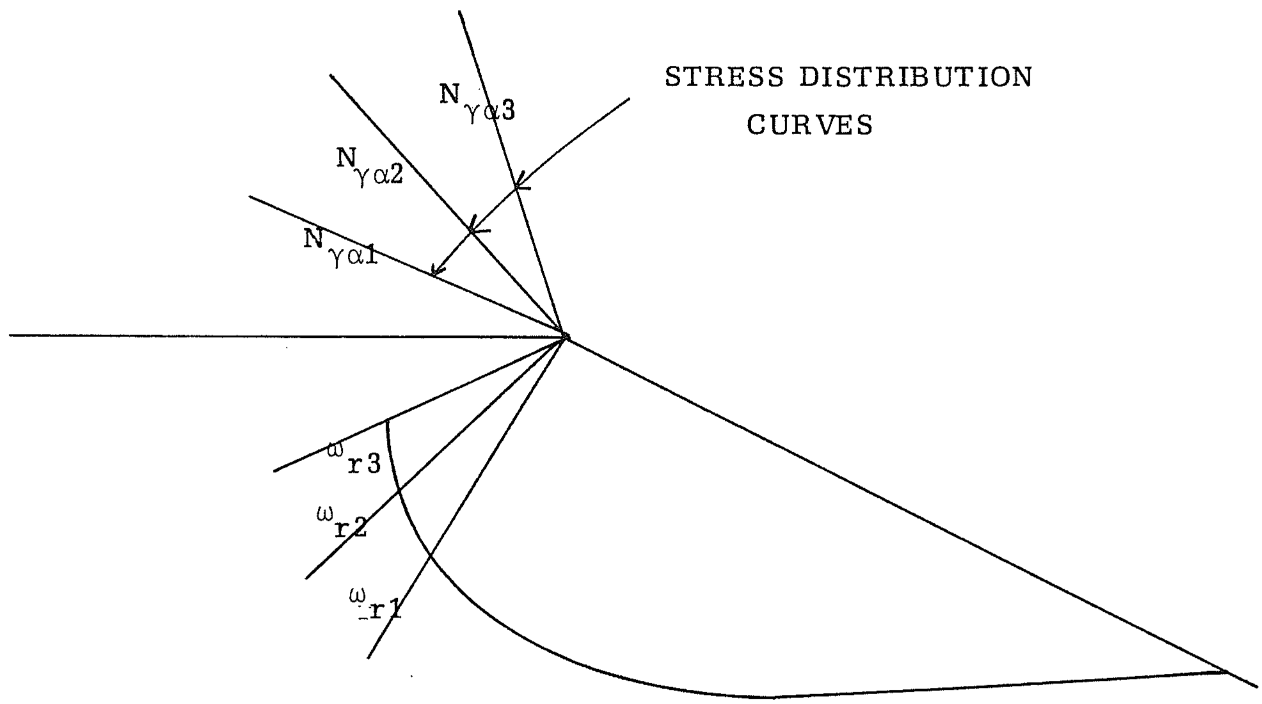

$\omega_{r1} > \omega_{r2} > \omega_{r3}$

$N_{\gamma 1} < N_{\gamma 2} < N\gamma 3$

FIGURE 4.12: SCHEMATIC ILLUSTRATION OF THE VARIATION OF $N_{\gamma\alpha}$ WITH ω_r

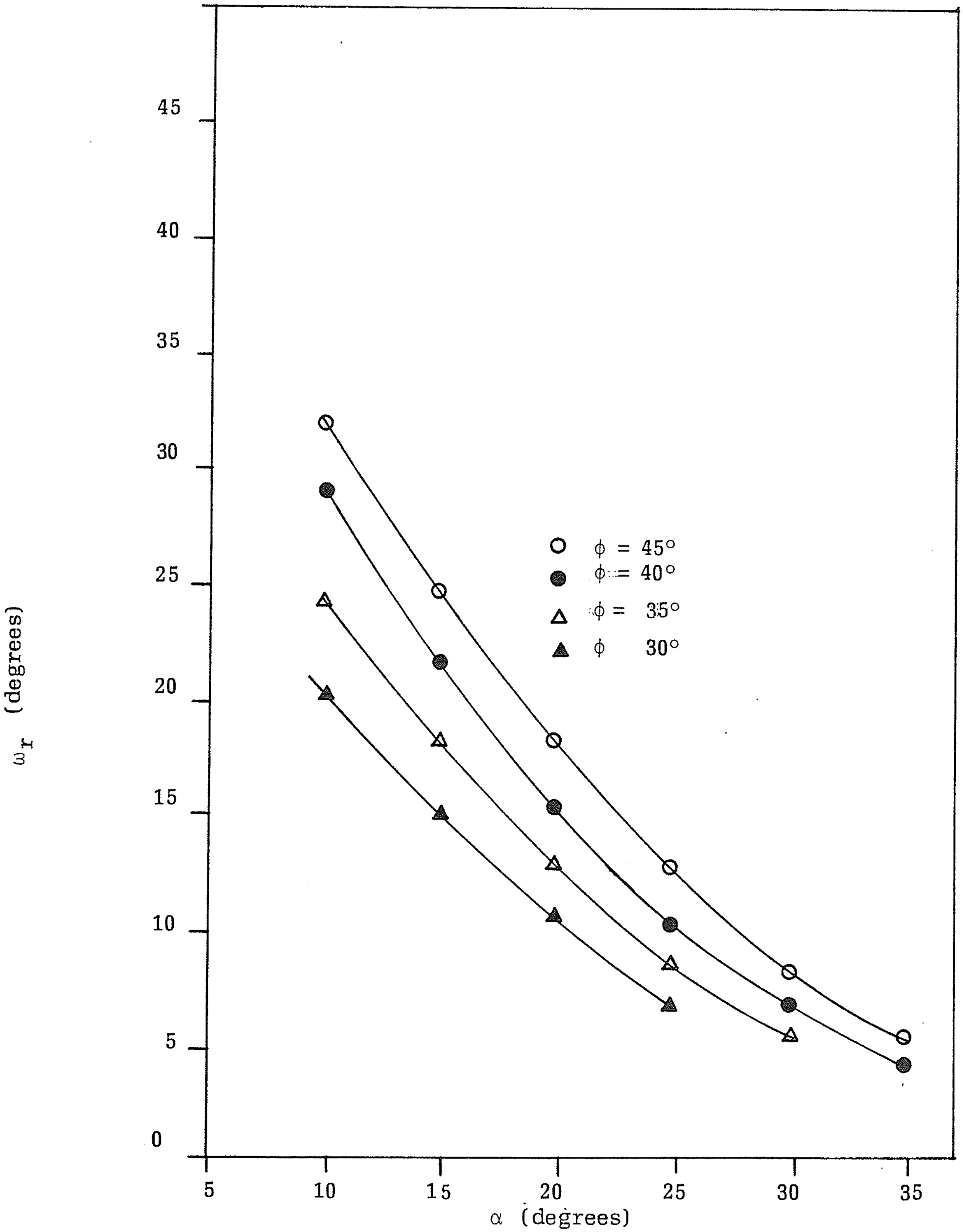

FIGURE 4.13: VARIATION OF ω_r WITH α (MODEL 4)

4.4. Validity Of The Models And Comments On The Assumptions Made in Their Formulation

A series of assumptions had to be made to allow development of the models for determining the shape of the trapped wedge beneath the footing. These now require further amplification, explanation and comment. For this discussion, Models 1 to 3 are treated together since the basic assumptions utilised in their formulation are essentially similar. The main assumptions incorporated in the formulation of Models 1 to 3 are as follows:-

(1) The sand medium was assumed to be weightless.

(2) The value of ω_ℓ in Fig. 4.1 was taken to be equal to the angle of internal friction of the soil ϕ.

(3) It was assumed that plastic straining and displacement of the failed masses on either side of the centre line of the footing take place simultaneously.

Assumption 3 applies to all of the models, that is to Model 4 as well as to Models 1 - 3.

4.4.1 Assumption 1

This assumption is common in both the limit equilibrium and limit analysis approaches to the bearing capacity problem (Chapter 2). It uses failure mechanisms based on logarithmic spirals (which are strictly correct only for weightless materials), and adapts them to produce estimates of the bearing capacity of sands with self-weight. Such approximate mechanisms provide estimated bearing capacity which compare favourably with stress characteristic solutions which do not presuppose the failure surface (Graham and Stuart: 1971). It might therefore be concluded at first sight, that the shapes of the failure mechanisms for sands with and without self-weight are not significantly different. In the development of Models 1 to 3, a weightless medium was assumed only for the purpose of determining an approximate shape for the trapped elastic wedge. It should be noted that the effect of the soil weight is included in subsequent calculations of bearing capacity.

4.4.2 Assumption 2

It is intuitively expected that, since the external soil boundary is on the left side of the footing (Figure 4.1) then the failure mechanism in this vicinity should approximate or converge to those which correspond to a footing on level ground, that is, a ϕ wedge may be expected beneath the left edge of the footing.

The experimental evidence to support this assumption is limited. However, the evidence that is available indicates that the assumption is reasonable. A summary of the values ω_r measured in experimental testing programs is presented on Table 4.1 (pg. 74). It can be deduced that the ratio of observed to theoretical values of ω_ℓ varies within the relatively narrow range of 0.95 to 1.35. More experimental data would be helpful to further substantiate this hypothesis.

4.4.3 Assumption 3

The manner in which failure progresses through the sand from the region which is obviously the weakest, that is, the region closest to the slope, into the more stable regions beneath the footing is not completely known. The problem is further complicated by its physical asymmetry.

The assumption of simultaneous failure to both sides of the footing is associated with the assumption that the soil behaviour is rigid-plastic (Figure 4.14) that is, negligible volume change is assumed prior to failure.

Graham (1968) and Hovan (1985) suggested that the idea of associating a relatively incompressible material such as a medium dense sand with rigid-plastic behaviour does not alter the basic validity of the stress-characteristic solution. This assumption is justified so long as the footing is forced to move downwards vertically, and is not free to rotate.

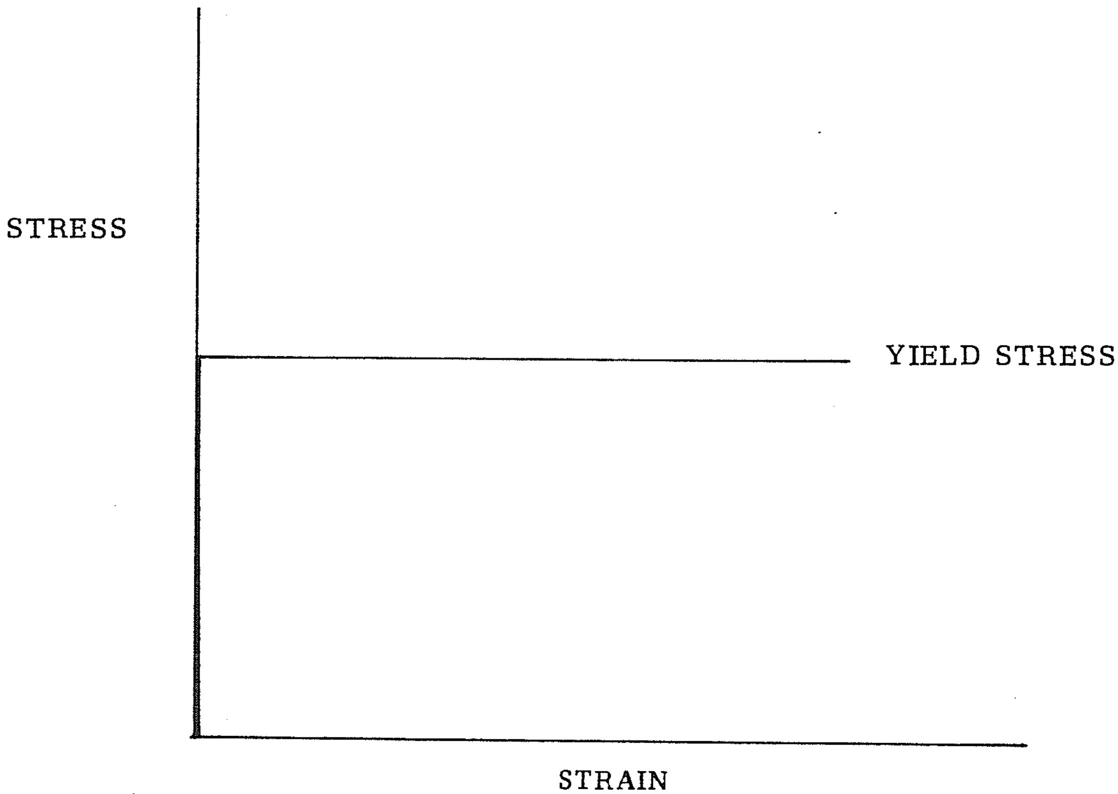

FIGURE 4.14: THE RIGID PLASTIC SOIL MODEL

Whether the footing is constrained to move downward or rotates as failure is induced will depend on the rigidity of the connections between the footing and the superstructure and the nature of the structural connections of the superstructure.

Small scale model tests in general do not try to simulate the rigidity of the superstructure. In fact they generally have free joints. Footings will therefore tend to move in the direction of least resistance. As a result, footings will tend to rotate and produce a failure mechanism which does not show any slip line fields in the stronger region, or the region close to the level ground. In actual structures such as bridges, the superstructure may be rigid or semi-rigid. In such cases the footing can be expected to have some constraint and to move vertically downwards, thereby inducing failure to both sides of the sand mass simultaneously. This thesis considers only footings which move vertically downwards with failure zones extending on both sides of the footing.

4.5 Comparison Of The Models

Figures 4.5 and 4.6 indicate that the amount of eccentricity of the wedge predicted by the models for any value of α is in the following ascending order of magnitude: Model 1, Model 3, Model 2, Model 4. That is, Model 1 predicts the smallest amount of eccentricity, while Model 4 predicts the highest eccentricity (Figure 4.14).

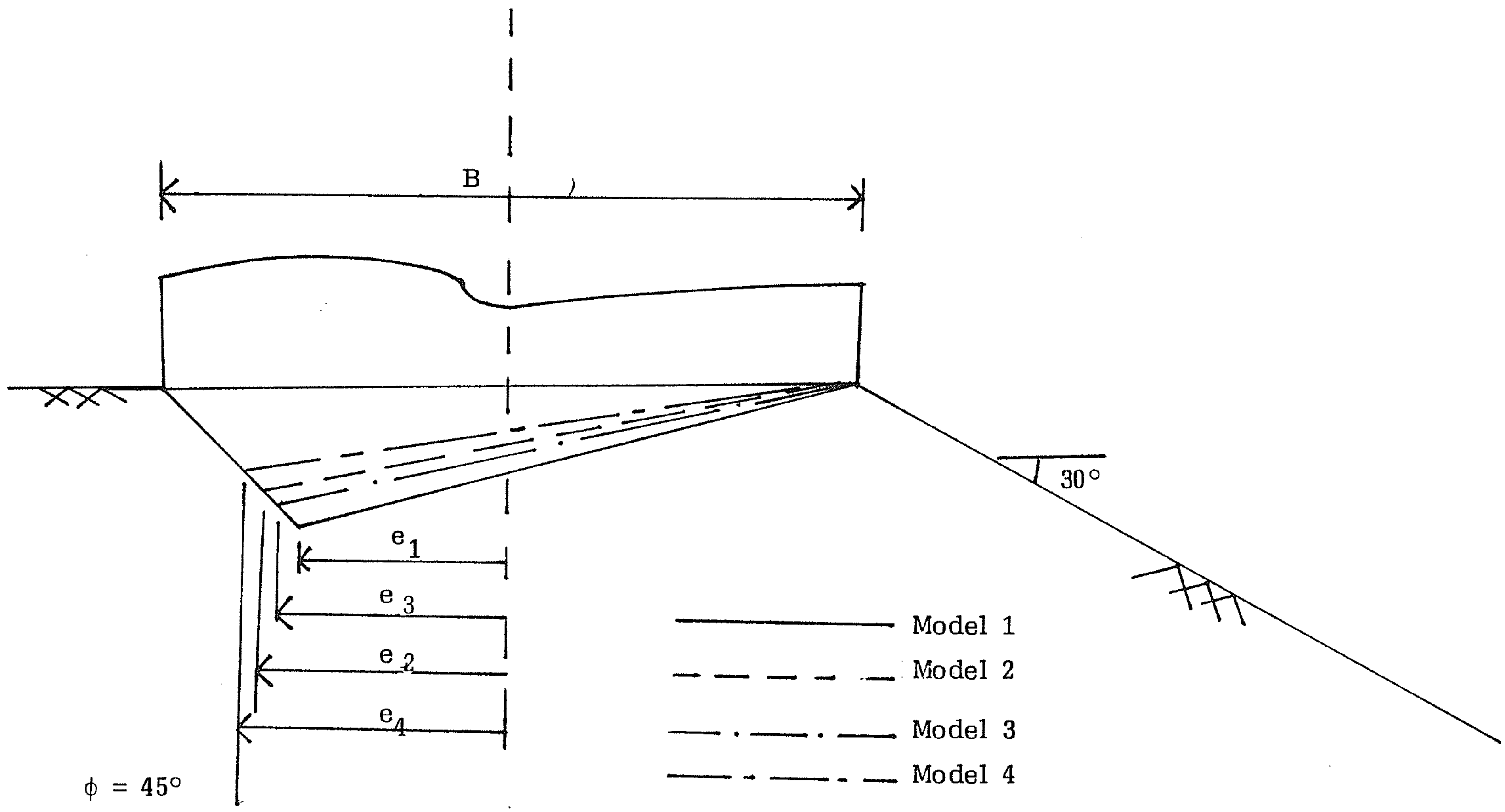

FIGURE 4.15 COMPARISON OF THE PREDICTED SHAPE OF THE TRAPPED WEDGE FOR MODELS 1 - 4 INCLUSIVE

The suitability of any model for subsequent use in the determination of the bearing capacity coefficient should be assessed on the basis of the following two criteria

(i) The validity of the assumptions used in the analysis and the rigour of the theory.

(ii) The level of agreement between the theoretical results, and the available experimental observations.

As noted in Section 4.3.8 Model 4 is by far the most rigorous in terms of the assumptions upon which it is based. It considers a failure mechanism which is considered to be the most realistic of the four that have been studied. At best, Models 1 to 3 are approximations to the likely failure mechanism. Hence from the point of view of criterion (i), Model 4 is the preferred model.

With respect to criterion (ii), Table 4.1 (p. 74), which compares the results from all the models, clearly shows that the best agreement observed and theoretical x_ℓ/x_r ratios is obtained for Model 3, while Model 1 gives the best agreement between observed and theoretical ω_r values. No firm conclusions can be drawn from these deductions since they are not consistent. Furthermore, the amount of experimental data which is available is quite limited.

On the basis of criterion 1 therefore Model 4 is the preferred model. Some analyses are also carried out using Model 1 since it provides a "lower bound" solution. It should perhaps be emphasized that the basis of comparison at this stage is with the geometry of the base wedge based on photographic evidence. It is well known for example, (Graham, 1968) that displacement (or strain) fields are much more difficult to model than loads or displacements. A later Section (Chapter 7) will compare theoretical predictions of N_γ with experimental values.

CHAPTER 5

FOOTING LOCATED AT THE CREST OF A SLOPE PARAMETRIC STUDY AND RESULTS

5.1 INTRODUCTION

The main variables which influence the bearing capacity of a footing at close proximity to a slope are the angle of internal friction of the soil, ϕ, the slope angle, α, the footing depth, D, and the distance, H, from the crest of the slope to the edge of the footing. In this Chapter, we are concerned only with the case of a footing located at the crest of a slope, that is $H = 0$. The case of a footing located away from the crest, is presented in Chapter 6. It is convenient to normalize the parameter D by dividing it by the footing breadth B. That is, it is expressed as the dimensionless parameter D/B. Analyses to determine the bearing capacity factor were carried out using Model 4 developed in Chapter 4 for ϕ ranging from 30 to 45 degrees and α ranging from 10 degrees to (ϕ -5) degrees for each value of ϕ considered. This thesis is concerned only with shallow footings hence analyses were done for $0.0 \leq D/B < 1.0$.

5.2 SURFACE FOOTINGS

In addition to the parameters which define the soil (ϕ) and slope geometry (α), the input parameters which are required for determination of the bearing capacity for the case under consideration, are those which define the geometry of the trapped elastic wedge in Chaper 4. That is, the ratio of x_ℓ / x_r and the value of ω_r. These parameters are in fact secondary parameters since they depend on ϕ and α. The values were obtained from Figures 4.6 and 4.13.

As outlined in Chapter 3, the surface footing, or zero surcharge condition is simulated by introducing a surcharge into the computation initially (Figure 5.1) and then enlarging the zone of computation until the assumed surcharge has no significant effect on the computed bearing capacity (Graham, 1968).

Using this method, and the computed shape of the wedge for Model 4 as outlined in Chapter 4, bearing capacity factors were calculated for ϕ ranging from 30 to 45 degrees and α from 10 to (ϕ - 5) degrees. The results are shown graphically on Figure 5.2a.

5.3. SHALLOW FOOTINGS

The addition of an artificial surcharge to the ground surface is an expedient mathematical procedure for handling the stress discontinuity at point O (Figure 5.1). The surcharge can also be considered to be real and to have the same effect as embedding the footing beneath the surface. The procedure for obtaining the bearing capacity factor which was alluded to in the preceding section involves diminishing the surcharge effect in a series of steps until its effect is negligible. The intermediate steps can however yield $N_{\gamma q}$ values corresponding to different depths of embedment . However, as noted by Graham

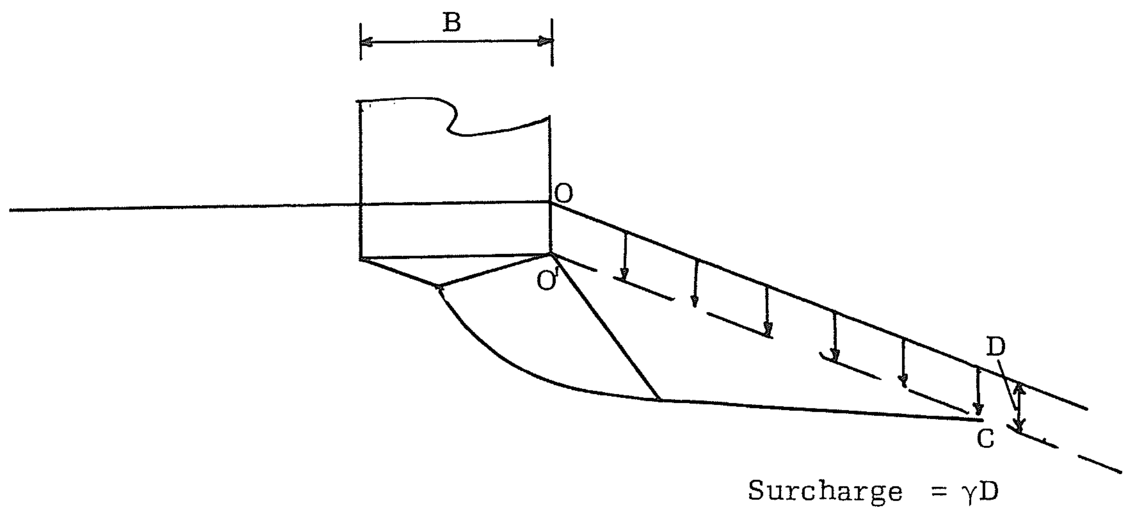

FIGURE 5.1 - EMBEDMENT DEPTH 'D' TREATED AS A SURCHARGE

and Stuart (1971), the convergence from the $N_{\gamma q}$ to the N_{γ} value is quite rapid. As a result, it was not possible to obtain a complete range of $N_{\gamma q}$ values corresponding to the required range of D/B values between 0 and 1. The limited results obtained using this approach are shown on Table 5.1 Also shown on Table 5.1. are values of $N_{\gamma q}$ obtained using the method outlined below. The values obtained from the latter method are generally lower than those obtained using the scale reduction method. The values obtained using the procedure outlined below range from 56-107% of those obtained using the scale reduction method.

The other procedure used for computing the bearing capacity factor consisted of treating the embedment depth D as a surcharge (Figure 5,1). The parameters σ and ψ on the "equivalent free surface" O'C were then calculated from the Mohr's circle (Figure 3.7) This means that the effect of the surcharge was included as both a vertical stress and shear stress along O'C. The governing equation for obtaining σ is

$$\sigma = \frac{1.0 + z}{1 + \sin\phi \cos 2\psi_i}$$

Since the values of the parameters x, z, σ and ψ are known for all points along O'C, then using the procedure outlined in Section 3, the entire slip line field in the region between the equivalent free surface and the edge of the passive zone could be computed.

ϕ (degrees)	α (degrees)	D/B	$N_{\gamma q}$ from scale reduction - (1)	$N_{\gamma q}$ equivalent free surface method (2)	(2)/(1) %
30	10	0.21	39.9	24	60
35	10	0.31	108.1	64	59
35	15	0.29	82.6	56	68
35	20	0.25	57.5	45	78
40	10	0.44	290.5	170	59
40	15	0.43	232.1	160	69
40	20	0.39	166.2	130	78
40	25	0.34	110.3	98	89
40	30	0.26	67.4	72	107
45	10	0.69	1001.0	560	56
45	15	0.65	742.6	480	65
45	20	0.61	538.9	410	76
45	35	0.56	372.9	330	88

TABLE 5.1 SUMMARY OF $N_{\gamma q}$ VALUES FOR FOOTING AT THE CREST OF A SLOPE.

- $N_{\gamma q}$ FROM 1st SCALE REDUCTION.

The entire computation starting from calculation of the parameters x , z, σ and ψ on the boundary O'C and determination of the slip line field was done using a specially written subroutine EDGPA3. A typical plot of the slip line field in this region is shown on Figure 5.4. The remainder of the slip line field up to the base of the footing and hence the bearing capacity factor was then computed using the basic program.

The complete set of results for α varying from 10 to (ϕ - 5) degrees, ϕ from 30 to 45 degrees and D/B=0.25, 0.50, 0.75 and 1.0 are shown on Figures 5.2 and 5.3.

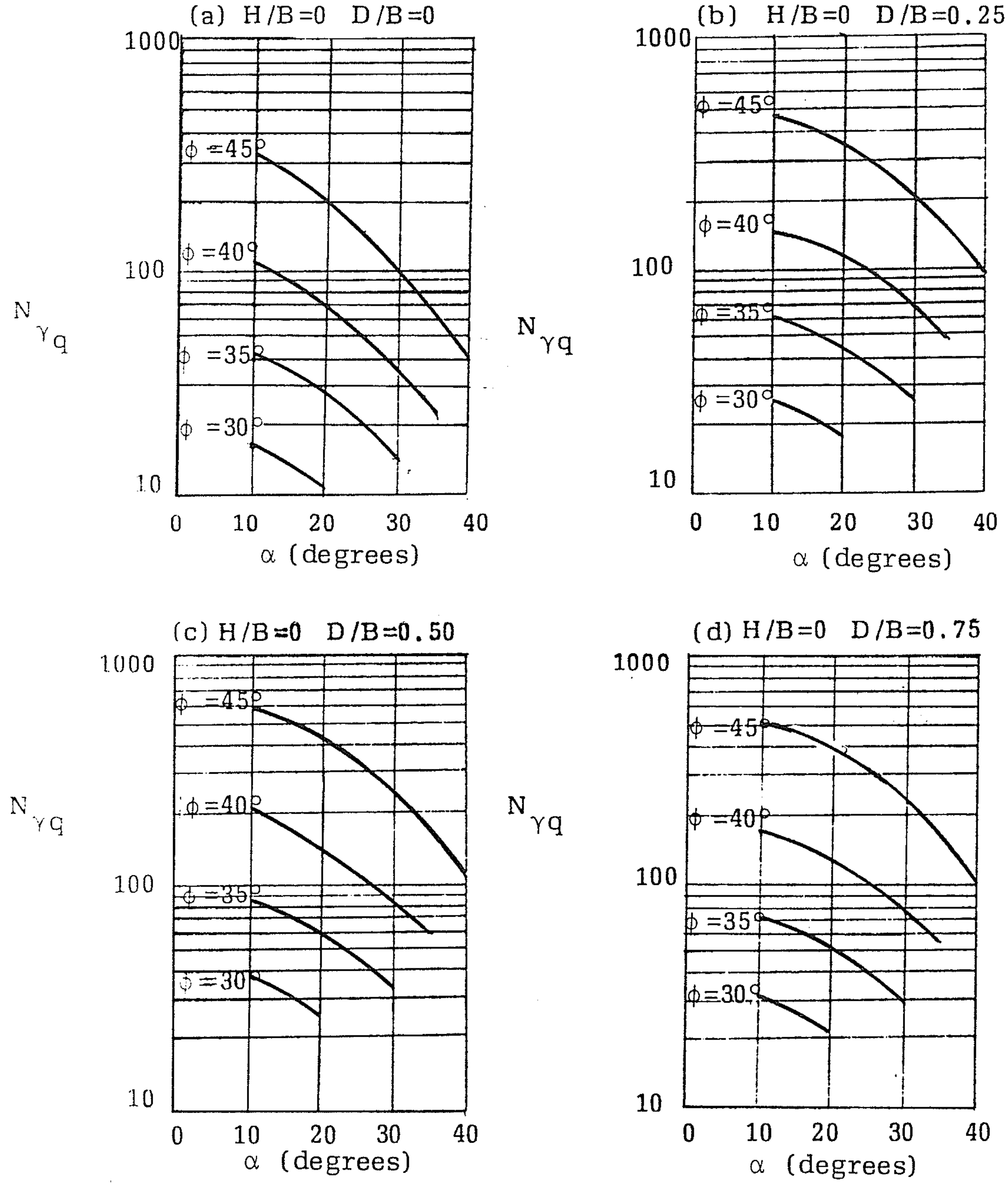

FIGURES 5.2: PLOT OF $N_{\gamma q}$ vs α FOOTING AT THE CREST OF THE SLOPE.

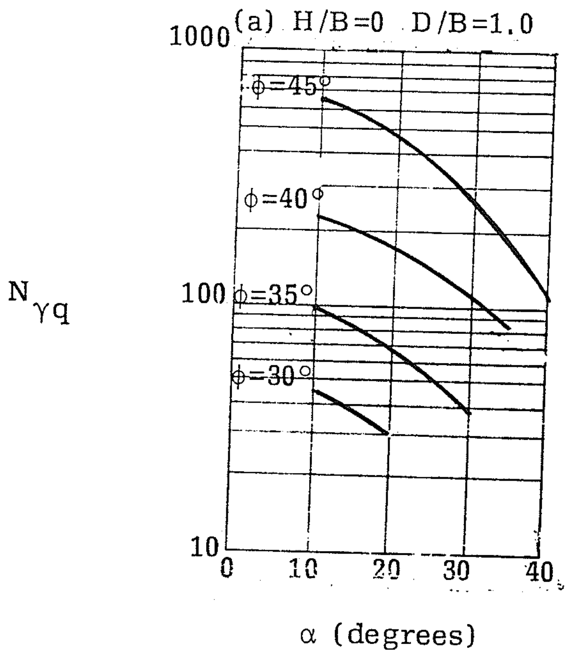

FIGURE 5.3 $N_{\gamma q}$ vs α FOR A FOOTING AT THE CREST OF A SLOPE

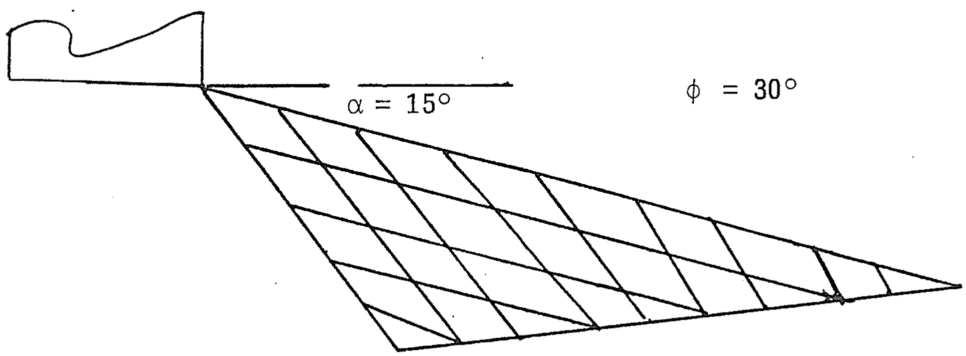

FIGURE 5.4: TYPICAL SLIP LINE FIELD FOR UNIFORM SURCHARGE ON SLOPE.

CHAPTER 6

FOOTING LOCATED AWAY FROM THE CREST OF THE SLOPE - PARAMETRIC STUDY AND RESULTS

6.1 INTRODUCTION

In addition to the variables ϕ, α and D which influence bearing capacity (Chapter 5), this chapter is particularly concerned with the influence of H, (the distance from the crest of the slope to the edge of the footing). It has been found convenient to normalize the parameters D and H, by dividing them by the footing breadth B. That is, they are expressed as the dimensionless parameters D/B and H/B respectively. Since only shallow footings were considered, analyses were carried out for $0 \leqq D/B \leqq 1.0$. The range of H/B values tested depended on the size of the zone within which the bearing capacity is influenced by the presence of the slope. At large values of H/B, the failure zone extends to the ground surface as if the slope were not present. This phenomenon is discussed further in Section 6.3. The maximum range considered was $0 \leqq H/B \leqq 3.0$.

6.2 THE EQUIVALENT SLOPE

The concept of an "equivalent slope" was used by Giroud and Vo-Nhiem to determine the bearing capacity of a footing located away from a slope (Figure 6. 1). The procedure for determining the equivalent slope, used in this thesis is outlined below.

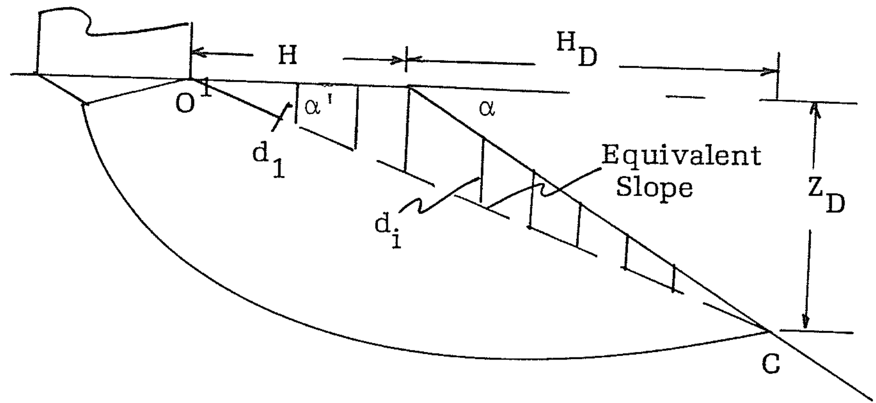

FIGURE 6.1 DEFINITION OF EQUIVALENT SLOPE

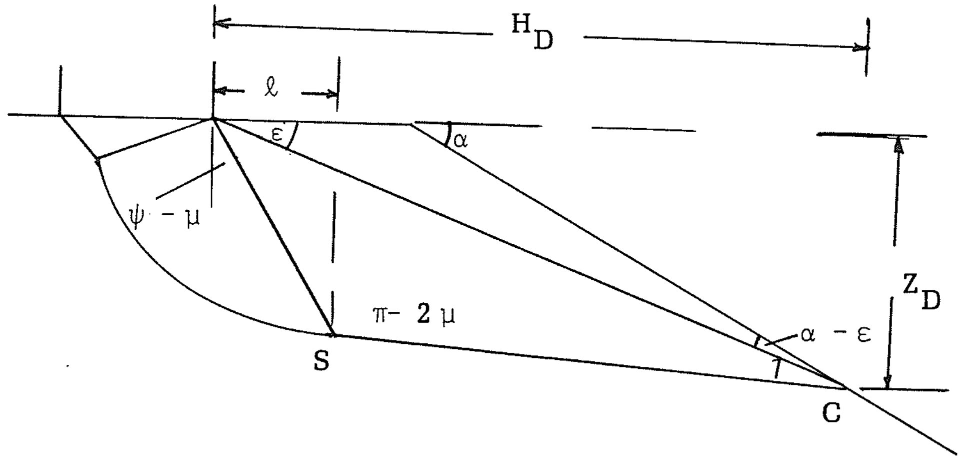

FIGURE 6.2 DETERMINATION OF THE "SIZE" OF THE FAILING DOMAIN.

Consider Figure 6.2 which shows the case of a footing located at the crest of a slope. The distance 'ℓ' is taken as the characteristic length and establishes the scale of the computation. From simple geometry, we obtain the following expressions for z_D and H_D respectively.

$$z_D = \ell \left\{ \frac{\sin(\alpha + \varepsilon)\sin(2\mu - \varepsilon) + \sin\varepsilon\cos(\psi + \mu)}{\cos(\alpha + \varepsilon)\sin(2\mu - \varepsilon)} \right\} \quad \ldots\ldots 6.1$$

and

$$H_D = \ell \left\{ \frac{1 + \sin\varepsilon\sin(\psi + \mu)}{\cos(\alpha + \varepsilon)\sin(2\mu - \varepsilon)} \right\} \quad \ldots\ldots 6.2$$

Once 'ℓ' is chosen or established by the analyst, all the quantities on the right hand side of Equations 6.1 and 6.2 are known or can be specified since, from the geometry of Figure 6.2, ε is given by $\varepsilon = \pi/2 - \alpha - \psi + \mu$.

It was therefore possible to calculate z_D and H_D values for any combination of ϕ, α and H. These parameters define the 'size' of the failure domain and the equivalent slope angle α', since $\alpha' = \tan^{-1}\{z_D/(H + H_D)\}$ (Figure 6.1).

6.3 THE CRITICAL CREST OFFSET Hc

It is now postulated that as the footing is moved further away from the crest of the slope that is, as H is increased (Figures 6.3a,b,c) both z_D and H_D also decrease until they become zero at some critical value H_c

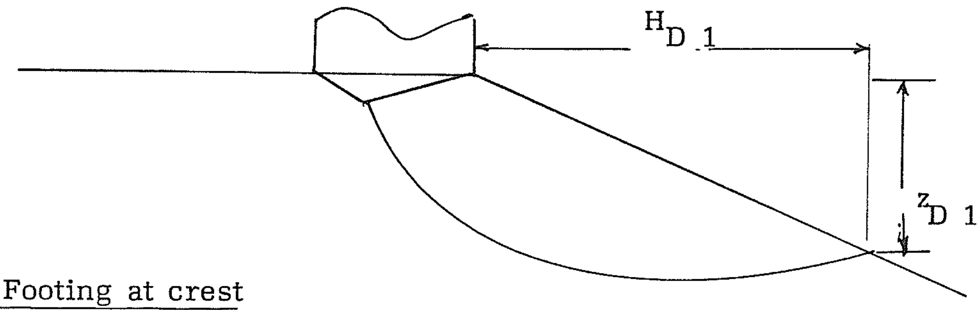

(a) Footing at crest

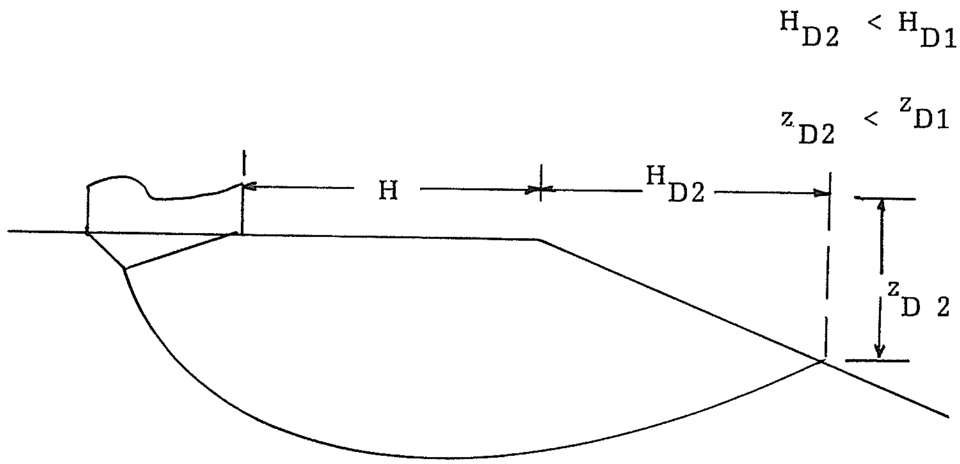

(b) Footing at a distance H from crest

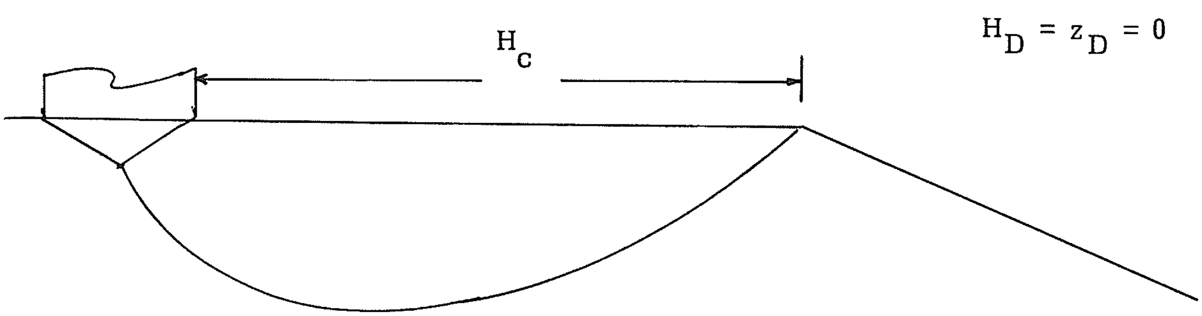

(c) Footing at a distance H_c from crest

FIGURE 6.3 THE EFFECT ON THE SLIP LINE FIELD OF MOVING THE FOOTING AWAY FROM THE SLOPE

(Figure 6.3c). This means that when $H \geq H_c$ the effect of the slope on the bearing capacity is not non-existent. For the case of a footing located at a distance H from the crest, where $0 < H < H_c$ the equivalent slope angle is defined in Figure 6.1 as

$$\alpha' = \tan^{-1}\{ z_D/(H + H_D) \} \qquad \ldots\ldots 6.3$$

An estimate of the distance H_c was obtained from the work of Suppiah (1981). Suppiah considered interfering footings and developed Figure 6.4 which gives an indication of minimum spacing between footings for zero interference. This can also be considered a measure of the "size" of the fialing domain. We can think of the slope as "interfering" with the slip line field as long as the footing is located at a distance from the crest which is smaller than the "size" of the failing domain. The values of H_c deduced from Suppiah's work are presented in Table 6.1.

ANGLE OF INTERNAL FRICTION ϕ (degrees)	H_c*
30	1.2B
35	2.0B
40	2.7B
45	3.5B

TABLE 6.1 ESTIMATED H_c VALUES (after Suppiah, 1981)

* It should be noted that edge to edge spacing is used in this thesis while Suppiah used centre to centre spacing for his parameter S.

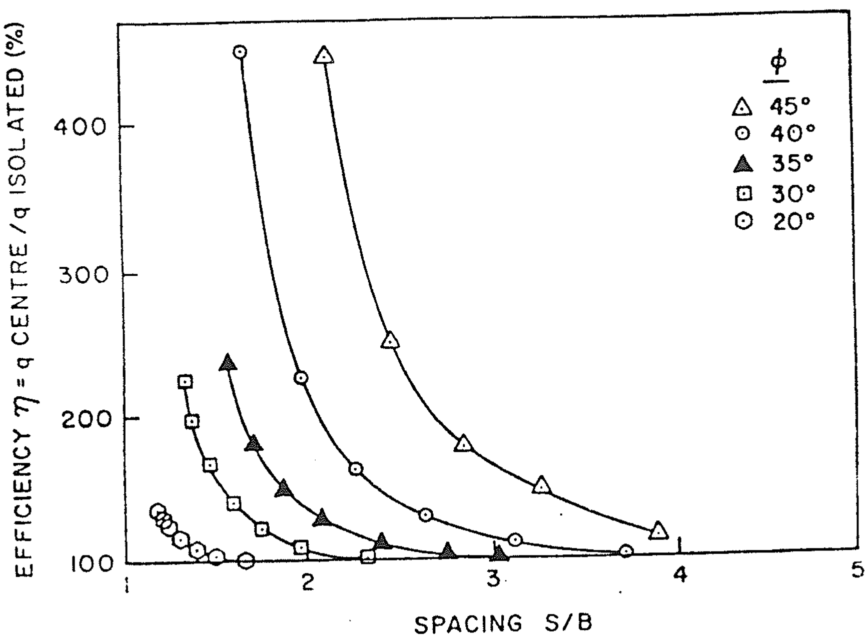

FIGURE 6.4 EFFECT OF FOOTING SPACING ON BEARING CAPACITY

(after Suppiah 1981)

6.4 DEFINITION OF THE FAILURE ZONE FOR $0 < H < H_c$

The manner in which z_D and H_D reduces to zero as H/B varies from zero to H_c/B is not known precisely. However, intuition suggests that the slope effect would be greater near to the slope, and would reduce as the distance from the slope increases. That is, the rate at which z_D decreases as H/B increases would be slow at first, but would increase as H/B increases. However, at this time, there is no definite observational nor scientific basis for modelling the way in which z_D varies. At this stage therefore, it is considered satisfactory to assume simply a linear relationship between z_D and H/B. Using the values of z_D calculated from Equation 6.1 and the H_c/B values from Table 6.1, curves showing the relationship between z_D and H/B for various values of ϕ and α have been prepared. These are shown on Figure 6.5.

It is also reasonable to assume that as H/B increases from 0 to H_c, that is, as the footing is moved away from the crest of the slope, the elastic wedge changes from the asymmetrical shape developed in Chapter 4, to a symmetrical ϕ wedge for a footing on level ground as utilised by Graham and Stuart (1971). Since there is no observational evidence currently available, it is again assumed that the parameters defining the geometry of the

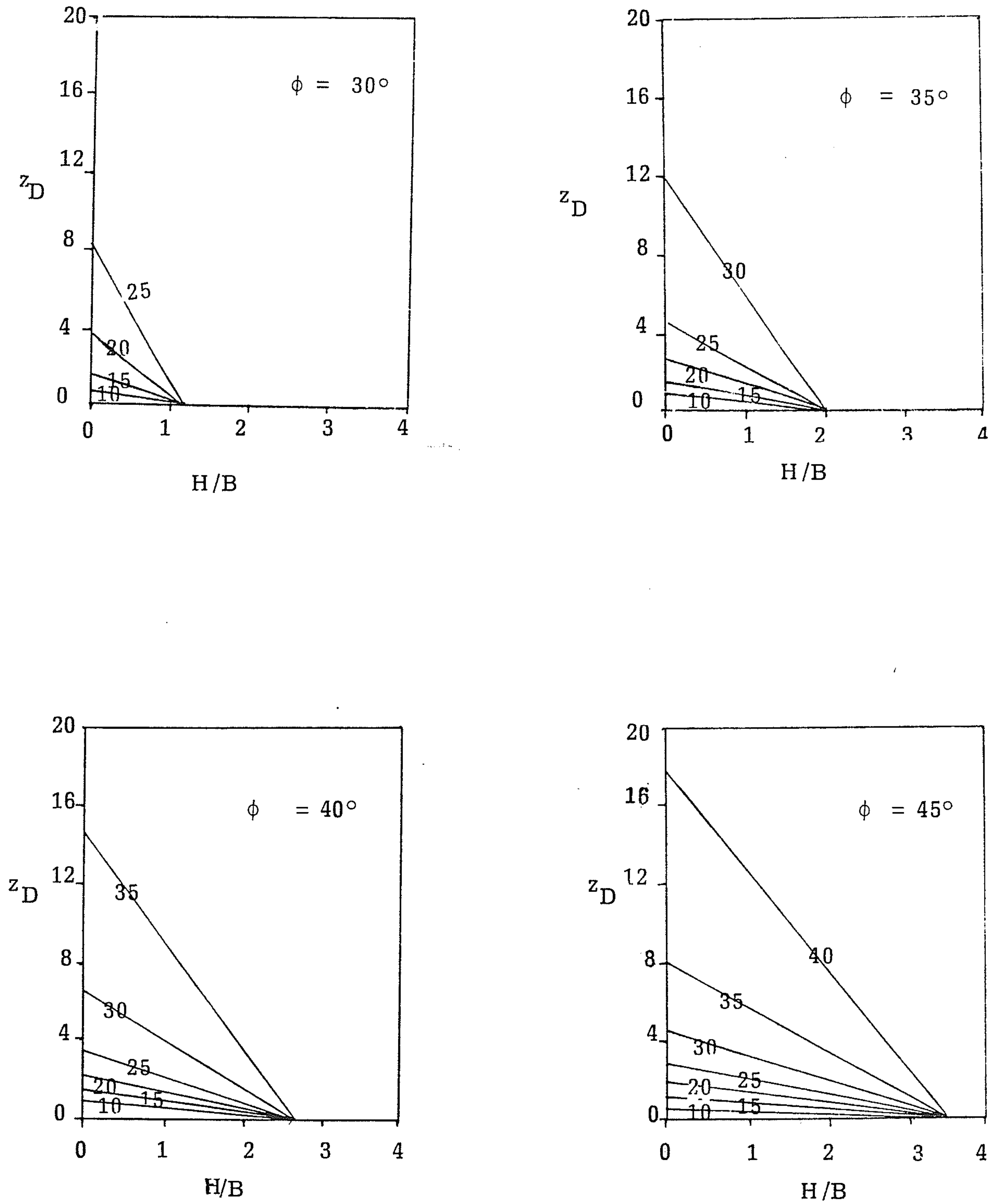

Note: The values on the curves are values of α.

FIGURE 6.5 PLOTS OF z_D vs H/B

the wedge, that is, ω_r and x_ℓ/x_r vary linearly as H/B varies from 0 to H_c. Graphical representation of the linear plots is shown on Figure 6.6. These figures were used to obtain intermediate values of x_ℓ/x_r for use in the subsequent analyses.

6.5 PARAMETRIC STUDY AND RESULTS

6.5.1 Surface Footings

For this case, the triangular surcharge on the equivalent free surface O'C (Figure 6.7.) was treated as an equivalent uniformly distributed surcharge. From the geometry, the equivalent uniformly distributed surcharge is given by

$$b' = H \sin \alpha' /2$$

Using the subroutine EDGPA3 (Chapter 5) which computes the slipline field in the region between the equivalent free surface and the edge of the passive zone, and the main program, the entire slipline field was calculated for various values of H/B, α and ϕ. The maximum value of H/B for a given ϕ, corresponds to that obtained from Table 6.1. ϕ values were from 30° to 45° and α values from 10° to $(\phi - 5)^\circ$.

6.5.2 Shallow Footings

For each value of ϕ and α and specified values of H/B, the values of z_D and H_D were determined from Equations 6.1 and 6.2 respectively, and the equivalent slope angle calculated from Equation 6.3.

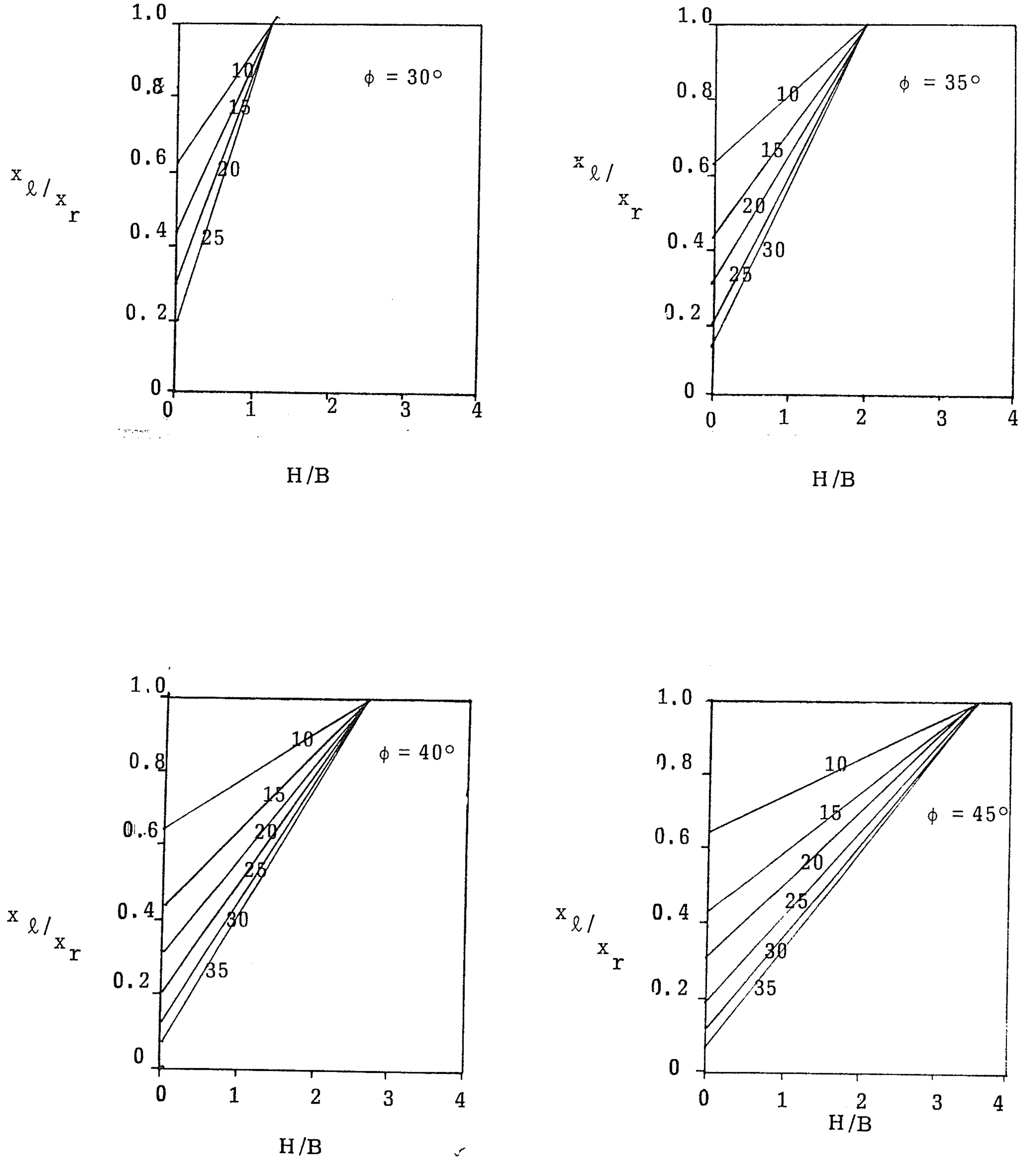

Note: The values on the curves are values of α.

FIGURE 6.6 PLOTS OF x_ℓ/x_r vs H/B

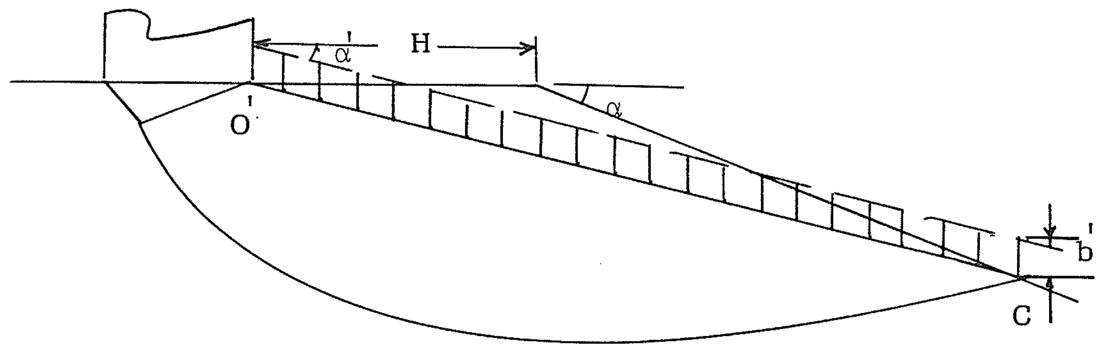

FIGURE 6.7: EQUIVALENT SURCHARGE FOR A SURFACE FOOTING

In order to set the scale of the failure domain and to simplfy the programming, the set back from the crest of the slope to the edge of the footing (H) was set to be equal to 1.0. The distance H + H_D was then expressed as n. (Figure 6.8). The value of n = 1.0 corresponds to the case of a footing at the point of "zero slope interference". Larger values of 'n' correspond to moving the footing further towards the crest of the slope. Based on the problem geometry (Figure 6.1 and 6.8), it was possible to determine values of n for the range of ϕ, α and H/B values being considered. For a given ϕ 'n' was found to vary over a very narrow range for different values of α as indicated on Figure 6.9, that is, 'n' was not very sensitive to changes in α, for a given ϕ. A plot of the average value of 'n' against H/B for $\phi = 45°$ is shown on Figure 6.9. The parameter 'n' being a ratio of distances and therefore a dimensionless quantity was found to be more useful than having to specify values of H_c, z_D and H in the analyses.

The next step in the analysis involves computing the stresses on the equivalent free surface O'C. The vertical stress at any point O'C is equal to γd_i. (Figure 6.1). The value of σ and ψ on O'C can therefore be determined from the Mohr's circle (Figure 6.10). These parameters are as follows:

$$\sigma = \frac{\sigma_v}{1+\sin\phi \quad \cos \ 2\psi} \qquad \ldots\ldots\ldots\ldots 6.3$$

and,

$$2\psi = \pi - \varepsilon - \sin^{-1}(\sin\varepsilon/\sin\phi) \qquad \ldots\ldots\ldots 6.4$$

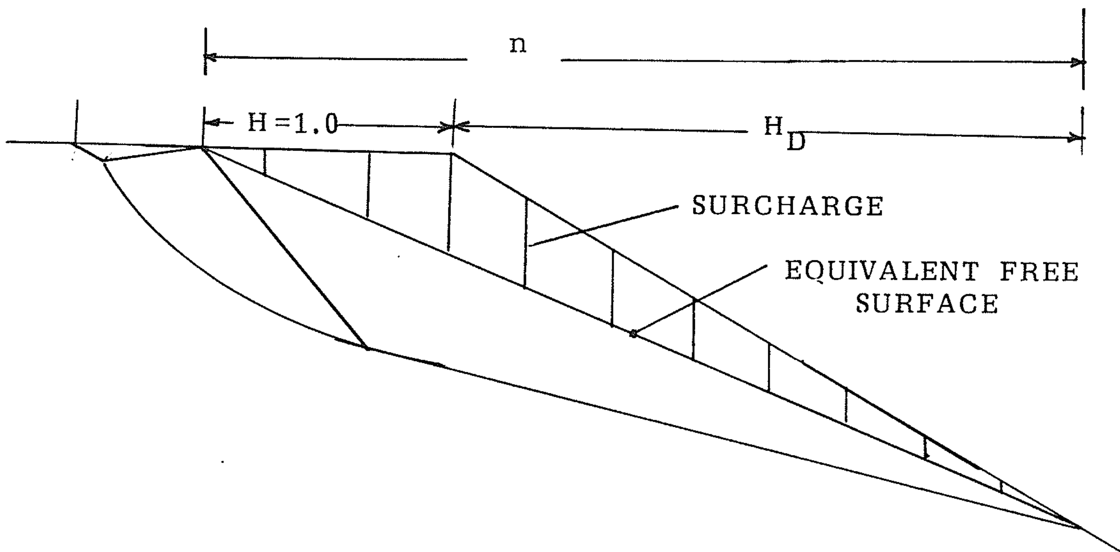

FIGURE 6.8 SIMPLIFICATION OF THE PROBLEM FOR PROGRAMMING

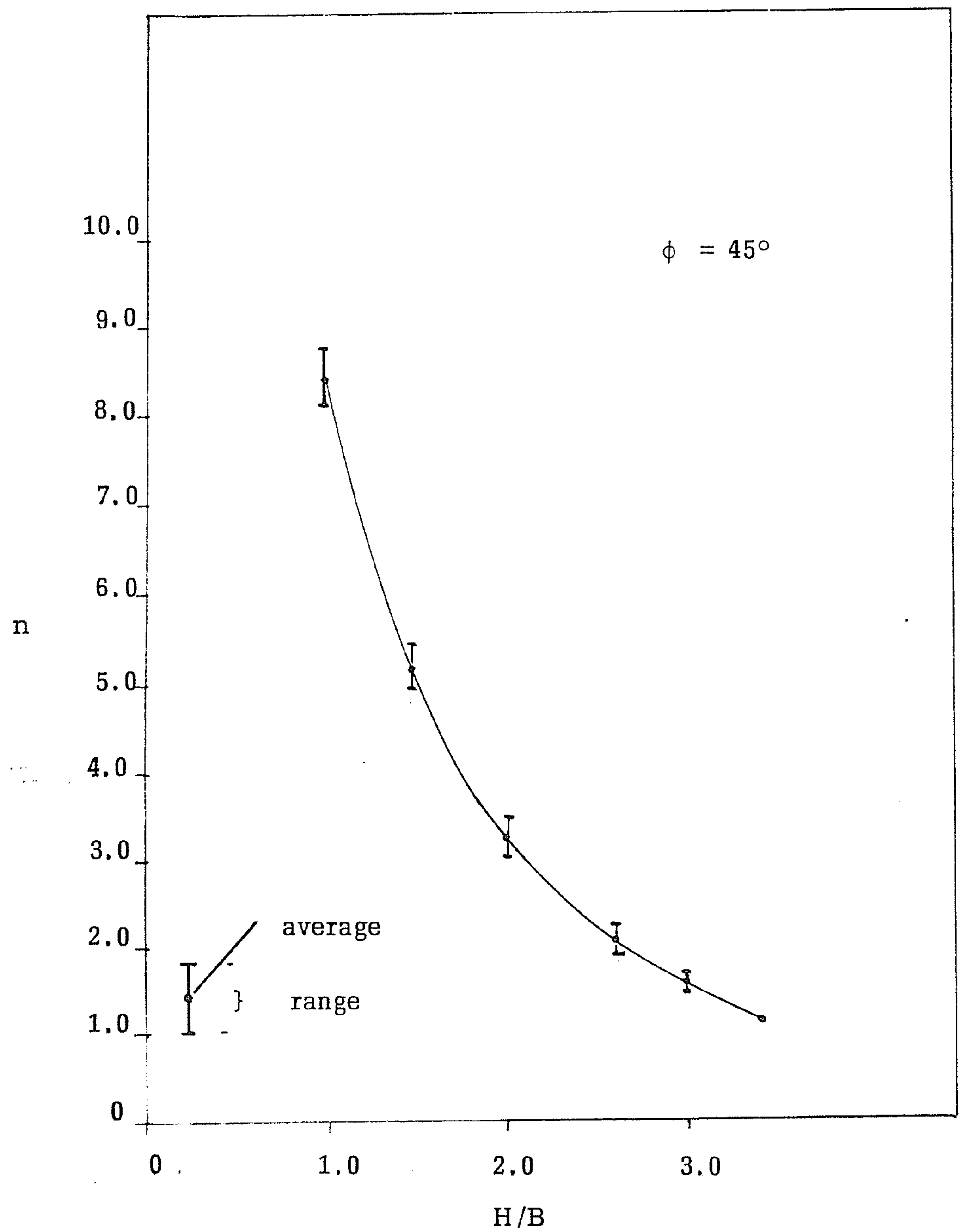

FIGURE 6.9 PLOT OF n vs H/B

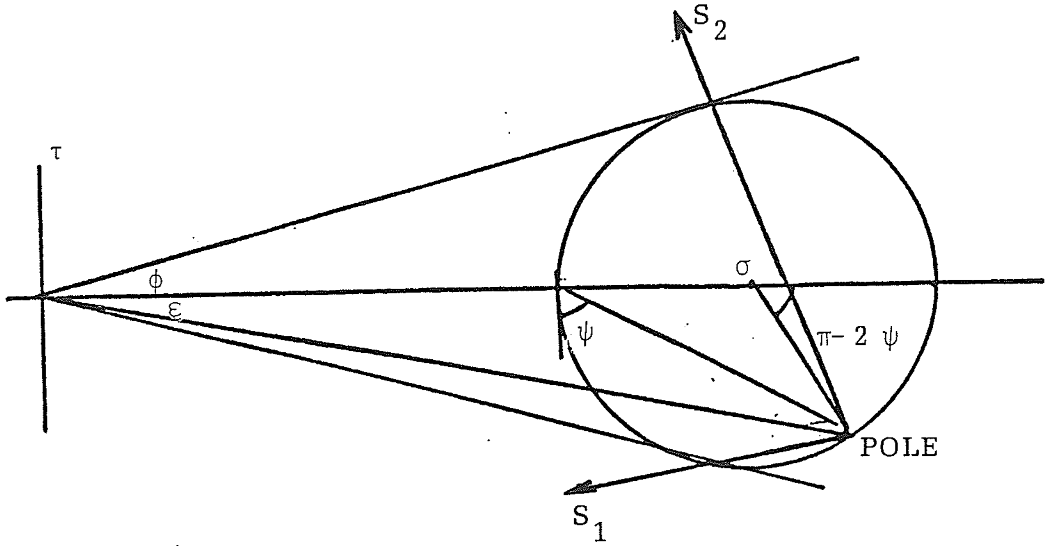

FIGURE 6.10 MOHR'S CIRCLE FOR STRESSES ON EQUIVALENT FREE SURFACE.

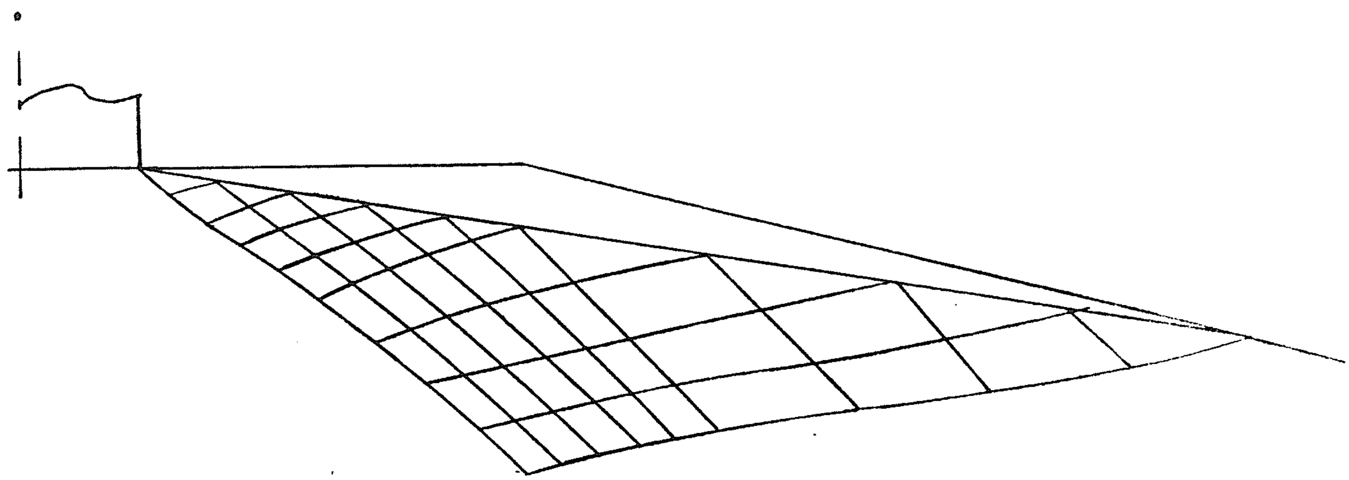

FIGURE 6.11 TYPICAL SLIP LINE FIELD IN THE REGION BETWEEN EQUIVALENT SLOPE AND PASSIVE ZONE.

The stress on O'C and the slip line field in the region between the equivalent free surface and the edge of the passive zone was then computed using the subroutine EDCPA2. This subroutine also computes the slip line field in the region between the equivalent surface and the edge of the passive zone. A typical result of the slip line field is shown on Figure 6.11. The main program was then used to compute the bearing capacity factor and the remainder of the slip line field. This analysis also yields a value for the footing width B.

Different embedment depths were then simulated by adding an artifical surcharge which was a known multiple of B, (that is 0.25B, 0.50B, 0.75B, and 1.0B) to the ground surface. The stresses on O'C were in this case computed by adding the true triangular surcharge to the artificial surcharge.

Values of $N_{\gamma q}$ were calculated for $\phi = 30°$ to $45°$, $\alpha = 10$ to $(\phi-5)$ degrees and $D/B = 0.0$ to 1.0. The range of H/B values analysed depends on ϕ and are shown on Table 6.1.

The results are presented in the form of graphs of $N_{\gamma q}$ vs α and are shown on Figures 6.11 to 6.16.

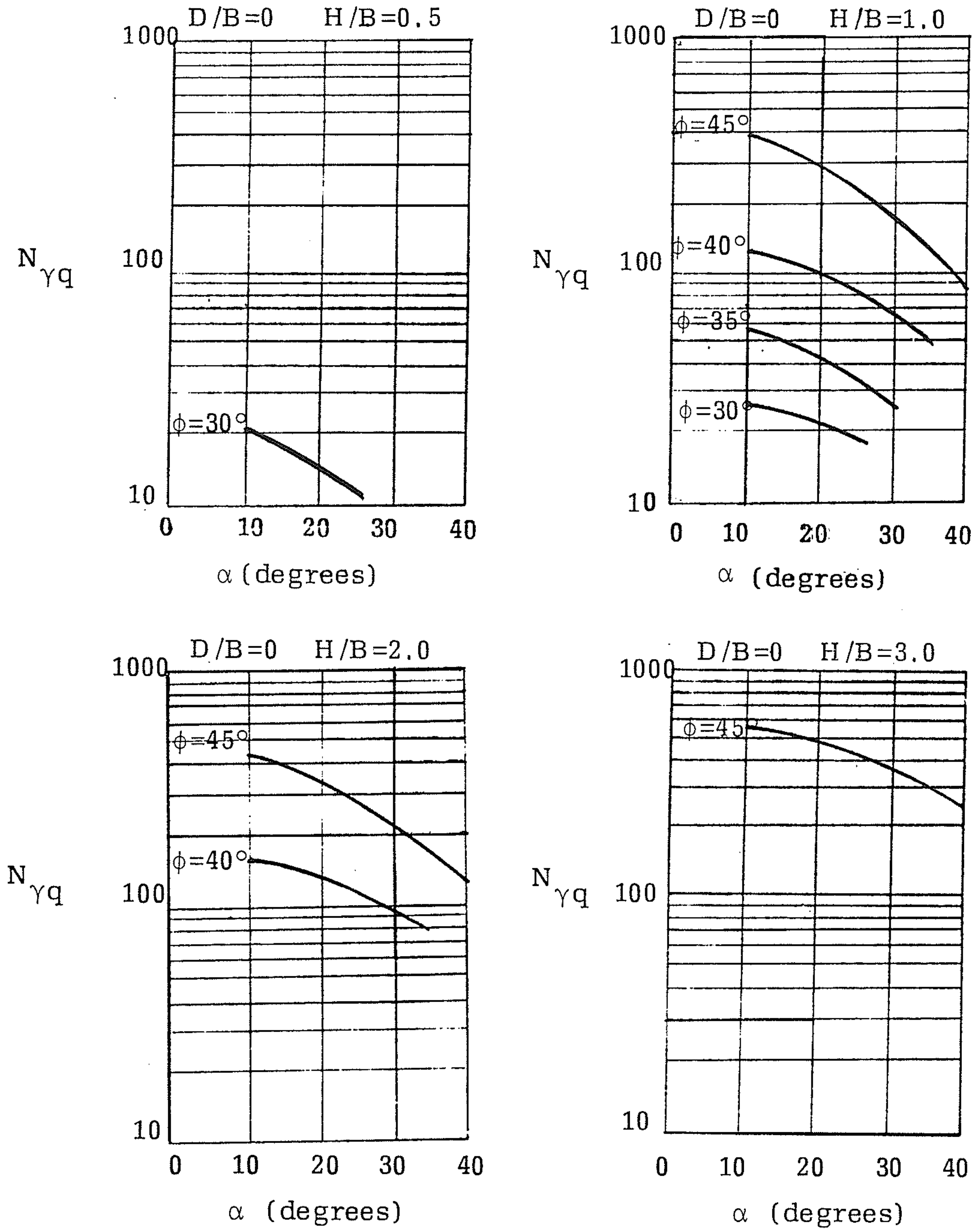

Note: Read in conjunction with Table 6.1

FIGURE 6.12 $N_{\gamma q}$ vs α (SURFACE FOOTING)

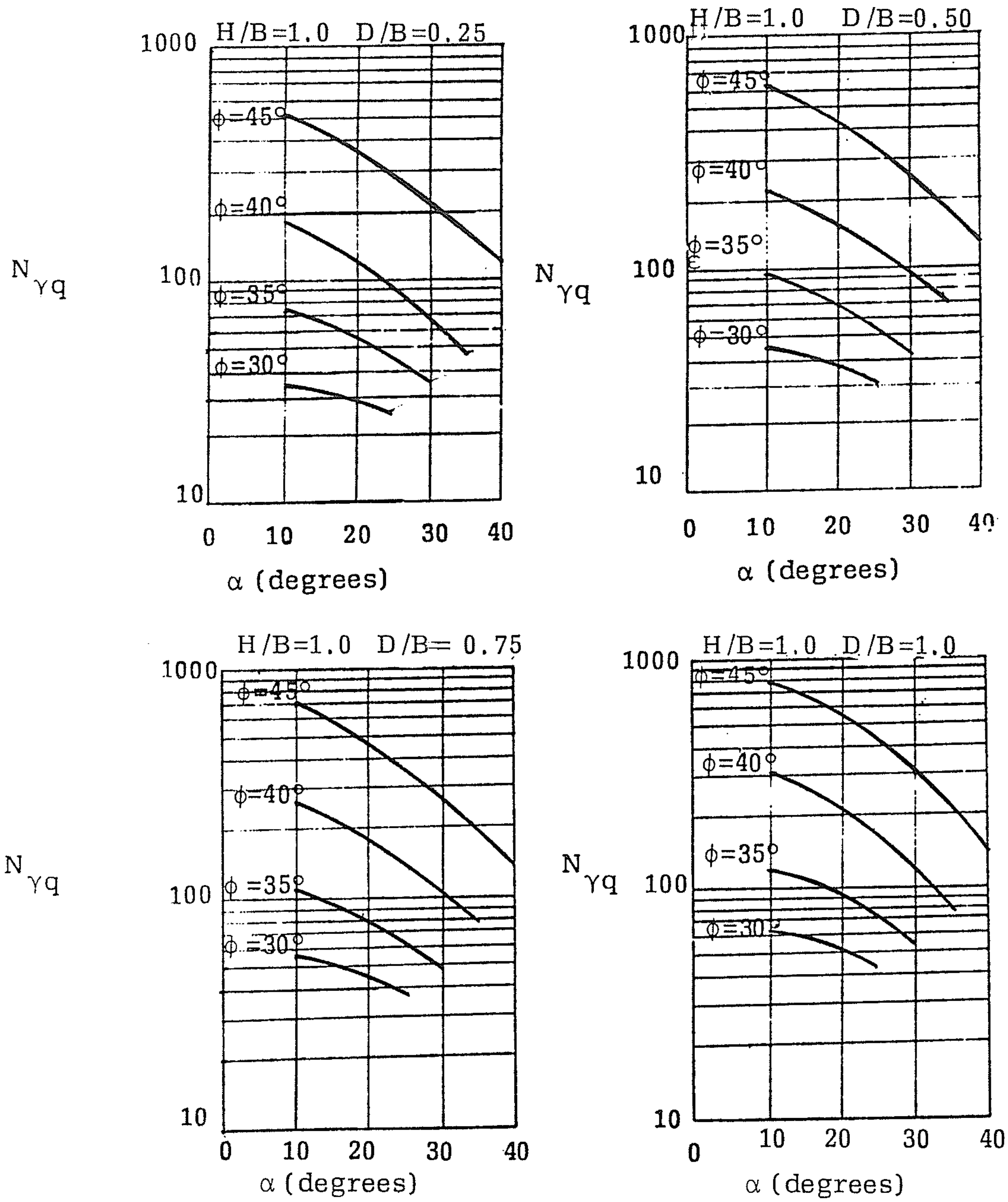

Note: Read in conjunction with Table 6.1

FIGURE 6.13 $N_{\gamma q}$ vs α (SHALLOW FOOTING)

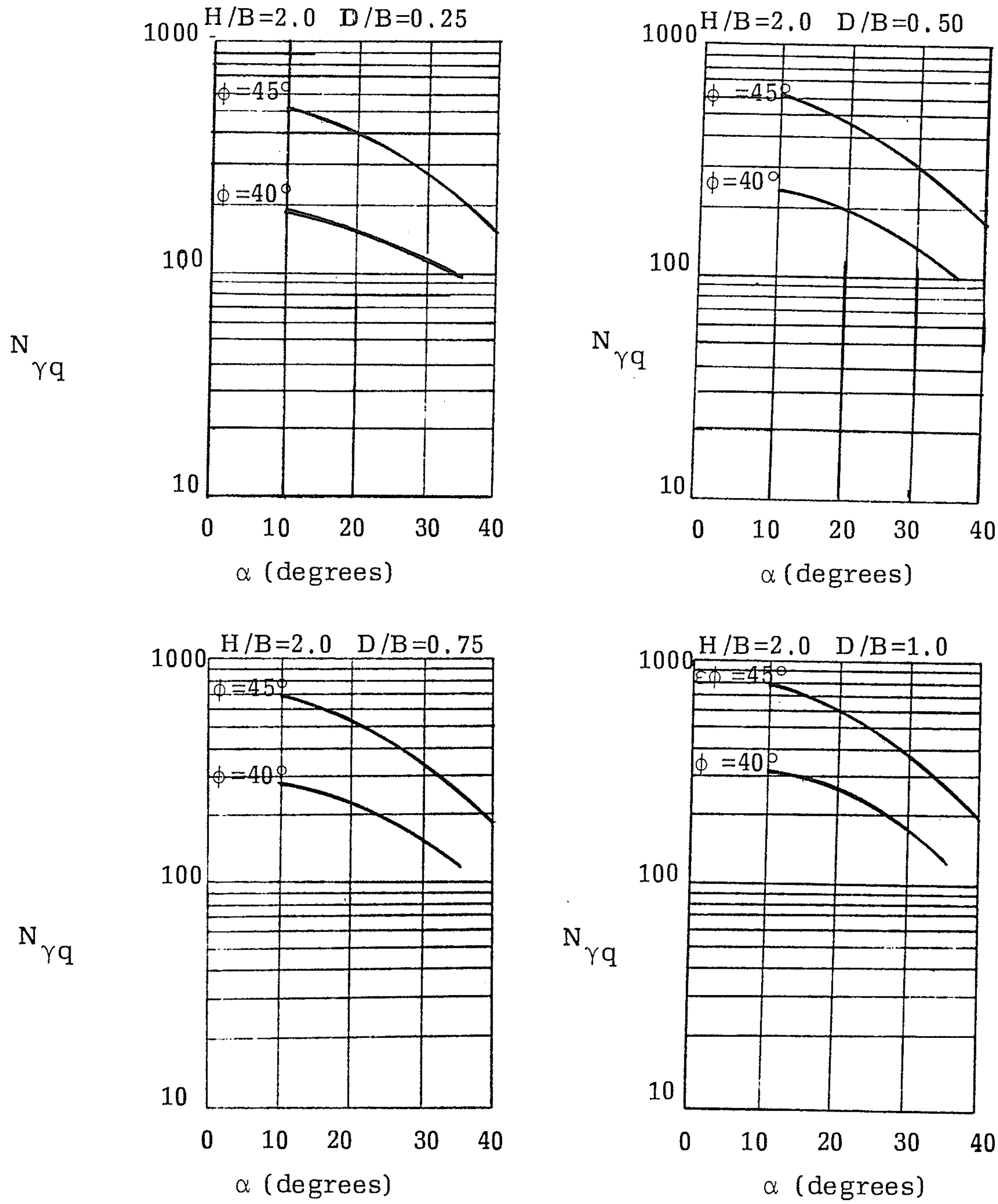

Note: Read in conjunction with Table 6.1.

FIGURE 6.14 $N_{\gamma q}$ vs α

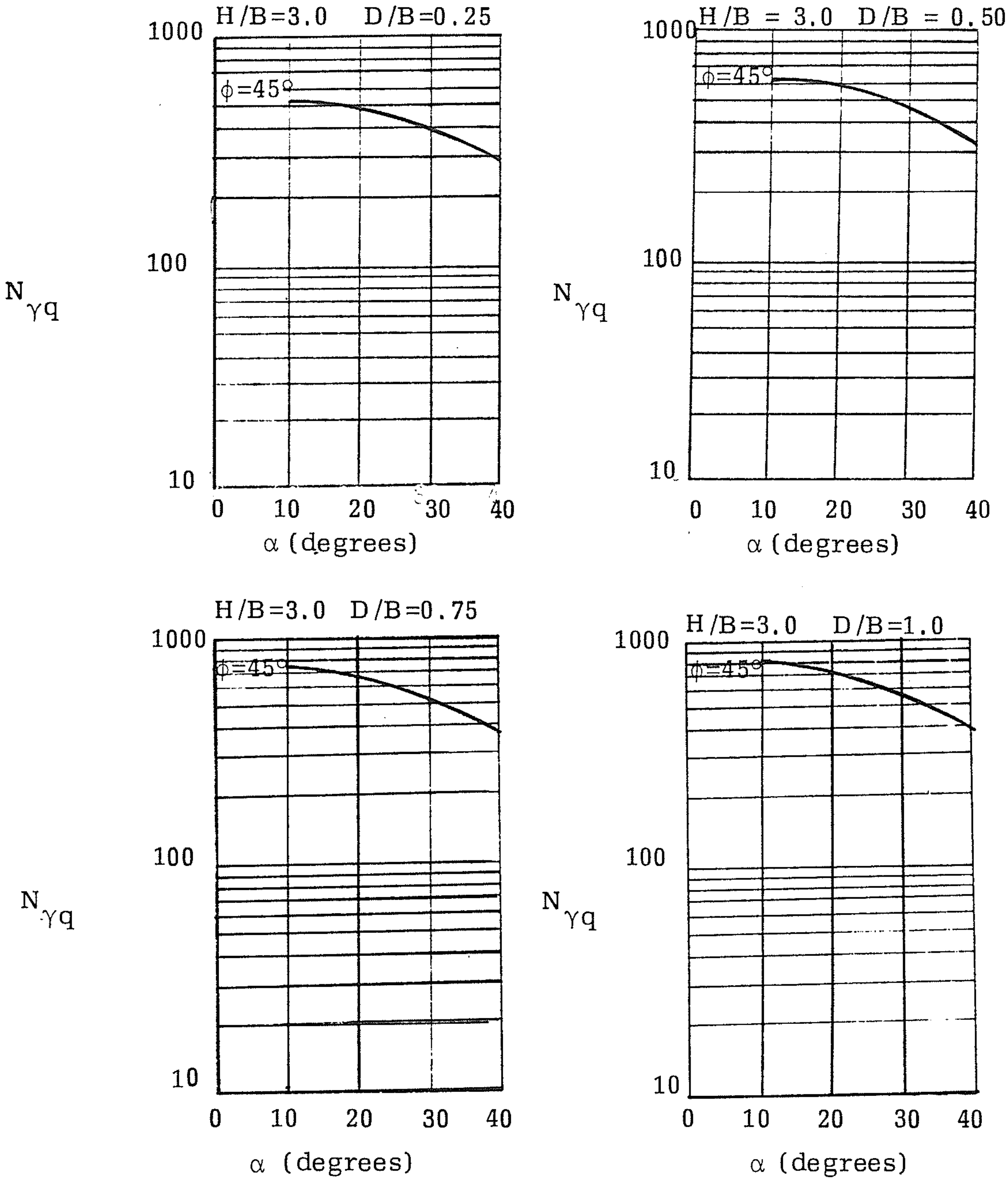

Note: Read in conjunction with Table 6.1

FIGURE 6.15 $N_{\gamma q}$ vs α

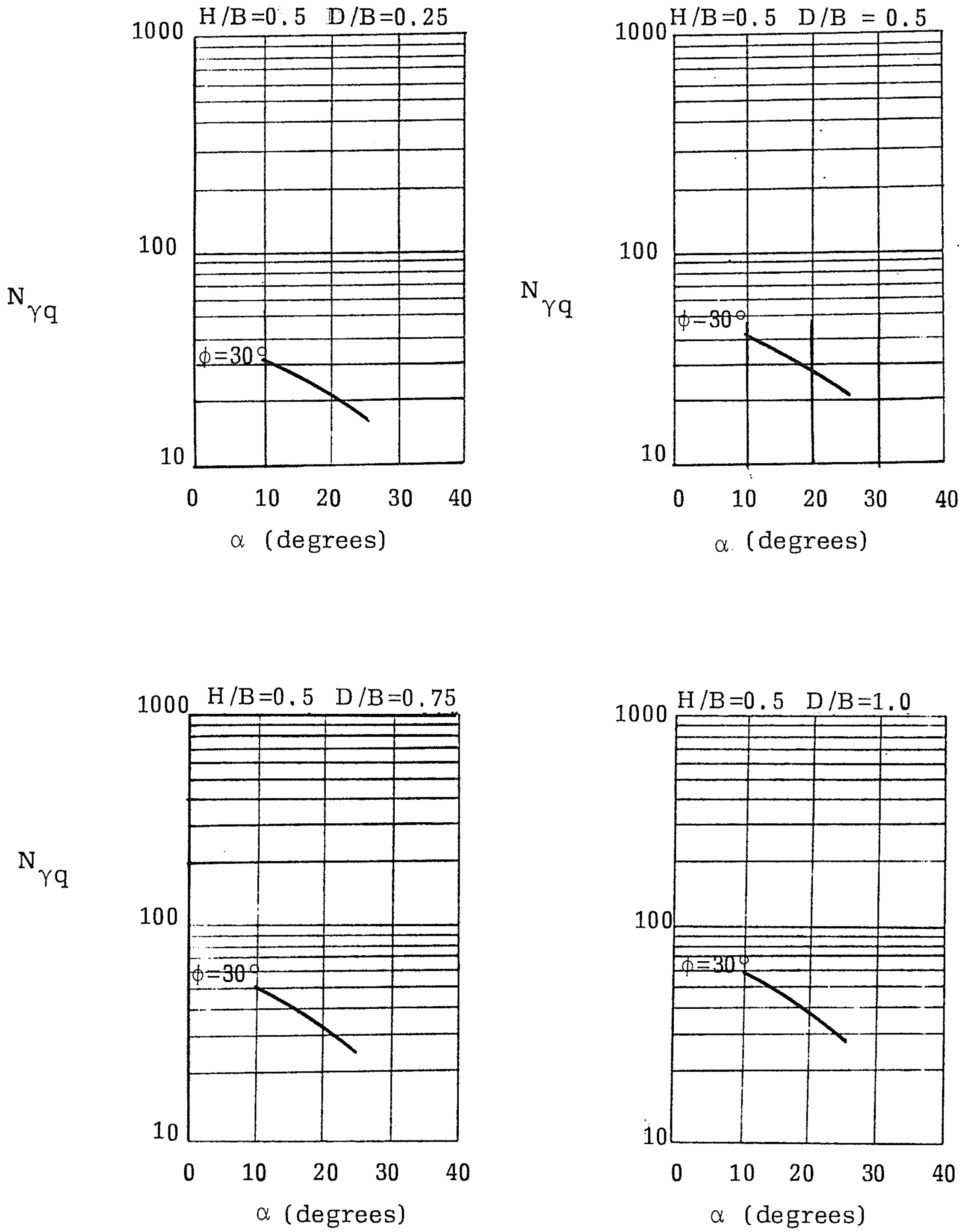

Note: Read in conjunction with Table 6.1

FIGURE 6.16 $N_{\gamma q}$ vs α

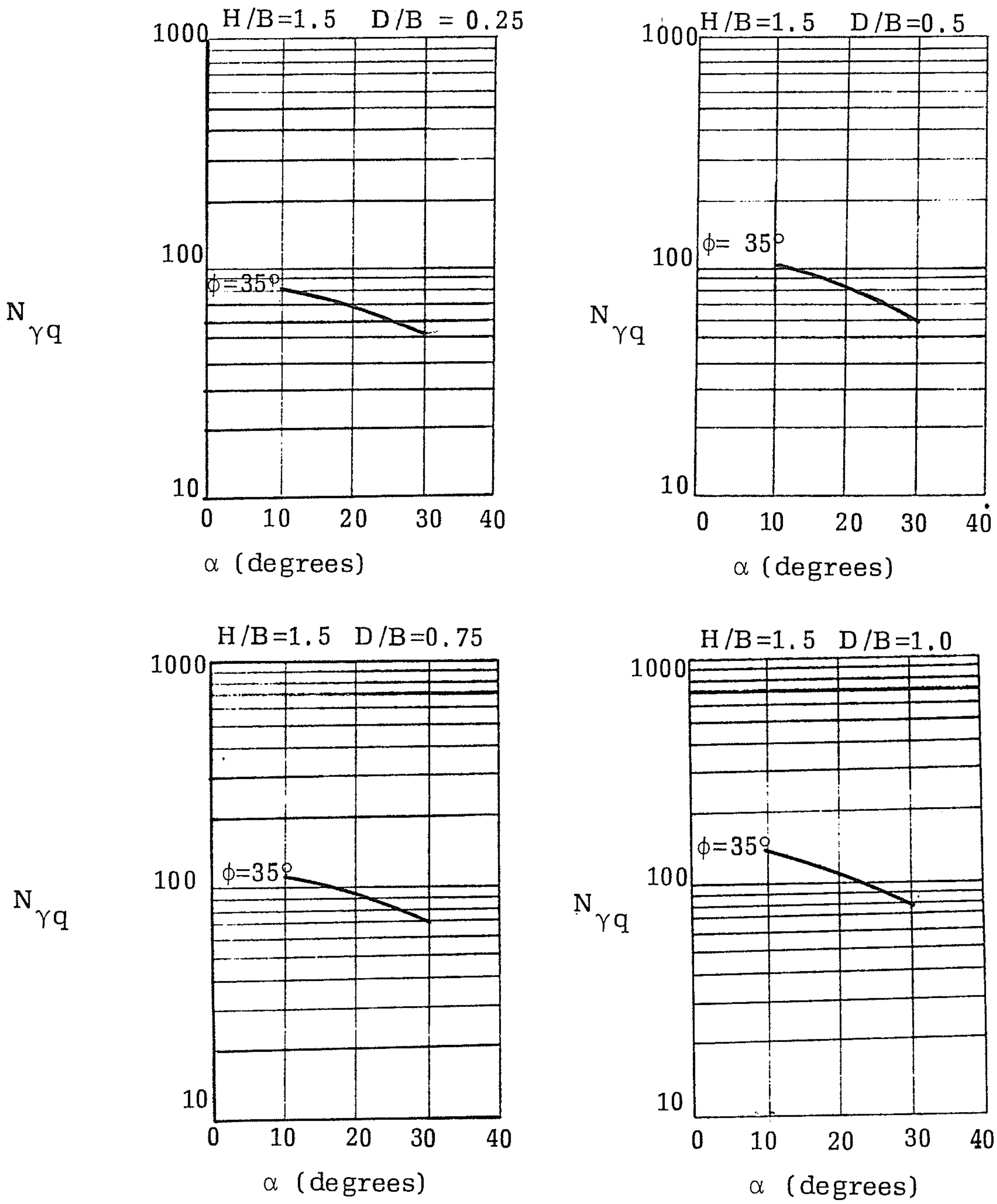

Note: Read in conjunction with Table 6.1

FIGURE 6.17 $N_{\gamma q}$ vs α

CHAPTER 7

COMPARISON OF RESULTS WITH OTHER THEORIES AND LARGE SCALE TEST RESULTS

7.1 INTRODUCTION

In this Chapter the results developed in this thesis and presented in Chapters 5 and 6 are compared with those from the existing available theories, and with available large scale test results. The large scale test results consist of work done by the Geotechnical Group at the University of Ottawa in 1977 and 1978. Tests were done in a box 15.0 m long 2.0 m wide and 2.2 m high. Footing sizes were 0.3 m and 0.6 m wide. All tests were done for a slope angle of 26.5 degrees.

7.2 COMPARISON OF RESULTS WITH EXISTING THEORIES

As noted in Chapter 2, most of the existing theories consider only the case of a surface footing at the crest of a slope. This condition is therefore used as the basis for the subsequent comparisons. The comparisons are made for a ϕ of 40 degrees and are shown graphically on Figure 7.1.

Figure 7.1 shows that for the location considered, in general, the Author's results for $N_{\gamma q}$ are higher than those from most of the other existing theories which cover a large range of $N_{\gamma q}$ values. Because of the limitations outlined in Chapter 2 and the significant scatter indicated in Figure 7.1, no further comparison with theoretical results is considered herein. The remainder of the Chapter is concerned with comparison between the Author's results and the results of large scale testing (Shields et al., 1977).

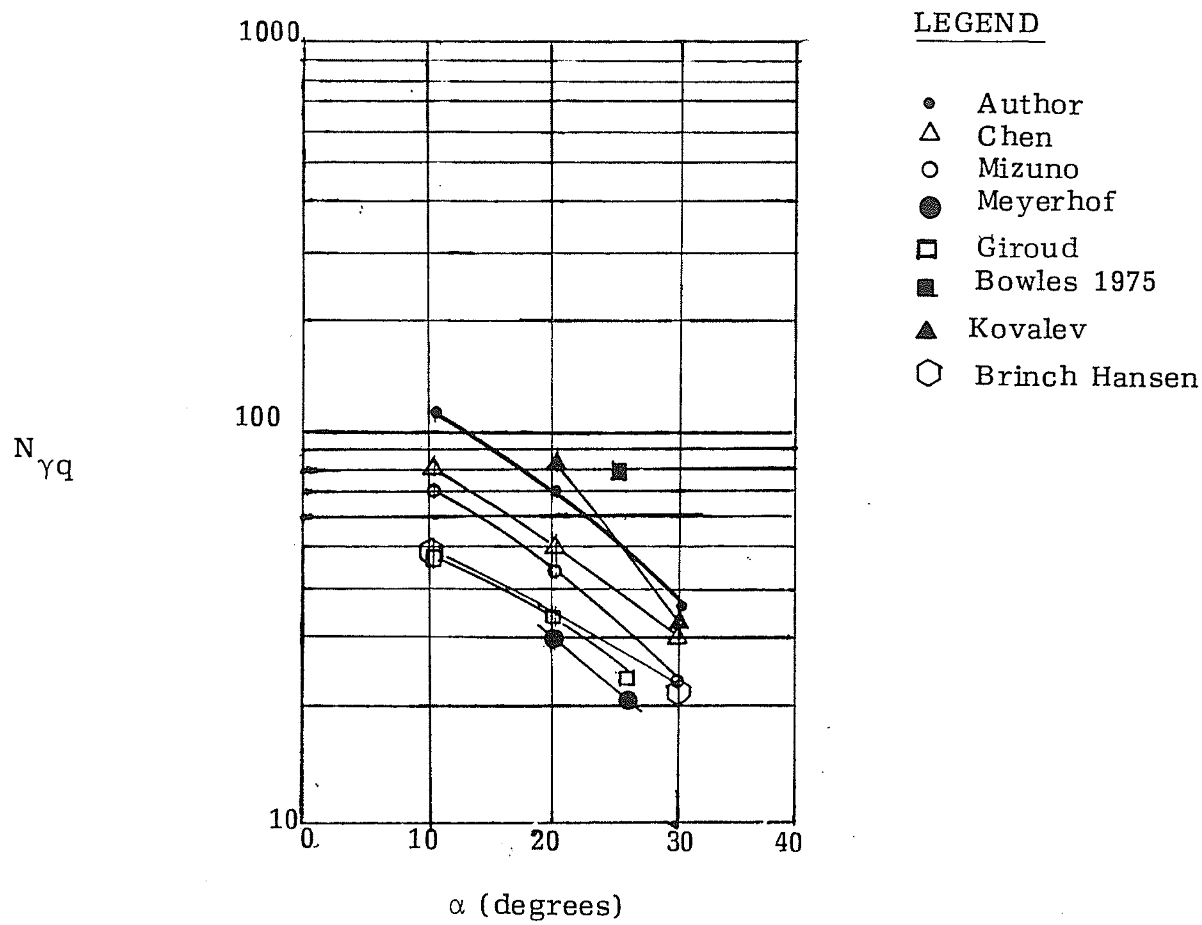

FIGURE 7.1 COMPARISON OF RESULTS FROM THIS THESIS WITH EXISTING THEORIES.

7.3 COMPARISON OF RESULTS WITH LARGE SCALE TEST RESULTS

The method of presentation of $N_{\gamma q}$ values first proposed by Shields et al., 1977 and shown in Figures 7.2 and 7.3 is used as the basis for comparison of the results.

Figure 7.2 compares the $N_{\gamma q}$ values computed by the Author with the $N_{\gamma q}$ values obtained by Shields et al. for compact sand (ϕ triaxial = 37°). The theoretical values for $\phi = 37°$ have been interpolated between the values of $\phi = 35°$ and $\phi = 40°$ presented earlier.

The Figure shows that for any given depth, the $N_{\gamma q}$ values obtained by the Author are higher than those obtained by Shields. A more detailed comparison is made in Table 7.1. This Table represents the case of compact sand with the following properties as indicated by Shields et al.

ϕ triaxial	= 37°
ϕ triaxial + 10 %	$\doteqdot$ 41°
ϕ plane strain	= 45°
ϕ shear box	= 45°

Table 7.1 indicates that there is reasonable agreement between the theoretical and experimental results for ϕ equal to the triaxial value. That is, ($N_{\gamma q}$-theoretical) /($N_{\gamma q}$-experimental) varies from 1.20 to 1.35. For ϕ equal to ϕ triaxial plus 10 %, (a common approximate method for converting from triaxial ϕ to plane strain ϕ), the ratio varies from 2.61 to 3.33.

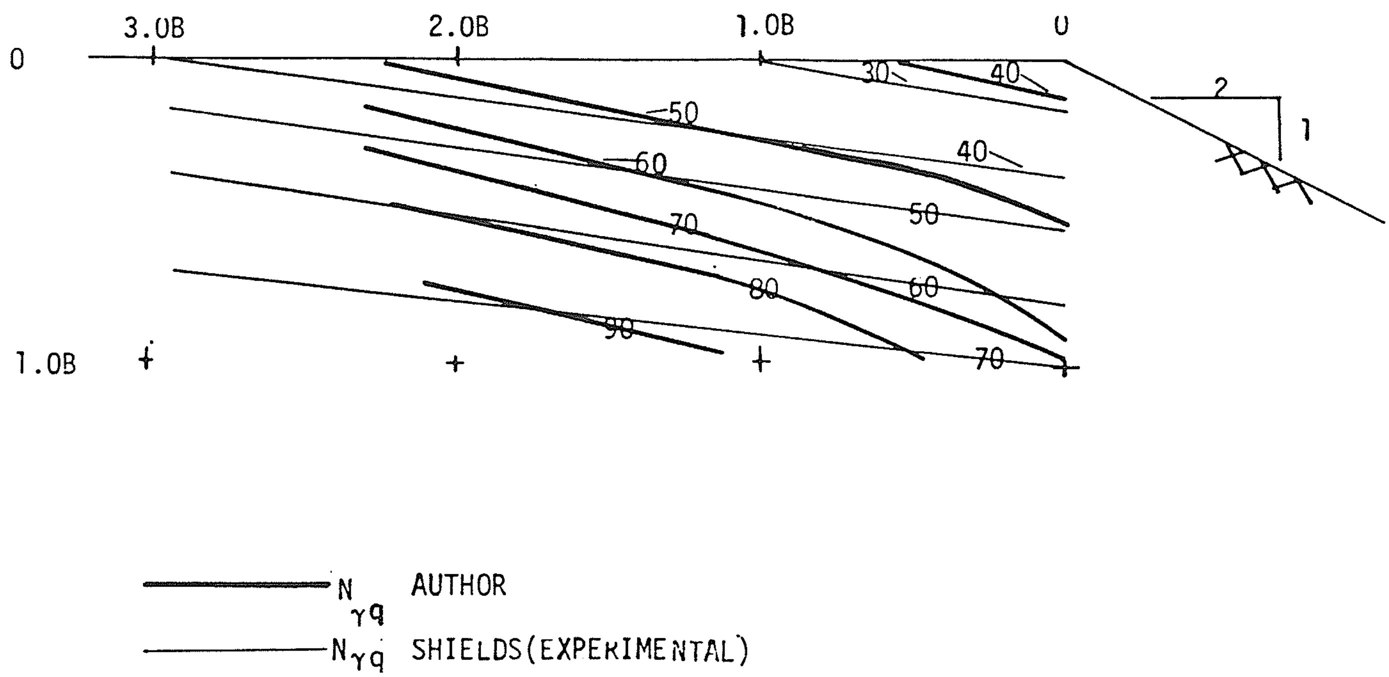

FIGURE 7.2 CONTOURS OF $N_{\gamma q}$ VALUES IN COMPACT SAND

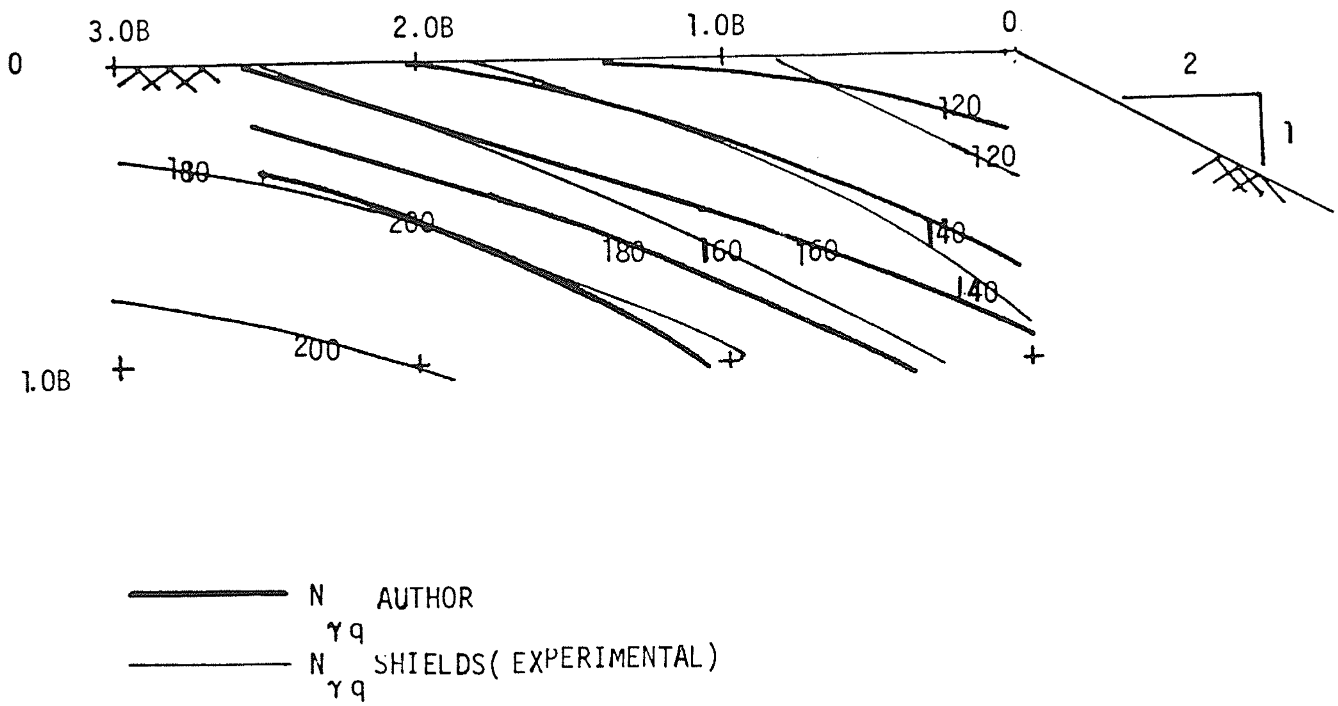

FIGURE 7.3 CONTOURS OF $N_{\gamma q}$ VALUES IN DENSE SAND

Table 7.2 presents comparisons for a dense sand with the following properties;

ϕ triaxial	$= 41°$
ϕ triaxial + 10 %	$= 45°$
ϕ plane strain	$= 48°$
ϕ shear box	$= 50°$

Again it is found that good agreement between the theoretical and experimental values is obtained for $\phi = \phi$ triaxial. The value of the ratio ($N_{\gamma q}$-theoretical)/($N_{\gamma q}$-experimental) ranges from 0.64 to 1.30. If the plane strain value is used, the ratio ranges from 1.40 to 2.50.

Although the plane strain ϕ would normally be expected to yield theoretical bearing capacity values which agree more closely with the experimental values, (Graham and Stuart, 1971), this is not the case for the theory presented here. Use of the plane strain ϕ-angle would seriously overestimate the bearing capacity.

H/B	D/B	$N_{\gamma q}$ (1) SHIELDS	$N_{\gamma q}$ AUTHOR $\varphi = 37^{0}$ (2)	$\varphi = 41^{0}$ (3)	(2)/(1)	(3)/(1)
0.0	0.0	24	29	64	1.21	2.67
0.0	0.5	45	58	140	1.29	3.11
0.0	1.0	70	84	176	1.20	2.51
0.0						
1.0	0.0	30	48	100	1.60	3.33
1.0	0.5	55	74	148	1.35	2.69
1.0	1.0	75	100	196	1.33	2.61

TABLE 7.1 COMPARISON OF RESULTS - COMPACT SAND.

H/B	D/B	$N_{\gamma q}$ (1) SHIELDS	$N_{\gamma q}$ AUTHOR $\varphi = 41^{\circ}$	$\varphi = 45^{\circ}$	(2)/(1)	(3)/(1)
0.0	0.0	100	64	140	0.64	1.40
0.0	0.5	120	140	300	1.16	2.50
0.0	1.0	150	176	320	1.17	2.13
1.0	0.0	120	100	200	0.83	1.67
1.0	0.5	150	148	300	0.98	2.00
1.0	1.0	180	196	380	1.09	2.11
2.0	0.0	150	148	260	0.98	1.73
2.0	0.5	175	208	350	1.19	2.00
2.0	1.0	200	260	450	1.30	2.25

TABLE 7.2 COMPARISON OF RESULTS - DENSE SAND

CHAPTER 8

CONCLUSIONS AND FURTHER RESEARCH

8.1 CONCLUSIONS

Bearing capacity coefficients $N_{\gamma q}$ have been calculated for footings at close proximity to a slope. The results are presented in the form of graphs of $N_{\gamma q}$ vs α for ϕ angles ranging from 30 to 45°, 0.0 < D/B < 1.0 and H/B values from 0 to 3.0B, (Figures 5.2, 5.3 and 6.11 to 6.17). The results agree within 64-160 % (average 115 %), with experimental values of $N_{\gamma q}$ when the triaxial value of ϕ is used. Calculation of $N_{\gamma q}$ using stress characteristics required an estimation of the shape of the trapped elastic wedge beneath the footing. This shape was modelled in the analysis.

8.2 FURTHER RESEARCH

It is well known that the value of ϕ varies with stress level because of the curvature of the Mohr envelope. This thesis takes no account of varying stress levels in the failing domain that is, a constant ϕ analysis was done. The solution could be improved by carrying out a variable-ϕ analysis (Graham and Hovan 1986).

The effect of scale (footing size) on the bearing capacity factor if considered in the analysis could also further refine and improve the results. This would then need model tests using a centrifuge, and work of this type is currently projected at the Laboratoire Centrale des Ponts et Chaussees, France. It would also need additional laboratory testing to characterize the sand in the way used in the analysis.

The proposed model for determination of the shape of the trapped elastic wedge needs to be confirmed by a comprehensive programme of testing, preferably large scale testing. In addition, further confidence in the theory may be established by a programme of experimental work to determine the $N_{\gamma q}$ values for various combinations of ϕ and α.

REFERENCES

Bauer, G.E. (1982) "Finite Element Analysis Of Footings In Granular Approach Fills" Proceedings, 4th Int. Conf. on Numerical Methods in Geomechanics, Edmonton, Canada (1982) Vol 2 pp. 741-747.

Bauer, G.E., Shields, D.H., Scott, J.D. (1978). "Final Report On The Bearing Capacity of Footings on Compacted Approach Fill.

Bauer, G.E. and Felio, G.Y. (1984). "Movements Of A Bridge Abutment" 3rd International Conference on Ground Movements and Structures, UWIST, Cardiff, 9-12 July 1984.

Bauer, G.E., and Mowafy, Y.M. (1985) "A non-linear Finite Element Analysis of Reinforced Embankments Under External Loading" Proceedings 5th International Conf. on Numerical Methods in Geomechanics, Nagoya, Japan, April 1-5,1985.

Bauer, G.E. Shields, D.H., Scott, J.D., Gruspier, J.E. (1981) "Bearing Capacity Of Footings In Granular Slopes" Proceeding 10th Int. Conf. on Soil Mech. and Foundation Eng. Stockholm 1981, Vol. 2 pp. 33-36.

Biarez, J, Burel, M, Wack, B. (1961) "Contribution A L'Etude De La Force Portante Des Fondations. Proc. 5th ICSMFE V1, pp 603-609.

Bowles, J.E. (1975), "Spread Footings" Foundation Engineering Handbook edited Winterhorn and Fang. New York, Van Nostrand Reinbold Co.

Bowles, J.E. (1977) "Foundation Analysis and Design" 2nd Edition, McGraw Hill Publishing Co.

Bozozuk, M (1978) "Bridge Foundations Move" Transportation Research Record 678- "Tolerable Movement of Bridge Foundations, Sand Drains, K-Test, Slopes, Culverts, pp. 17-21.

Brinch Hansen, J. (1957) "The Internal Forces In a Circle of Rupture" Danish Geotechnical Institute Bulletin No. 2

Brinch Hansen, J. (1961) "A General Formula For Bearing Capacity" Danish Geotechnical Insitute, Bulletin No. 11.

Brinch Hansen, J. (1965) "The Philosophy of Foundation Design" Design Criteria, Safety Factors And Settlement Limits" Proceedings of a Symposium held at Duke University, April 1965, pp 9-13.

REFERENCES (2)

Brinch Hansen, J. (1966) "Comparison of Methods for Stability Analysis" Danish Geotechnical Institute - Bulletin No. 21.

Hansen, J (1970) "A Revised and Extended Formula For Bearing Capacity" Danish Geotechnical Institute Bullettin No. 28.

Chen, W.F. and Davidson, H.L. (1973) "Bearing Capacity Determination By Limit Analysis" Journal of the Soil Mechanics and Foundations Division, ASCE, Vol. 99, No. SM6, June 1973, pp. 433-449.

Chen, W.F. (1975) "Limit Analysis and Soil Plasticity" Developments in Geotechnical Engineering 7, Elsevier Scientific Publishing Company.

De Beer (1965) " Bearing Capacity and Settlement of Shallow Foundations on Sand" Proceedings of a Symposium held at Duke University, April 1965, Edited by A.S. Vesic.

De Beer, E.E. (1970) "Experimental Determination of the Shape Factors and Bearing Capacity Factors of Sand" Geotechnique 20 No. 4 pp. 387-411.

Dembicki, E, Odrobinski, W., Mrozek, W. (1981) "Bearing Capacity of Subsoils under Strip Foundations". Proceedings 10th Int. Conf. on Soil Mechanics and Foundation Eng. Stockholm 1981 Vol. 2 pp 91-94.

Felio, G.Y and Bauer, G.E, (1984) "Monitoring and Performance of A Bridge Abutment" International Conference on Case Histories in Geotechnical Engineering UMR, SDt. Louis, Missouri, U.S.A. May 6-11, 1984.

Graham, J. (1968) "Plane Plastic Failure in Cohesionless Soils". Geotechnique 18 pp. 301-316.

Graham, J. (1974) "Plasticity Solutions to Stability Problems in Sand" CGJ Vol. 11, No. 2 May 1974, pp 238-247.

Graham, J., Raymond, G.P., Suppiah, A. (1984) "Bearing Capacity of Three Closely Spaced Footings on Sand." Geotechnique 34, No. 2 pp. 173-182.

Graham, J. and Stuart, J.G. (1971) "Scale and Boundary Effects in Foundation Analysis." JSMFD ASCE, Vol. 97 No. SM 11, Nov. 1971.

REFERENCES (3)

Graham, J. and Hovan, J.M.(1985) "Stress Characteristics for Bearing Capacity in Sand Using A Critical State Model" Presented at Canadian Congress of Applied Mechanics, June 1985.

Giroud, J. P. and Tran Vo-Nhiem (1971) " Force Portante D'une Foundation Sur Une Pente". Annales de L'Institut Technique du baitment et des Travanx Publics Supplement No. 283 - 284, July, Aug, 1971.

Gorbunon-Possadov, M.I. (1965) "Calculations for the Stability Of a Sand Bed By A Solution Combining The Theories Of Elasticity and Plasticity." Proc. 6th ICSMFE Montreal, V2 pp. 51-55.

Habib, P. (1985) "Effet D'Echelle Et Surfaces De Clissement . Revue francaise de geotechnique No. 31, pp. 5-10.

Hovan, J.M. (1985) " Computation of Bearing Capacity and Passive Pressure Coefficients in Sand Using Stress-Characteristics and Critical State". A thesis presented to U.M. in partial fulfilment for degree of M.Sc.

International Road Federation (1984) "Limit States Design For Highway Bridges" - Geotechnical Considerations". 10th IRF World Meeting, Rio de Janerio, October 1984.

Kimura, T., Kusakabe, O., Saitoh, K., (1985) "Geotechnical Model Tests Of Bearing Capacity Problems In a Centrifuge" Geotechnique 35,No. 1 pp. 33-45.

Kovalev, I.V. (1964) "De La Resistance Ultime De Foundations Limitees Par Un Talus" Traduction du russe; extrait du recueil des travaux de LIIZLT, fascicule 225, " Nekotorye voprosy tonnele - i - mostostroeniy " Leningrad, URSS (1964) Traduction francaise effective par L.C.P.C., Paris 1973.

Kuskabe, O., Kimura, T., Yamaguchi, H. (1981) "Bearing Capacity of Slopes Under Strip Loads On The Top Surfaces" Soils and Foundations Vol. 21 No. 4 Dec. 1981, Japanese Society of Soil Mechanics and Foundation Engineering.

Lebegue, Y. (1973) "Essais De Fondations Superficielles Sur Talus" Proceedings 8th ICSMFC Vol. 4.3 pp 313.

REFERENCES (4)

Lee, I. W-Y (1978) "Bowles Bearing Capacity Factors For Cohesionless Soils" Thesis submitted in partial fulfillment of the requirements for the degree of Bachelor of Applied Science, Dept. of Civil Engineering, University of Ottawa, Ontario, Canada, January 1978.

Lee, I, W-Y (1981) "Determination of Bearing Capacity Factors For Cohesionless Slopes" Hong Kong Engineer, November 1981.

Lundgren, H. and Mortensen, K. (1953) "Determination by the Theory of Plasticity of the bearing capacity of continuous footings on sand." Proceedings 3rd Int. Conf. Soil Mechanics and Foundation Eng. Vol. 1, Zurich 1953.

Meyerhof, G.G. (1951) "The Ultimate Bearing Capacity Of Foundations" Geotechnique 2, (4) pp. 301-32.

Meyerhof, G.G. (1985) " The Ultimate Bearing Capacity of Foundations On Slopes" Proceedings 4th International Conference on Soil Mechanics and Foundation Engineering, London 1957, Vol pp. 384-386.

Meyerhof, G.G. (1963) Some Recent Research On The Bearing Capacity Of Foundations" CGJ Vol. 1 No. 1 September 1963.

Meyerhof, G.G. (1984) "Safety Factors and Limit States Analysis In Geotechnical Engineering" CGJ Vol. 21 (1984) pp. 1-7.

Mizuno, T. (1948) "On The Bearing Power Of Soil In A Two-Dimensional Problem" Proceeding 2nd International Conference of Soil Mechanics and Foundation Engineering, Rotterdam Vol. 3, pp.44-46.

Mizuno, T. (1953) "On The Bearing Power Of Soil Under A Uniformly Distributed Circular Load" Proceedings 3rd International Conference S.M.FE, Zurich, Vol. 1, pp. 446-449.

Mizuno, T,. Tokumitsu, Y and Kawakami, H. (1960) "On The Bearing Capacity Of A Slope Of Cohesionless Soil" Soils and Foundations Vol. 1, No. 2 November 1960. Japanese Society of Soil Mechanics and Foundation Engineering.

Mowafy, Y. (1984) "Reinforced Soil Embankment subjected to Surface Loading" Ph.D Thesis Proposal, Department of Civil Engineering, Carleton University, Ottawa, Canada, November 1984.

REFERENCES (5)

Myslivec, A., Kysela, Z., (1978) "The Bearing Capacity of Building Foundations" Elsevier Scientific Publishing Co.

Mizuno, T., Tokumitsu, Y., Kawakami, H. (1960) "On the Bearing Capacity of a Slope of Cohesionless Soil". Soils and Foundations Vol. 1 No. 2 Nov. 1960, pp. 30-37.

Peynircioglu, H. (1948) "Test On Bearing Capacity of Shallow Foundations On Horizontal Top Surfaces Of Sand Fills and the Behaviour Of Soils Under Such Foundations" Proceedings 2nd ICSMFE Rotterdam, V3 pp. 144-205.

Selvadurai, A.P.S. Nicholas, T.J., Bauer, G. "Finite Element Analysis of Load-Settlement Behaviour of Foundations near Slopes" Final Report to Ontario Joint Transportation and Commu-ications Research programme - ProjectO-1.

Shields, D.H., Scott, J.D., Bauer, G.E., Deschienes, J.H., Barsvary, A.K. (1973) "Bearing Capacity of Foundations Near Slopes" Proceeding 9th International Conference on Soil Mechanics and Foundation Engineering, Moscow 1973, V pp. 715-179.

Shields, D.H., Deschienes, J.H., Scott, J.D., Bauer, G.E. (1979) "Advantages of Founding Bridge Abutments On Approach Fills."

Sokolovski, V.V. (1960) "Statics of Soil Media" Butterworths Scientific Publications, London, England.

Suppiah, A (1981) "Interference of three parallel, strip Surface Footings On Sand". A Thesis submitted to the Faculty of Graduate Studies of the University of Manitoba in partial fulfillment of the re-quirements for the degree of Master of Science.

Tenier, P., Morlier, P. (1982) "Influence De Surcharge Concentrees Sur La Stab-ilite Des Talus" CGJ Vol. 19, 1982.

Terzaghi, K. (1943) "Theoretical Soil Mechanics" John Wiley and Sons Inc.

Vesic, A.S. (1973) "Analysis of Ultimate Loads of Shallow Foundations" JSMFD ASCE Vol. 99, No. SM 1, January 1973.

APPENDIX 1.

LISTING OF COMPUTER PROGRAM

```
  802   CONTINUE
C
        DO 803 I=H1,10
        Z(I,I)=(X(I,I)*TANEP)-(((ENN-1.)/(H-2))*TAN(ALPHA)*(I-H))
     1            +(Z(10,10))
  803   CONTINUE
C
        FIRPSI=PI-EPSILO-ARSIN(SIN(EPSILO)/SIN(PHI))
        COSPSI=COS(FIRPSI)
        DO 804 I=1,10
        SIGMA(I,I)=Z(I,I)/(1.+(SNPHI*COSPSI))
C23456789
  804   CONTINUE
C
        DO 811 I=2,H
        Z(I,I)=Z(I,I)-(Z(1,1))
C23456789
  811   CONTINUE
C
C
        DO 890 I=H1,9
        Z(I,I)=Z(I,I)+(X(I,I)-X(H,H))*TAN(ALPHA)-(Z(10,10))
  890   CONTINUE
C
        Z(1,1)=0.0
        Z(10,10)=(ENN-1.0)*TAN(ALPHA)
C
C23456789
        DO 807 I=1,10
        PSI(I,I)=FIRPSI/2.
  807   CONTINUE
        DO 806 J=1,9
        W2=10-J
        DO 805 I=1,W2
C
        X1=X(I+J-1,I)
        X2=X(I+J,I+1)
C
        SIGMA1=SIGMA(I+J-1,I)
        SIGMA2=SIGMA(I+J,I+1)
C
        Z1=Z(I+J-1,I)
        Z2=Z(I+J,I+1)
C
        PSI1=PSI(I+J-1,I)
        PSI2=PSI(I+J,I+1)
        E=1
C
        CALL NUPT
C
        X(I+J,I)=XX
        Z(I+J,I)=ZZ
        SIGMA(I+J,I)=SIMA
        PSI(I+J,I)=PSSI
C2345678
  805   CONTINUE
  806   CONTINUE
C
        PRINT 100
  100   FORMAT( '1', ////// 10X,'BOUNDARY OF THE PASSIVE ZONE')
        PRINT 200
  200   FORMAT(/// 14X,'X',11X,'Z',10X,'SIGMA',14X,'PSI' )
C
        DO 808 I=1,10
        CALL RESOUT(I,1)
  808   CONTINUE

C
        PRINT 200
C
        DO 809 J=2,10
        PRINT 16,J
C23456789
   16   FORMAT(//4X,'RADIAL NO', 2X,I3)
        DO 810 I=J,10
        PRINT 15,X(I,J),Z(I,J),SIGMA(I,J),PSI(I,J)
   15   FORMAT(4X,F6.3,5X,F6.3,5X,F8.3,4X,F8.3)
  810   CONTINUE
  809   CONTINUE
C23456789
  899   CONTINUE
        RETURN
        END
C
C
C

            SUBROUTINE EDGPA3
C
C
C
C
      REAL PHI,EPSILO,ALPHA,FIRPSI,COSPSI
      COMMON PHI,BETA,DELTA,TOL,CONVG,SIZE,ALPHA,EPSILO
      INTEGER H,E
      COMMON L,K,C
      REAL M
      REAL XX,ZZ,SIMA,PSSI,PHHI
      COMMON /TATA/ X1,X2,XX,Z1,Z2,ZZ,PHHI
      COMMON /TITI/ SIGMA1,SIGMA2,SIMA
      COMMON /TETE/ PSI1,PSI2,PSSI
      COMMON /TOTO/ PI,SNPHI,CSPHI
      COMMON /OUI/ PP,QQ,CONTRO
      INTEGER PP,QQ
      REAL MU
      COMMON  MU,PHIP,PHIT
      REAL X(40,40),Z(40,40),SIGMA(40,40),PSI(40,40)
      COMMON /LALA/ X,Z,SIGMA,PSI
      INTEGER W,H1,W2,I,J
      INTEGER P(40),Q(40)
      COMMON /LOLO/ P,Q
      COMMON /NEW/ CSPSI,HOR,ANG
      REAL DIF,DI,TNPHI,HD,HEQUIV,HPRIME
       COMMON NPSI,E,HD
       COMMON /KAYO/ BED,HEQUIV,BDILES,HPRIME,GEL
C
        IF(BED .GT. 0) GO TO 767
        SHE=50.0
        HD=40.0
       HEQUIV=HD*(TAN(ALPHA))*(1.-HD/(SHE*2.0))
       HPRIME=HEQUIV
C23456789
  767  CONTINUE
C
        DO 71 I=1,10
        Z(I,I)=HEQUIV
   71   CONTINUE
C
        X(1,1)=0.0
C
        DO 72 I=2,10
        W=I-1
        X(I,I)=X(W,W)+(SHE/9.0)
```

```
      C23456789
896      72   CONTINUE
      C
897           FIRPSI=PI-ALPHA-ARSIN(SIN(ALPHA)/SIN(PHI))
898           CSPSI=COS(FIRPSI)
899           DO 73 I=1,10
900           SIGMA(I,I)=Z(I,I)/(1.+(SNPHI*CSPSI))
      C23456789
901      73   CONTINUE
      C
      C23456789
902           DO 74 I=1,10
903           PSI(I,I)=FIRPSI/2.
904      74   CONTINUE
      C
905           Z(I,I)=0.0
      C
906           DO 75 I=1,10
907           Z(I,I)=X(I,I)*TAN(ALPHA)
908      75   CONTINUE
909           E=1
910           DO 76 J=1,9
911           W2=10-J
912           DO 77 I=1,W2
      C
913           X1=X(I+J-1,I)
914           X2=X(I+J,I+1)
      C
915           SIGMA1=SIGMA(I+J-1,I)
916           SIGMA2=SIGMA(I+J,I+1)
      C
917           Z1=Z(I+J-1,I)
918           Z2=Z(I+J,I+1)
      C
919           PSI1=PSI(I+J-1,I)
920           PSI2=PSI(I+J,I+1)
      C
921           CALL NUPT
      C
922           X(I+J,I)=XX
923           Z(I+J,I)=ZZ
924           SIGMA(I+J,I)=SIMA
925           PSI(I+J,I)=PSSI
      C2345678
      C2345678
926      77  CONTINUE
927      76  CONTINUE
      C
928           PRINT 100
      C23456789
929     100   FORMAT('1',////// 10X,'BOUNDARY OF THE PASSIVE ZONE')
930           PRINT 200
931     200   FORMAT(/// 14X,'X',11X,'Z',10X,'SIGMA',14X,'PSI')
      C
932           DO 78 I=1,10
933           CALL RESOUT(I,1)
      C2345678
934      78   CONTINUE
      C
935           PRINT 200
      C
936           DO 79 J=2,10
937           PRINT 16,J
      C23456789
938      16   FORMAT(//4X,'RADIAL NO', 2X,I3)
939           DO 80 I=J,10

940           PRINT 15,X(I,J),Z(I,J),SIGMA(I,J),PSI(I,J)
941      15   FORMAT(4X,F6.3,5X,F6.3,5X,F8.3,4X,F8.3)
      C
942      80   CONTINUE
943      79   CONTINUE
      C23456789
944     899   CONTINUE
945           RETURN
946           END
      C
      C
      C*************************************************************
      C
      C        INPUT DATA IS LISTED AS FOLLOWS
      C       PHI,DELTA,BETA,TOL,CONVG,SIZE,ALPHA
      C        CONTROL
      C        L,K
      C
      C
      C
      C*************************************************************
      C

      $ENTRY
```

```
            Q(I)= QQ
     250    CONTINUE
      C
     117    IF(H .LT. L) GO TO 300
            RAD1=RAD+L-2
            PRINT,RAD1
      C
      C23456789
            IF(BED .EQ. 0) THEN DO
*EXTENSION*  OTHER COMPILERS MAY NOT ALLOW IF-THEN-ELSE, DO CASE, STRUCTURED LOOP, OR REMOTE BLOCK STATEMENTS
            GEL=0.2
            ELSE
            GO TO 979
            END IF
     979    CONTINUE
      C
      C
            CALL NGAMA(RAD)
      C
      C
      C
      C
            DIF=(SIGMA(L,RAD1)-10*SIGMA(2,RAD))
            DIF=DIF/SIGMA(L,RAD1)
            DIF=ABS(DIF)
            PRINT 200, SIGMA(L,RAD1) ,SIGMA(2,RAD),DIF,CONVG
      C234567
     200 FORMAT(////////20X,'******************************',
        1                    //20X,'*     SIGMA(L,RAD+L-2)=',F12.6,' *',
        2                    //20X,'*     SIGMA(2,RAD)=',F12.6,'     *',
        3                    //20X,'*     DIF=',F8.5,'              *',
        4                    //20X,'*     CONVG=',F8.5,'              *',
        5                    //20X,'**********************************')
      C
      C
             BED=BED+1
             Z(1,1)=BDILES*BED/4.
             Z(10,10)=Z(1,1)
             GEL=Z(1,1)
             IF(BED .LE. 4) THEN
*EXTENSION*  OTHER COMPILERS MAY NOT ALLOW IF-THEN-ELSE, DO CASE, STRUCTURED LOOP, OR REMOTE BLOCK STATEMENTS
            GO TO 888
            ELSE
            GO TO 999
            END IF
      C23456789
     999    CONTINUE
      C
      C
            ME=5
            IF(ME .EQ. 5) GO TO 777
            IF(DIF .GT. CONVG) THEN
*EXTENSION*  OTHER COMPILERS MAY NOT ALLOW IF-THEN-ELSE, DO CASE, STRUCTURED LOOP, OR REMOTE BLOCK STATEMENTS
            Z(2,1)=Z(2,1)-X(2,1)*TAN(EPSILO)
            NPSI=PI-EPSILO-(ARSIN(SIN(EPSILO)/SIN(PHI)))
            CSPSI=COS(NPSI)
            DO 500 I=2,L
           SIGMA(I,1)=(Z(I,1)-(X(I,1)*TAN(EPSILO))-(Z(2,1)))/(1.+(SNPHI
        1          *COS(PSI(I,1))))
            SIGMA(I,1)=SIGMA(I,1)+(SIGMA(L,1)/10.0)
               SIGMA(I,1)=SIGMA(I,1)+(SIGMA(L,1)/10.0)
     500    CONTINUE
            Z(2,1)=Z(2,1)+X(2,1)*TAN(EPSILO)
            KS=K+SPI
            DO 510 J=2,KS
               X(2,J)= (X(L,W+J))/10.0
               Z(2,J)= (Z(L,W+J))/10.0
               SIGMA(2,J)=(SIGMA(L,W+J))/10.0
               PSI(2,J)=PSI(L,W+J)
     510    CONTINUE
            PRINT 22,C
            PRINT 27,X(2,RAD),Z(2,RAD),SIGMA(2,RAD),PSI(2,RAD)
      27    FORMAT(////10X,'X(2,RAD)=',F5.2,
      C2345678
        1   //10X          ,'Z(2,RAD)=',F5.2,
        2   //10X          ,'SIGMA(2,RAD)=',F12.8,
        3   //10X        ,'PSI(2,RAD)=',F12.8//)
      C
            PRINT 30,C
      30    FORMAT('1',//////14X,'RESULTS OF FIRST SPIRAL AFTER ',I3,
        1   ' SCALE REDUCTION')
            PRINT 19
      C
            DO 415 J=1,RAD
               CALL RESOUT(2,J)
     415    CONTINUE
            GO TO 450
      C
      C
            ELSE
            GO TO 222
            END IF
     222    PRINT 333
     333    FORMAT('1',//////20X,'****************************** ',
        1                     /20X,'*                            *',
        2                     /20X,'*  END OF FINAL COMPUTATION  *',
        3                     /20X,'*  ZERO SURCHARGE CASE       *',
        4                    /20X,'*  REGULAR RADIAL ZONE       *',
        5                     /20X,'*                            *',
        6                     /20X,'******************************'//)
            DO 555 J=2,RAD
               PRINT 890,J
               PRINT 891
     890       FORMAT(////10X,'J=',I3)
     891       FORMAT(10X,'*****')
               PRINT 19
               DO 666 I=1,L
                  CALL RESOUT(I,J)
     666       CONTINUE
     555    CONTINUE
      C
      C
               DO 557 I=1,L
                  PRINT 893,I
                  PRINT 896
     893          FORMAT('1',////10X,'I=',I3)
     896          FORMAT(10X,'*****')
                  PRINT 19
                  DO 669 J=2,RAD
                     CALL RESOUT(I,J)
     669          CONTINUE
     557       CONTINUE
      C
     103      PRINT 104
     104        FORMAT( 20X,'*************')
                  PRINT 756
     756          FORMAT('1',////45X,'**************************',
        1                        /45X,'*                        *',
        2                        /45X,'*  EXTRA DOMAIN CREATED  *',
        3                        /45X,'*  BY SCALE REDUCTIONS   *',
        4                        /45X,'*                        *',
        5                        /45X,'**************************'//)
```

```
C23456789
  777     CONTINUE
              STOP
              END
C
C
C*****************************************************************

        SUBROUTINE HEADIN
              REAL PHI
              COMMON PHI,BETA,DELTA,TOL,CONVG,SIZE,ALPHA,EPSILO
              INTEGER L,K,C
              COMMON L,K,C
              REAL XX,ZZ,SIMA,PSSI,PHHI
              COMMON /TATA/ X1,X2,XX,Z1,Z2,ZZ,PHHI
              COMMON /TITI/ SIGMA1,SIGMA2,SIMA
              COMMON /TETE/ PSI1,PSI2,PSSI
              COMMON /TOTO/ PI,SNPHI,CSPHI
              INTEGER PP,QQ,CONTRO
              COMMON /OUI/ PP,QQ,CONTRO
              REAL MU
              COMMON MU ,PHIP ,PHIT
              REAL X(40,40),Z(40,40),SIGMA(40,40),PSI(40,40)
              COMMON /LALA/ X,Z,SIGMA,PSI
              INTEGER P(40),Q(40)
              COMMON /LOLO/ P,Q
              COMMON NPSI,E,HD
              COMMON /NEW/ CSPSI,HOR,ANG
C
C
        PRINT 10,PHI,BETA,DELTA,TOL,CONVG,SIZE,ALPHA,EPSILO,ANG
   10     FORMAT('1',//////////10X,'     PHI=',F5.1,
     1    //10X        ,'     BETA=',F5.1,
     2    //10X        ,'     DELTA=',F5.1,
     3    //10X        ,'     TOL=',F7.5,
     4    //10X        ,'     CONVG=',F7.5,
     5    //10X        ,'     SIZE=',F6.3,
     7    //10X        ,'     ALPHA=',F5.1
     1    //10X        ,'     EPSILON=',F5.1,
     1    //10X        ,'     EPS/ALPHA=',F5.2)
          RETURN
          END
C
C*****************************************************************
C
C23456789

          SUBROUTINE POLCOM
C
C         THIS SUBROUTINE COMPUTES SIGMA AND PSI FOR ALL
C         POINTS AT THE POLE INCLUDING THE BOUNDARY POINT
C
          REAL PHI
          COMMON PHI,BETA,DELTA,TOL,CONVG,SIZE,ALPHA,EPSILO
          INTEGER L,K,C
          COMMON L,K,C
          REAL XX,ZZ,SIMA,PSSI,PHHI
          COMMON /TATA/ X1,X2,XX,Z1,Z2,ZZ,PHHI
          COMMON /TITI/ SIGMA1,SIGMA2,SIMA
          COMMON /TETE/ PSI1,PSI2,PSSI
          COMMON /TOTO/ PI,SNPHI,CSPHI
            INTEGER PP,QQ,CONTRO
          COMMON /OUI/  PP,QQ,CONTRO
          REAL MU
          COMMON MU,PHIP,PHIT
          REAL X(40,40),Z(40,40),SIGMA(40,40),PSI(40,40)
```

```
          COMMON /LALA/ X,Z,SIGMA,PSI
          INTEGER P(40),Q(40)
          INTEGER KK,K1,I,J
          REAL PSII,PSIF,INT,FIRSIG,FINSIG,TNPHI,FINPHI
         COMMON /LOLO/ P,Q
         COMMON NPSI,E,HD
         COMMON /NEW/ CSPSI,HOR,ANG
C
C
          PSII=PSI(1,1)
          MU=PI/4.-PHI/2.
C2345678
  400     PSIF=MU+BETA
C
  405     INT= (PSII-PSIF)/K
         KK=K-1
          PRINT,' '
           PRINT,'*********************************************'
          PRINT,' '
         PRINT,'              POLE COMPT  < >  FIRST SPIRAL:(1,J)  '
          PRINT,' '
          PRINT,' '
          PRINT 14
          PRINT,' '
          DO 350 J=2,K
          X(1,J)=X(1,1)
          Z(1,J)=Z(1,1)
          TNPHI=TAN(PHI)
          FIRSIG=EXP(ALOG(SIGMA(1,J-1))+INT*2.*TNPHI)
          SIGMA(1,J)=FIRSIG
          PSI(1,J)=PSI(1,J-1)-INT
          PRINT 12,X(1,J),Z(1,J),SIGMA(1,J),PSI(1,J)
C2345678
   12    FORMAT(11X,F8.5,3X,F8.5,E15.6,3X,F8.5)
  350     CONTINUE
          PRINT,' '
         PRINT,'*********************************************
       1*************************************************'
        IF (CONTRO .EQ. 1) GO TO 64
          PRINT,' '
          PRINT,'                 SECOND SPIRAL '
          PRINT,' '
          PRINT 19
C234568
   19 FORMAT(////17X,'X',13X,'Z',13X,'SIGMA',12X,'PSI',
     1              17X,'P',4X,'Q'/)
          PRINT,' '
   64 CONTINUE
          PRINT,' '
          DO 355 J=2,K
          X1= X(1,J)
          Z1= Z(1,J)
          SIGMA1= SIGMA(1,J)
          PSI1= PSI(1,J)
          X2= X(2,J-1)
          Z2= Z(2,J-1)
          SIGMA2= SIGMA(2,J-1)
          PSI2= PSI(2,J-1)
          E=0
C
          CALL NUPT
C
          X(2,J)=XX
          Z(2,J)=ZZ
          SIGMA(2,J)= SIMA
          PSI(2,J)= PSSI
```

```
$JOB WATFIV
C
C
C
C         MAIN PROGRAM
C
C23456789
      REAL PHI
      COMMON PHI,BETA,DELTA,TOL,CONVG,SIZE,ALPHA,EPSILO
      INTEGER L,K,C,E
      COMMON L,K,C
      REAL XX,ZZ,SIMA,PSSI,PHHI
      COMMON /TATA/ X1,X2,XX,Z1,Z2,ZZ,PHHI
      COMMON /TITI/ SIGMA1,SIGMA2,SIMA
      COMMON /TETE/ PSI1,PSI2,PSSI
      COMMON /TOTO/ PI,SNPHI,CSPHI
      INTEGER PP,QQ,CONTRO
      COMMON /OUI/ PP,QQ,CONTRO
      REAL MU
      COMMON  MU,PHIP,PHIT
      REAL X(40,40),Z(40,40),SIGMA(40,40),PSI(40,40)
      COMMON /LALA/ X,Z,SIGMA,PSI
      INTEGER SPI,RAD,W,H,H1,KS,L1,LK,I,J,RAD1
      REAL DIF,DI,TNPHI
      REAL NY,FIRSIG
      INTEGER P(40),Q(40)
      COMMON /LOLO/ P,Q
      REAL NPSI,HOR,HEQUIV,BDILES,HPRIME
      INTEGER BED
      COMMON NPSI,E,HD
      COMMON /NEW/ CSPSI ,HOR,ANG
      COMMON /KAYO/ BED,HEQUIV,BDILES,HPRIME,GEL
C
C
      PI=ARCOS(-1.)
      READ,PHI,DELTA,BETA,TOL,CONVG,SIZE,ALPHA
      EPSILO=ALPHA*0.52
      ANG=EPSILO/ALPHA
      READ,CONTRO
      IF(CONTRO .EQ. 1) THEN DO
*EXTENSION*  OTHER COMPILERS MAY NOT ALLOW IF-THEN-ELSE, DO CASE, STRUCTURED LOOP, OR REMOTE BLOCK STATEMENTS
      PRINT 43
   43 FORMAT('1',///////20X,'*****************************',
     1                    /20X,'*                           *',
     2                    /20X,'*      CONTROL=1            *',
     3                    /20X,'*                           *',
     4                    /20X,'*      PARTIAL RESULTS      *',
     5                    /20X,'*         PRINTOUT          *',
     6                     20X,'*                           *',
     7                    /20X,'*****************************')
      ELSE
      GO TO 44
      END IF
   44 CONTINUE
C
C
      READ,L,K
      IF (ABS(BETA) .LE. 0.0001) BETA=0.0001
C
C          INITIALISATION
C
      CALL HEADIN
      PRINT 825
  825 FORMAT('1',///////////////20X)
      PRINT,'        *******************************************'
      PRINT,'        *                                         *'
----------------------------------------------------------------------------------------------------
      PRINT,'        *  THE PROGRAM COMPUTES THE FAILURE LINES  *'
      PRINT,'        *  FOR A FOOTING AT THE TOP OF A SLOPE IN  *'
      PRINT,'        *  COHESIONLESS SOIL. THE COMPUTATION      *'
      PRINT,'        *  PRESENTS A FEATURE WHICH CONSISTS OF    *'
      PRINT,'        *  TRAPPING THE FAILURE LINES AROUND THE   *'
      PRINT,'        *  POLE BY IMPLEMENTING VARIOUS SCALE      *'
      PRINT,'        *  REDUCTIONS WITH A DIMINISHING SURCHARGE *'
      PRINT,'        *  EFFECT.                                 *'
      PRINT,'        *******************************************'
C
C
       L1=40
       DO 3 I=1,L1
          P(I)=0
          Q(I)=0
    3  CONTINUE
       PHI=PHI*PI/180.
      BETA= BETA*PI/180.
      DELTA= DELTA*PI/180.
      ALPHA=ALPHA*PI/180.
      EPSILO=EPSILO*PI/180.
      CSPHI=COS(PHI)
      SNPHI=SIN(PHI)
      TNPHI=TAN(PHI)
C
C
       BED=0
C23456789
  888 CONTINUE
C
           CALL EDGPA2
C
C
           L1=40
           LK=40
C
C
           DO 1 I=1,10
           DO 2 J=2,LK
              X(I,J)=0.0
              Z(I,J)=0.0
              SIGMA(I,J)=0.0
              PSI(I,J)=0.0
C23456789
    2      CONTINUE
    1      CONTINUE
           DO 601 I=11,L1
           DO 602 J=1,LK
              X(I,J)=0.0
              Z(I,J)=0.0
              SIGMA(I,J)=0.0
              PSI(I,J)=0.0
C23456789
  602    CONTINUE
  601      CONTINUE
C
           C=1
C
           CALL POLCOM
C
           SPI=L-1
C
C
C     FIRST TIME COMPUTATION
C
C
      C=0
```

```
      450 C=C+1
          PRINT 22,C
       22 FORMAT('1',////25X,'*******************************',
         1        /25X,'*                             *',
         2        /25X,'*   SCALE ITERATION C=',I3,'  *',
         3        /25X,'*                             *',
         4        /25X,'*   REGULAR DOMAIN            *',
         5        /25X,'*                             *',
         6        /25X,'*******************************')
           IF( C.EQ.1 ) THEN DO
TENSION*  OTHER COMPILERS MAY NOT ALLOW IF-THEN-ELSE, DO CASE, STRUCTURED LOOP, OR REMOTE BLOCK STATEMENTS
             RAD=K+1
               W=0
          ELSE DO
             RAD=K+SPI
               W=SPI-1
          END IF
          DO 100  J=1,RAD
            IF(CONTRO .EQ. 1) GO TO 53
           PRINT,' '
           PRINT,' '
           PRINT,' '
          PRINT 41,J
          PRINT 39
       39 FORMAT(10X,' *****')
       41 FORMAT(10X,' J=',I3)
           PRINT 19
C23456789
       19  FORMAT(// 17X,'X',13X,'Z',13X,'SIGMA',11X,'PSI'
         1       ,18X,'P',4X,'Q',/)
       53 CONTINUE
C
            IF(J .EQ. 1) GO TO 50
            DO 75 I=3,L
               X1= X(I-1,J)
               Z1= Z(I-1,J)
               SIGMA1=SIGMA(I-1,J)
               PSI1=PSI(I-1,J)
               X2= X(I,J-1)
               Z2= Z(I,J-1)
               SIGMA2=SIGMA(I,J-1)
               PSI2=PSI(I,J-1)
               E=0
C
C
               CALL NUPT
C
               X(I,J)= XX
               Z(I,J)= ZZ
               SIGMA(I,J)= SIMA
               PSI(I,J)=PSSI
               P(I)= PP
               Q(I)= QQ
       75 CONTINUE
       50 GO TO 51
       51 IF(CONTRO .EQ. 1) GO TO 100
          IF(J.EQ.1) THEN
TENSION*  OTHER COMPILERS MAY NOT ALLOW IF-THEN-ELSE, DO CASE, STRUCTURED LOOP, OR REMOTE BLOCK STATEMENTS
          PRINT 19
             DO 80 I=2,L
                CALL RESOUT(I,1)
       80      CONTINUE
            ELSE
               GO TO 100
          END IF
      100 CONTINUE
```

```
C
C         END OF REGULAR RADIAL ZONE COMPUTATION
C
          IF(CONTRO .EQ. 1)GO TO 67
          PRINT,' '
          PRINT,' '
          PRINT,' '
          PRINT 25
       25 FORMAT( 11X,'RADIAL ZONE COMPUTATION COMPLETED')
          PRINT 26
       26 FORMAT( 11X,'*********************************')
          PRINT 678
      678 FORMAT('1',////25X,' COMPUTATION OF THE EXTRA DOMAIN',
         1               //25X,' ******************************')
       67 CONTINUE
          H=2
          J=RAD
      300 H=H+1
          J=J+1
          H1=H+1
          IF(CONTRO .EQ. 1) GO TO 68
          PRINT, ' '
          PRINT,' '
          PRINT,' '
          PRINT 47,J,H
       47 FORMAT(10X,'J=',I3,5X,'FIRST SPIRAL=',I3)
          PRINT 59
       59 FORMAT(10X,'*****',5X,'***************')
          PRINT 19
       68 CONTINUE
C
          X1=X(H-1,J-1)
          Z1=Z(H-1,J-1)
          SIGMA1=SIGMA(H-1,J-1)
            PSI1=PSI(H-1,J-1)
          X2=X(H,J-1)
          Z2=Z(H,J-1)
          PSI2=PSI(H,J-1)
          SIGMA2=SIGMA(H,J-1)
C
          CALL ENDPT
C
          X(H,J)=XX
          Z(H,J)=ZZ
          SIGMA(H,J)=SIMA
          PSI(H,J)=PSSI
C
          IF(H1 .GT. L) GO TO 117
          DO 250 I=H1,L
             X1= X(I-1,J)
             Z1= Z(I-1,J)
              SIGMA1= SIGMA(I-1,J)
             PSI1= PSI(I-1,J)
             X2= X(I,J-1)
             Z2= Z(I,J-1)
             SIGMA2= SIGMA(I,J-1)
             PSI2= PSI(I,J-1)
             E=0
C
             CALL NUPT
C
             X(I,J)= XX
             Z(I,J)=ZZ
             SIGMA(I,J)= SIMA
             PSI(I,J)= PSSI
             P(I)= PP
```

```
      C       SOIL MASS
      C
      C
              REAL PHI
              COMMON PHI,BETA, DELTA,TOL,CONVG, SIZE, ALPHA,EPSILO
              INTEGER L,K,C
              COMMON L,K,C
              REAL XX,ZZ,SIMA,PSSI,PHHI
              COMMON /TATA/ X1,X2,XX,Z1,Z2,ZZ,PHHI
              COMMON /TITI/ SIGMA1,SIGMA2,SIMA
              COMMON /TETE/ PSI1, PSI2,PSSI
              COMMON /TOTO/ PI, SNPHI, CSPHI
              INTEGER PP, QQ, CONTRO
              COMMON /OUI/ PP,QQ,CONTRO
              REAL MU
              COMMON MU,PHIP,PHIT
              REAL X(40,40),Z(40,40),SIGMA(40,40),PSI(40,40)
              COMMON /LALA/ X,Z,SIGMA,PSI
              INTEGER P(40),Q(40)
              REAL ENDPSI
              REAL ZIGMA2,PZI2,SUM2,DIFF2,CSSUM2
              REAL B,XI,F,U,PHHHI
              INTEGER I,J
              COMMON /LOLO/ P,Q
              COMMON NPSI,E,HD
              COMMON /NEW/ CSPSI,HOR,ANG
      C
              PP=1
              QQ=1
              SIMA=(SIGMA1+SIGMA2)/2.
         301   ENDPSI=MU+BETA
         305  PSSI=ENDPSI
         302  ZIGMA2=(SIGMA1+SIGMA2)/2.
              PZI2=(PSSI+PSI2)/2.
              SUM2=SIN(PZI2+MU)
              DIFF2=SIN(PZI2-MU)
              CSSUM2=COS(PZI2+MU)
              B=-1.*(DIFF2)/(2.*ZIGMA2*SNPHI*CSSUM2)
               IF(ABS(BETA)  .LT. 0.0001) BETA=0.0001
              ZZ=Z1*TAN(BETA)-X1-Z2*SUM2/CSSUM2+X2
              ZZ=ZZ/(TAN(BETA)-(SUM2/CSSUM2))
              XI=ALOG(SIGMA2)/(2.*TAN(PHI))+PSI2+B*(ZZ-Z2)
              F=EXP(2.*TAN(PHI)*(XI-PSSI))
              U=ABS((F-SIMA)/F)
      C
              IF (U .LE. TOL) GO TO 303
      C
              SIMA=F
              PP=PP+1
      C
              IF(PP-100) 302,302,303
      C2345678
         303  XX=X1+(ZZ-Z1)*TAN(BETA)
              IF (CONTRO .EQ. 1) GO TO 26
              PRINT 13,     XX,ZZ,SIMA,PSSI,PP,QQ
          13  FORMAT(11X,F12.8,3X,F12.8,3X,E15.5,3X,F12.8,8X,I4,1X,I4)
              PRINT 306
         306  FORMAT('+','
           1
           2 BOUNDARY')
         26   CONTINUE
              RETURN
              END
      C
      C****************************************************************
      C
```

```
              SUBROUTINE EDGEPA
      C
      C
      C       THIS SUBROUTINE COMPUTES SIGMA FOR EACH SPECIFIED POINT
      C       AT THE EDGE OF THE RECTILINEAR PASSIVE ZONE
      C
              REAL PHI
              COMMON PHI,BETA,DELTA,TOL,CONVG,SIZE,ALPHA,EPSILO
              INTEGER L,K, C
              COMMON L,K,C
              REAL XX,ZZ,SIMA,PSSI,PHHI
              COMMON /TATA/ X1,X2,XX,Z1,Z2,ZZ,PHHI
              COMMON /TITI/ SIGMA1,SIGMA2,SIMA
              COMMON /TETE/ PSI1, PSI2, PSSI
              COMMON /TOTO/ PI,SNPHI,CSPHI
              INTEGER PP,QQ,CONTRO
               REAL MU
              COMMON MU,PHIP,PHIT
              REAL X(40,40),Z(40,40),SIGMA(40,40),PSI(40,40)
              COMMON /LALA/ X,Z,SIGMA,PSI
              INTEGER P(40),Q(40)
              INTEGER CC,I,J
                REAL DI,NUZ,NSIMA
             COMMON /LOLO/P,Q
              COMMON NPSI,E,HD
             REAL NPSI
              COMMON /NEW/ CSPSI,HOR,ANG
      C
      C
              IF(C .EQ. 0)THEN
XTENSION*  OTHER COMPILERS MAY NOT ALLOW IF-THEN-ELSE, DO CASE, STRUCTURED LOOP, OR REMOTE BLOCK STATEMENTS
              CC=2
              C=1
              ELSE
              CC=3
              END IF
              DO 23 I=CC,L
              MU=PI/4.-PHI/2.
              TN=TAN((NPSI/2.)-(MU))
              Z(I,1)=X(I,1)*(1./TN-TAN(ALPHA))
              SIMA=(1.0+Z(I,1))/(1.+(SNPHI*CSPSI))
              SIGMA(I,1)=SIMA
              PSI(I,1)=(PI-ALPHA-(ARSIN(SIN(ALPHA)/SIN(PHI))))/2.
             IF(ALPHA .GT. 0.0)THEN
XTENSION*  OTHER COMPILERS MAY NOT ALLOW IF-THEN-ELSE, DO CASE, STRUCTURED LOOP, OR REMOTE BLOCK STATEMENTS
               Z(I,1)=Z(I,1)+(X(I,1)*TAN(ALPHA))
                ELSE
                GO TO 23
                END IF
          23   CONTINUE
             RETURN
      C2345678
             END
      C
      C****************************************************************
      C
      C2345678

                SUBROUTINE PPLANE
                REAL PHI
                COMMON PHI,BETA,DELTA,TOL, CONVG,SIZE,ALPHA,EPSILO
                INTEGER L,K,C
                COMMON L,K,C
                REAL XX,ZZ,SIMA,PSSI,PHHI
                COMMON /TATA/ X1,X2,XX,Z1,Z2,ZZ,PHHI
                COMMON /TITI/ SIGMA1,SIGMA2,SIMA
```

```
      P(J)= PP
      Q(J)= QQ
C2345678
  355 CONTINUE
C      CALCULATION OF A BOUNDARY POINT
C
      X1= X(1,K)
      Z1= Z(1,K)
      SIGMA1= SIGMA(1,K)
      PSI1= PSI(1,K)
      X2= X(2,K)
      Z2= Z(2,K)
      SIGMA2= SIGMA(2,K)
      PSI2= PSI(2,K)
C
      CALL ENDPT
C
      K1= K+1
      X(2,K1)=XX
      Z(2,K1)=ZZ
      SIGMA(2,K1)=SIMA
      PSI(2,K1)=PSSI
      P(K1)=PP
      Q(K1)=QQ
      PRINT,' '
       PRINT,'**************************************************
     1*********************************************'
      PRINT,' '
      PRINT,' '
       PRINT,' '
      PRINT,'            FINAL 2-ND SPIRAL WITH THE LAST POINT:
     1 (2,K+1)'
      PRINT,' '
      PRINT,' '
       PRINT 11
C23456789
   11 FORMAT(14X,'X',10X,'Z',10X,'SIGMA',9X,'PSI',15X,'P',4X,'Q')
   14 FORMAT(14X,'X',10X,'Z',10X,'SIGMA',10X,'PSI')
       PRINT,' '
     PRINT,' '
      DO 65 J=1,K1
      PRINT 16,X(2,J),Z(2,J),SIGMA(2,J),PSI(2,J),P(J),Q(J)
   16 FORMAT(11X,F8.5,3X,F8.5,E15.5,3X,F8.5,9X,I4,1X,I4)
   65 CONTINUE
      RETURN
      END
C
C*********************************************************************
C

      SUBROUTINE NUPT
      REAL PHI
      COMMON PHI,BETA,DELTA,TOL,CONVG,SIZE,ALPHA,EPSILO
      INTEGER L,K,C,E
      COMMON L,K,C
      REAL XX,ZZ,SIMA, PSSI,PHHI
      COMMON /TATA/ X1,X2,XX,Z1,Z2,ZZ,PHHI
      COMMON /TITI/ SIGMA1 ,SIGMA2 ,SIMA
      COMMON /TETE/ PSI1, PSI2, PSSI
      COMMON /TOTO/ PI,SNPHI,CSPHI
      INTEGER PP, QQ, CONTRO
      COMMON /OUI/ PP, QQ, CONTRO
      REAL MU
      COMMON  MU,PHIP,PHIT
      REAL X(40,40),Z(40,40),SIGMA(40,40),PSI(40,40)
      COMMON /LALA/ X,Z,SIGMA, PSI

      INTEGER P(40),Q(40)
      REAL ZIGMA1,ZIGMA2,PZI1,PZI2,SUM1,SUM2
      REAL DIFF1,DIFF2,CSDIF1,CSSUM2
      REAL A,B,ETA,XI,F,G,U,V
      INTEGER I,J
      REAL TNPHI,PHHHI
       COMMON /LOLO/ P,Q
      COMMON NPSI,E,HD
      COMMON /NEW/ CSPSI,HOR,ANG
C
C
      SIMA=(SIGMA1+SIGMA2)/2.
      PSSI =(PSI1+PSI2)/2.
      PP=1
      QQ=1
      MU=PI/4.-PHI/2.
  201 ZIGMA1=(SIMA+SIGMA1)/2.
      ZIGMA2=(SIMA+SIGMA2)/2.
      PZI1=(PSSI+PSI1)/2.
      PZI2=(PSSI+PSI2)/2.
      SUM1=SIN(PZI1+MU)
      SUM2=SIN(PZI2+MU)
      DIFF1=SIN(PZI1-MU)
      DIFF2=SIN(PZI2-MU)
      CSDIF1=COS(PZI1-MU)
      CSSUM2=COS(PZI2+MU)
      A=SUM1/(2.*ZIGMA1*SNPHI*CSDIF1)
      B=-1.* (DIFF2)/(2.*ZIGMA2*SNPHI*CSSUM2)
       ZZ=Z1*DIFF1/CSDIF1-Z2*SUM2/CSSUM2-X1+X2
      ZZ=ZZ/(DIFF1/CSDIF1-SUM2/CSSUM2)
      TNPHI=TAN(PHI)
      ETA=ALOG(SIGMA1)/(2.*TNPHI)-PSI1+A*(ZZ-Z1)
      XI=ALOG(SIGMA2)/(2.*TNPHI)+PSI2+B*(ZZ-Z2)
      F=EXP((XI+ETA)*TNPHI)
      G=(XI-ETA)/2.
      U=ABS((F-SIMA)/F)
      V=ABS((G-PSSI)/G)
C
      IF(V .GT. U) GO TO 202
      IF(U .LE. TOL) GO TO 203
      SIMA=F
      PP=PP+1
      IF(PP-100) 201,201,203
C23456789
  202 IF(V .LE. TOL) GO TO 203
      PSSI=G
      QQ=QQ+1
      IF(QQ-100) 201,201,203
  203 XX=X1+(ZZ-Z1)*DIFF1/CSDIF1
      XX=(XX+X2+(ZZ-Z2)*SUM2/CSSUM2)/2.
C
      IF(E .EQ. 1) GO TO 16
      PRINT 13, XX,ZZ,SIMA,PSSI,PP,QQ
C2345678
   13 FORMAT(11X,F12.8,3X,F12.8,3X,E15.5,3X,F12.8,8X,I4,1X,I4)
   16 CONTINUE
      RETURN
      END
C
C**********************************************************************
C

      SUBROUTINE ENDPT
C
C     THIS SUBROUTINE CALCULATES CONDITIONS AT A NEW BOUNDARY
C     POINT FROM A KNOWN BOUNDARY POINT AND A POINT WITHIN THE
```

```
      COMMON /TETE/ PSI1,PSI2,PSSI
      COMMON /TOTO/ PI,SNPHI,CSPHI
      INTEGER PP,QQ,CONTRO
      COMMON /OUI/ PP,QQ, CONTRO
      REAL MU
      COMMON MU,PHIP,PHIT
      REAL X(40,40),Z(40,40),SIGMA(40,40),PSI(40,40)
      COMMON /LALA/ X,Z,SIGMA,PSI
      INTEGER P(40),Q(40)
      REAL PHIPL1,PHIPL2
      COMMON /LOLO/ P,Q
      COMMON NPSI,E,HD
      COMMON /NEW/ CSPSI,HOR,ANG
C
C
      PHIT=PHI
      PHIPL1=32.8328
      PHIPL2=36.
C
      IF(PHIT .LT. PHIPL1) GO TO 10
      IF(PHIT .GT. PHIPL2) GO TO 20
C
      PHIP=1.6667*ALOG(PHIT)-2.3362
     PHIP=EXP(PHIP)
      PHIP=PHIP*PI/180
      GO TO 35
C2345678
   10 PHIP=PHIT
     PHIP=PHIP*PI/180.
      GO TO 35
C2345678
   20 PHIP=1.2944*ALOG(PHIT)-1.002
      PHIP=EXP(PHIP)
      PHIP=PHIP*PI/180
      GO TO 35
C
   35 RETURN
C
      END
C*****************************************************************
C
C

      SUBROUTINE RESOUT(A,B)
C
C
C
      REAL PHI
      COMMON PHI,BETA,DELTA,TOL,CONVG,SIZE,ALPHA,EPSILO
      INTEGER L,K,C
      COMMON L,K,C
      REAL XX,ZZ,SIMA,PSSI,PHHI
      COMMON /TATA/ X1,X2,XX,Z1,Z2,ZZ,PHHI
     COMMON /TITI/ SIGMA1,SIGMA2,SIMA
      COMMON /TETE/ PSI1,PSI2,PSSI
      COMMON /TOTO/ PI,SNPHI,CSPHI
      INTEGER PP,QQ,CONTRO
      COMMON /OUI/ PP,QQ,CONTRO
      REAL MU
      COMMON MU,PHIP,PHIT
      REAL X(40,40),Z(40,40),SIGMA(40,40),PSI(40,40)
      COMMON /LALA/ X,Z,SIGMA,PSI
      INTEGER A,B
        INTEGER P(40),Q(40)
      COMMON /LOLO/ P,Q
      COMMON NPSI,E,HD

       COMMON /NEW/ CSPSI,HOR,ANG
C
      PRINT 20,X(A,B),Z(A,B),SIGMA(A,B),PSI(A,B),P(A),Q(A)
   20 FORMAT(11X,F12.6,3X,F12.6,E15.5,3X,F12.6,5X,I4,1X,I4)
C
      RETURN
      END
C
C***************************************************************
CC

      SUBROUTINE NGAMA(RAD)
C
      REAL PHI,HOR,OFFS,D,HEQUIV,HPRIME
      COMMON PHI,BETA,DELTA,TOL,CONVG,SIZE,ALPHA,EPSILO
      INTEGER L,K,C
      COMMON L,K,C
      REAL XX,ZZ,SIMA,PSSI,PHHI
      COMMON /TATA/ X1,X2,XX,Z1,Z2,ZZ,PHHI
      COMMON /TITI/ SIGMA1,SIGMA2,SIMA
      COMMON /TETE/ PSI1,PSI2,PSSI
      COMMON /TOTO/ PI,SNPHI,CSPHI
      INTEGER PP,QQ,CONTRO
      COMMON /OUI/ PP,QQ,CONTRO
      REAL MU
      COMMON  MU,PHIP,PHIT
      REAL X(40,40),Z(40,40),SIGMA(40,40),PSI(40,40)
      COMMON /LALA/ X,Z,SIGMA,PSI
      INTEGER P(40),Q(40)
      REAL COSPSI,SIMAV(30),NGAMMA,F,E,SOMME,RATIO
      INTEGER  L1,RAD,I,J,H,RAD1,RAD3
      COMMON /LOLO/ P,Q
      COMMON NPSI,E,HD
      COMMON /NEW/ CSPSI,HOR,ANG
      COMMON /KAYO/ BED,HEQUIV,BDILES,HPRIME,GEL
C
      RAD1=RAD+L-2
      RAD3=RAD+L-3
C
      I=0
      H=0
      J=RAD-2
C23456789
    4 H=H+1
      J=J+1
      I=I+1
      PSI(H,J)=2.*PSI(H,J)
      COSPSI=COS(PSI(H,J))
      PSI(H,J)=PSI(H,J)/2.
     SIMAV(I)=SIGMA(H,J)*(1+SNPHI*COSPSI)
      IF(H .LT. L ) GO TO 4
     PRINT 670,SIMAV(1)
  670 FORMAT(////20X,'SIMAV1=',E15.5)
     PRINT 680,SIMAV(10)
  680 FORMAT(////20X,'SIMAVL=',E15.5)
      I=2
      H=2
      J=RAD
      NGAMMA=0.0
      SOMME=0.0
      AREA1=0.0
    6 I=I+1
C23456789
      H=H+1
      J=J+1
      SOMME=(SIMAV(I-1)+SIMAV(I))/2.
```

```
      SOMME=SOMME*(X(H,J)-X(H-1,J-1))
      AREA1=AREA1+SOMME
     L1=L
      IF(I .LT. L1) GO TO 6
      AREA1=ABS(AREA1)
      B=X(L,RAD1)
      XL=0.80*B
      B=XL+B
      BDILES=ABS(B)
C23456789
 878  CONTINUE
      AREA2=(BDILES-ABS(X(L,RAD1)))*SIMAV(10)*0.5
      AREA=AREA1+AREA2
      NGAMMA=NGAMMA+AREA
      RATIO=1./BDILES**2
      NGAMMA= NGAMMA*RATIO*2.
C
      PRINT 10,NGAMMA
  10  FORMAT('1',////////20X,'NGAMMA=',F9.4 )
C
      B=(BDILES*SIZE)/(X(L,1))
      PRINT 12,B
  12  FORMAT(/////20X,'BREADTH =',F9.4)
      D=GEL
      D=D/BDILES
C
      PRINT 11,D
  11  FORMAT(////////20X,'D/B=',F9.4)
      RETURN
      END
C***************************************************************
C
C
C23456789

      SUBROUTINE PAXCOR
C
C
      REAL PHI
      COMMON PHI,BETA,DELTA,TOL,CONVG,SIZE,ALPHA,EPSILO
      INTEGER L,K,C
      COMMON L,K,C
      REAL XX,ZZ,SIMA,PSSI,PHHI
      COMMON /TATA/ X1,X2,XX,Z1,Z2,ZZ,PHHI
      COMMON /TITI/ SIGMA1,SIGMA2,SIMA
      COMMON /TETE/ PSI1,PSI2,PSSI
      COMMON /TOTO/ PI,SNPHI,CSPHI
     INTEGER PP,QQ,CONTRO
      REAL MU
      COMMON MU,PHIP,PHIT
      REAL X(40,40),Z(40,40),SIGMA(40,40),PSI(40,40)
      COMMON /LALA/ X,Z,SIGMA,PSI
      INTEGER P(40),Q(40)
      COMMON /LOLO/ P,Q
      COMMON NPSI,E,HD
       REAL NPSI
       COMMON /NEW/ CSPSI,HOR,ANG
C
      REAL EX,TIN
C
C
C
      MU=PI/4.-PHI/2.
      EX=NPSI/2-MU
      EX=TAN(EX)
C

      DO 33 I=2,L
      TIN=EX/9.
C23456789
      X(I,1)=TIN*(I-1)
C2345678
  33  CONTINUE
      RETURN
      END
C
C

         SUBROUTINE EDGPA2
C
C
C
C
C
     REAL PHI,EPSILO,ALPHA,FIRPSI,COSPSI
     COMMON PHI,BETA,DELTA,TOL,CONVG,SIZE,ALPHA,EPSILO
     INTEGER H,E
     COMMON L,K,C
     REAL M
     REAL XX,ZZ,SIMA,PSSI,PHHI
     COMMON /TATA/ X1,X2,XX,Z1,Z2,ZZ,PHHI
     COMMON /TITI/ SIGMA1,SIGMA2,SIMA
     COMMON /TETE/ PSI1,PSI2,PSSI
     COMMON /TOTO/ PI,SNPHI,CSPHI
     COMMON /OUI/ PP,QQ,CONTRO
     INTEGER PP,QQ
     REAL MU
     COMMON  MU,PHIP,PHIT
     REAL X(40,40),Z(40,40),SIGMA(40,40),PSI(40,40)
     COMMON /LALA/ X,Z,SIGMA,PSI
     INTEGER W,H1,W2,I,J
     INTEGER P(40),Q(40)
     COMMON /LOLO/ P,Q
     REAL HOR
     COMMON /NEW/ CSPSI,HOR,ANG
     REAL DIF,DI,TNPHI,ENN
      COMMON NPSI,E,HD
      COMMON /KAYO/ BED,HEQUIV,BDILES,HPRIME,GEL
C
C
      SINEP=SIN(EPSILO)
      TANEP=TAN(EPSILO)
C
      H=6
      X(1,1)=0
     HOR=1.0
     DO 800 I=2,H
     W=I-1
      X(I,I)=X(W,W)+HOR/5.0
C23456789
 800  CONTINUE
C
     ENN=2.034
      H1=H+1
      DO 801 I=H1,10
      X(I,I)=X(H,H)+((I-H)*(ENN-1.)/(H-2))
 801  CONTINUE
      IF(BED .GT. 0) GO TO 889
      Z(1,1)=(HOR/10.)*2.0
      Z(10,10)=(HOR/10.)*2.0
 889  CONTINUE
C
      DO 802 I=2,H
      Z(I,I)=(X(I,I)*TANEP)+(Z(1,1))
```